ETH zürich

Diss. ETH No. 24746

Experimental Investigations and Application of Ionic Liquids in Small Self-lubricating Porous Journal Bearings

A thesis submitted to attain the degree of
DOCTOR OF SCIENCES of ETH ZURICH
(Dr. sc. ETH Zurich)

presented by

Mathis A. Trachsel
MSc ETH ME, ETH Zurich
born on Oktober 24, 1981
citizen of Zürich

accepted on the recommendation of
Prof. Dr. Jürg Dual, examiner
Prof. Dr. Konrad Wegener, co-examiner
Dr. Raniero Pittini, co-examiner

2017

Preface

This work was carried out in cooperation between the *Institute of Mechanical Systems* (IMES), Department of Mechanical and Process Engineering (D-MAVT) at the Swiss Federal Institute of Technology ETH Zurich and *maxon motor ag*, located in Sachseln, Obwalden, from 2013 to 2017. Many people contributed to overcome difficulties in different domains, I like to thank:

- Prof. Dr. Jürg Dual, for giving me the great opportunity of carrying out this thesis, inspiring discussions, freedom in choosing the direction of research and the huge amount of initial motivation during the lectures *Mechanik 1, 2* in the first semesters at ETH and later.
- Dr. Raniero Pittini, for being a great boss and supervisor for many years at *maxon motor* and having supported activities in research, including this thesis, in such a motivating and critical way, that is was a great pleasure to work on all sorts of problems and escape every dilemma.
- James Bartolo, my desk neighbour, for help in English and MATLAB.
- Franz Fölmli and Gerhard Brambrink, for fruitful discussions on experimental aspects and help in the domain of design and construction.
- Twan Mennink and Özge Drama, for basic hardware concepts and help in LabView.
- Mario Weder, for many interesting discussions, valuable advices and inputs and for sharing the passion for cycling.
- All the members of IMES at ETH, an equally great place ever since my Bachelor thesis, for their support, discussions and fun.

Zurich, Summer 2017 *Mathis A. Trachsel*

Contents

Abstract

Small, self-lubricated porous journal bearings are widely applied in all kind of different machinery and applications and produced in enormous quantities. Their low cost, high resistance with respect to impacts and overload make them a very important and successful bearing solution to support a rotating shaft carrying a radial load.

For small journal bearings, supporting shafts with diameters in the range of mm, as applied in small machines, standard techniques of friction analysis cannot be used, because the boundary conditions of the specific application cannot be represented. Due to this, different friction values result when compared to the real application and the measurements obtained are not precise enough.

This work addresses systematic investigations of small journal bearings lubricated with Ionic Liquids, which present a novel generation of fluids with promising properties and good lubrication performance. A setup was designed and built so as to represent the application of such bearing systems in a small electric motor of $20\,\mathrm{mm}$ in diameter and imposes identical mechanical boundary conditions as experienced in such motors. A nominal shaft diameter of $3\,\mathrm{mm}$ was used for the experiments. The important parameter of the radial clearance was altered by using precise shafts of different diameters. The radial loading on the bearings was varied in the range from $0.2\,\mathrm{N}$ to $10\,\mathrm{N}$.

A novel procedure for calibration allows to take into account deviations from perfect symmetry, as they are encountered on every part of the mechanical system. This new calibration allows to significantly increase measurement precision. In the case of miniature bearings, as they are used in this work, deviations from the ideal geometry cannot be neglected because measurement precision would suffer dramatically.

The setup developed allows for the simultaneous detection of friction and relative displacement between shaft and bearing, a key parameter in hydrodynamic lubrication theory. This gives additional insight into the bearing kinematics and allows to increase the precision of friction measurements even more, if measured values of shaft-bearing eccentricity are considered for the calculation of the friction torque. Using the developed setup, a nominal resolution of $50\,\mathrm{nNm}$ could be obtained with displacement measurements recorded at $150\,\mathrm{nm}$ nominal resolution.

An analysis of the displacement signal in the frequency domain was performed in order to give additional insight into the system dynamics and detection of whirling phenomena, which typically come along with an increase in friction. To avoid any misinterpretation of measured friction data, knowledge of the whirling state is important.

Viscous heating in the lubricant film strongly effects the lubricant temperature and therefore its viscosity and was also taken into account. Considering effects of viscous heating is especially important at high speeds. The setup under test allows for rotational speeds up to $25000\,\mathrm{rpm}$. Using a combined experimental, numerical and analytical approach, a thermal model was developed and lubricant temperature and therefore fluid viscosity can be determined for Stribeck measurements under variation of speed. Experiments were performed using Newtonian viscosity standards, which provide constant viscosity over a wide range of shear rates. The effect of porous bearing material on friction was investigated as well, under variation of relevant parameters as rotational speed and radial clearance, applying the corresponding theory and the measurement technique developed.

Several selected Ionic Liquids were applied as lubricant in porous, self-lubricating journal bearings and compared to an established standard lubricant. Using these new fluids, the measured friction can be described applying the same models as in the case of the Newtonian reference oil. It was found that in the domain of mixed lubrication several low viscosity Ionic Liquids provide lower friction than the highly developed, non-Newtonian standard lubricant taken as reference.

Zusammenfassung

Kleine, selbstschmierende, poröse Sinterlager werden in riesigen Stückzahlen hergestellt, sind weit verbreitet und werden in den verschiedensten Anwendungen und Maschinen eingesetzt. Wegen ihren geringen Produktionskosten und ihrer Unempfindlichkeit gegenüber Lastspitzen und Schlägen sind sie ein wichtiges Konstruktionselement um eine radial belastete, drehende Welle zu stützen.

Etablierte Messtechniken zur Erfassung von Drehmomenten oder zur Messung von Reibung aus dem Gebiet der Tribologie können nicht einfach auf das System eines Miniatur-Gleitlagers, mit einer Welle mit Durchmesser im Bereich von wenigen mm, angewendet werden, weil die Randbedingungen der spezifischen Anwendung nicht reproduziert werden können. Die erfassten Messwerte würden die Situation in der realen Anwendung nicht genau genug repräsentieren.

In dieser Arbeit wird die Anwendung einer neue Generation von Fluiden, ionischen Flüssigkeiten, als Schmiermittel in kleinen porösen Sinterlagern untersucht. Die neuartigen Flüssigkeiten haben viel versprechende physikalische Eigenschaften und eine gute Schmierfähigkeit.

Es wurde ein Versuchsaufbau gebaut und charakterisiert, um die Anwendung der Gleitlager in einem kleinen Elektromotor mit 20mm Durchmesser abzubilden und die gleichen mechanischen Randbedingungen wie in der Anwendung im Motor zu erzeugen. Für die experimentellen Untersuchungen wurde eine Welle mit 3mm Durchmesser verwendet. Der radiale Fluidspalt, ein wichtiger Parameter in der Lagertechnik, kann durch die Verwendung von Wellen mit unterschiedlichen Durchmessern verändert werden. Die auf das Lager wirkende Radiallast wurde im Bereich von 0.2N bis 10N variiert. Ein neuartiges Kalibrierungs-Verfahren erlaubt es, Abweichungen von der idealen Geometrie zu berücksichtigen, welche auf jedem mechanischen Teil anzutreffen sind. Dies erhöht die Messgenauigkeit signifikant, da im

Falle von kleinen Lagern, wie sie in dieser Arbeit verwendet wurden, diese Abweichungen nicht vernachlässigt werden können.

Der entwickelte Versuchsaufbau erlaubt die gleichzeitige Erfassung von Lagerreibung und der relativen Verschiebung zwischen Welle und Lager, ein wichtiger Parameter in der Theorie der Gleitlager. Dies gibt einen wertvollen Einblick in die Kinematik der Lager und erhöht die Messgenauigkeit noch weiter, wenn die gemessenen Daten für die Berechnung der Lagerreibung verwendet werden. Mit dem Messaufbau wird eine nominelle Messgenauigkeit von 50nNm für das Reibmoment erreicht. Die relative Verschiebung wird mit 150nm Auflösung erfasst.

Eine Analyse der Daten der relativen Bewegung zwischen Welle und Lager im Frequenzbereich gibt einen zusätzlichen Einblick in die Dynamik des Systems, speziell auf Wirbel-Phänomene, welche zusammen mit einer Erhöhung der Reibung auftreten. Um die Messdaten der Reibung nicht falsch zu interpretieren, ist die Kenntnis des dynamischen Zustandes sehr wichtig.

Die Erwärmung des Schmierfilmes wegen viskoser Energiedissipation beeinflusst die Temperatur des Schmierfilms signifikant und somit auch dessen Viskosität. Vor allem bei Messungen mit hohen Geschwindigkeiten bis zu 25000U/min ist dieser Effekt deutlich in der Messung der Reibung sichtbar. Mit einem Ansatz bestehend aus Messungen, numerischen Simulationen und analytische Modellen wurde ein thermisches Modell entwickelt, um die Fluidfilm-Temperatur im Spalt und somit auch die Schmiermittel-Viskosität für verschiedene Stribeck-Messungen unter Variation der Rotationsgeschwindigkeit der Welle zu bestimmen. Hierfür wurden Messungen mit Newtonschen Referenz-Ölen durchgeführt, welche über einen weiten Bereich von Geschwindigkeiten eine von der Scherrate unabhängige Viskosität aufweisen. Zusammen mit einer Veränderung der involvierten relevanten Parametern wurde der Einfluss der Lagerporen auf die Reibung mit der entwickelten Messtechnik untersucht und mit der entsprechenden Theorie modelliert.

Ausgewählte Ionische Flüssigkeiten wurden in porösen Sinterlagern eingesetzt, gemessen und mit Standard Schmierstoffen verglichen. Bei der Anwendung dieser Fluide kann die gemessene Reibung mit den gleichen Modellen beschrieben werden wie im Falle der Newtonschen Referenz-Öle. Im Bereich der Mischreibung zeigten einige niedrigviskose Fluide weniger Reibung als der hoch entwickelten nicht-Newtonsche Standard Schmierstoff.

Nomenclature

Greek Letter Variables

α	heat transfer coefficient	W/m^2K
β	slip coefficient	[-]
$\dot{\gamma}$	shear rate	$1/s$
λ	heat conductivity	W/mK
ϵ	relative eccentricity	[-]
κ	bearing permeability	m^2
η	fluid viscosity	Pa s
Θ	slip parameter $\frac{1}{\sqrt{\kappa}/\beta c}$	[-]
ρ	density	kg/m^3
τ	shear stress	Pa
φ	contact angle	
ω	shaft speed	rad/s
μ	measured coefficient of friction	[-]

Latin Letter Variables

A	area	m^2
B	bearing circumferential length	m
C	Center of bearing bore	
c	radial clearance	m
cw	clock wise direction	
ccw	counter clock wise direction	
C	heat capacity	J/K
d_c	cylinder diameter, 12	mm
e	eccentricity	m
d_s	shaft diameter	m
$\boldsymbol{e}$	unit vector	
F_b	rope force on the side of the balance	N
F_w	rope force on the side of the weight	N
F_r	radial load on the shaft	N
g	gravity, 9.81	ms^{-2}
$h(x)$	fluid gap	m
l_b	bearing length, 3	mm
L	bearing length, 3	mm
m_c	mass of cylinder with bearings, 13.13	g
n	shaft speed	rpm

M_{meas}	measured friction torque	Nm
M_s	friction torque at support	Nm
M_{HD}	modeled hydrodynamic friction	Nm
M_{THD}	modeled friction THD	Nm
$M_{THD,p}$	modeled friction THD incl. pores	Nm
O	Center of the shaft	
P_{ij}	internal heat flux from i to j	W
p	pressure	Pa
$\dot{Q}_f$	frictional heating	W
$\dot{Q}_{sup}$	heating of support	W
$\dot{Q}_i$	convective heat fluxes	W
$\boldsymbol{r}_{OS}$	vector from O to S	
$\boldsymbol{r}_{CS}$	vector from C to S	
r_s	shaft radius	m
r_c	cylinder radius	m
r_b	distance of F_b from the axis of rotation	m
r_w	distance of F_w from the axis of rotation	m
Δr_x	horizontal component of deviations	m
R_i	Reynolds number	[-]
R	heat resistance	K/W

S	Center of outer cylinder	
s_x	horizontal laser distance measurement	
s_y	vertical laser distance measurement	
T_f	friction torque	Nm
T_g	torque induced by gravity	Nm
T	temperature	K
t	time	s
$\boldsymbol{u}$	speed vector	m/s
Δx	horizontal displacement of bearing	m

1 Introduction

Nature cannot be fooled.

Richard Feynman, 1918-1988

1.1 Lubrication and bearing technology

Some of the first applications of lubrication were documented some 4000 years ago: On a painting discovered on the tomb of Tehuti-Hetep, who lived in the Middle Kingdom of Egypt, we can clearly see people responsible for applying a liquid, probably water, under the sled transporting a heavy statue (see detail view in Fig. 1.1). Most probably this was done to reduce the friction force while dragging the sled. During this time, also olive oil was

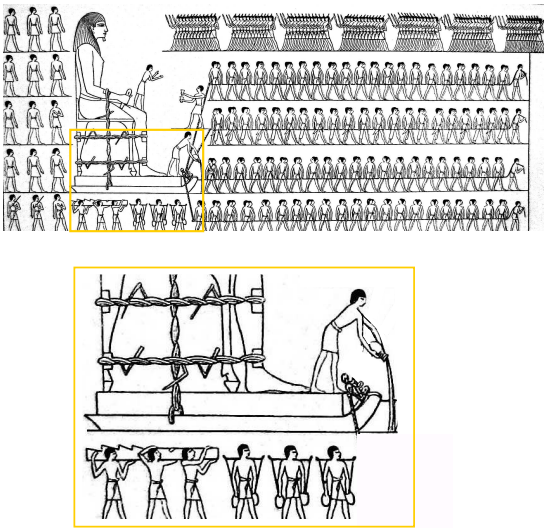

Fig. 1.1: *Documented application of lubrication in 1880 BC. A colossal statue is moved by 172 men with the help of a fluid added under the sled. [33]*

used to transport large stones. Later animal fats were applied to lubricate chariot wheels [7].

Even though first concepts in ball bearing design are old (see Fig. 1.2), their successful implementation on a large scale had to wait until suitable materials became available. When wooden tools were replaced with brass and iron, animal and vegetable oils were applied as lubricant, sometimes as mixtures. After the middle ages, whale and porpoise oil was widely used. The first mineral oil was successfully extracted in Pennsylvania, in the middle of the 19th century, starting the rise of the petroleum industry.

Crude oil was first used as a lubricant in a cotton spinning mill in Pittsburgh, Pennsylvania, in 1845 [7].

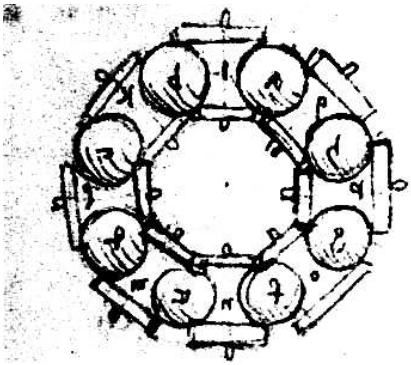

Fig. 1.2: *Ball bearing concept by Leonardo da Vinci (*1452)*

The principle of applying some deformable material as grease or oil between two solids sliding with respect to each other was tremendously successful: Friction and wear got reduced. Bearing technology finally allowed the building of complex machines which, with some maintenance, did not exhibit significant wear and frictional losses. A Fluid in between the two sliding components is able to provide a load-carrying pressure and therefore separate the two bodies. Any liquid, a deformable material, reacts to a shearing deformation it is exposed to, by means of a specific force arising by viscosity and geometry. Due to the typically small resulting values of friction, the energy spent to overcome friction can be further reduced using an intelligent bearing design. Most importantly, any energy losses can be extracted in the form of thermal energy and typically do not provide any wear.

Refining petroleum products allowed to create lubricants with different ratings of viscosity to meet the new requirements of high speed machines working at different temperatures. Various additives and mixtures later allowed to tune the lubricants according to the specific needs, e.g. high pressure additives favor lubrication properties in the domain of boundary lubrication and non Newtonian, shear thinning lubricants reduce friction and energy losses at high speed. Since the middle of the 20th century [7], synthetic liquid lubricants again improved lubrication performance providing high-temperature stability, decreased volatility and superior viscosity-temperature properties.

Due to the enormous amount of machinery emerging from modern industry, the number of bearing systems installed increased dramatically. Optimization with respect to friction, wear and other parameters of bearing performance therefore are very important to save energy and cost. Due to this fundamental demand from industry, bearing and lubrication technology also gained importance in the field of research which spread in all different

directions.

In small electric motors, the bearing friction losses are of special importance: The efficiency of the electromagnetic part is limited due to the small size. The mechanical losses, which can mainly be found in the bearings, provide potential for improvement in efficiency, a reduction in thermal losses and therefore an increase in overall performance.

1.1.1 Types of Bearings

The type of bearings most commonly applied in small electric motors are shown in Fig. 1.3. They can be broadly classified as: a) porous, self-lubricating sintered bronze bearings and b) ball bearings. Independent from

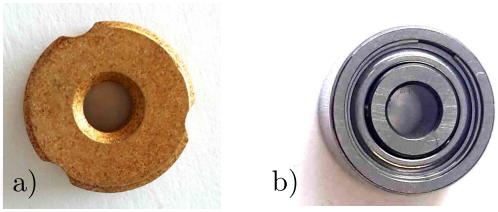

Fig. 1.3: *Typical bearings of* 10 *mm outer and* 3 *mm inner diameter:*
a) Sintered porous bronze journal bearings of type B50.
b) Ball bearing by GRW: 623-2Z ABEC3P C10/15 GPR J 15

the bearing technology applied, the friction induced by the relative motion can either be expressed as friction torque M, with respect to the centre of rotation, or in dimensionless form, related to the normal radial loading F_r applied, as coefficient of friction μ:

$$\mu = \frac{M/r_s}{F_r} \tag{1.1}$$

with shaft radius r_s. Due to their totally different principle of reducing friction, the measured friction presented in so called Stribeck curves under variation of speed and radial loading F_r, show important, characteristic differences for the two types of bearings as illustrated in Fig. 1.4: In the representation of the friction torque M, shown in Fig. 1.4a), the ball bearings exhibit values of friction that merely depend on the radial loading applied

and start at low speed at around $10.5\,\mu Nm$ to become higher with increasing speed. Friction torque values M for the journal bearings in contrast, strongly depend on the radial load applied at low speed, reduce with increasing speed to only slightly depend on the radial load at higher speeds. In the representation of friction in dimensionless form μ (1.1), displayed in

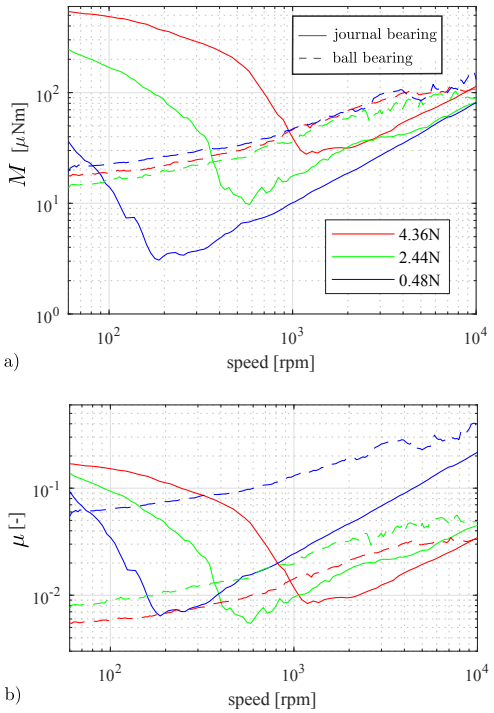

Fig. 1.4: *Comparison of friction for self-lubricating journal bearings with radial clearance $c = 12\mu m$ and standard ball bearings. Both for $3\,mm$ inner and $10\,mm$ outer diameter, radial loadings $F_r = 0.48\,N,\ 2.44\,N$ and $4.36\,N$. Representation of measurement data as friction torque in a) and as dimensionless coefficient of friction in b).*

Fig. 1.4b), a different situation is found: Journal bearings start at low speed at similar values of friction μ, independent from the loading and also the

values of minimum dimensionless friction μ is similar. The friction values μ of the ball bearings strongly depend on the radial loading applied. At low radial loading, ball bearings show much higher friction μ when compared to the journal bearings, except for very low speed.

For the porous, self-lubricating journal bearings, which are in the focus of this thesis, the Stribeck curves are characterized by the fluid structure interaction, which strongly depends on speed. Therefore different important domains in the Stribeck-curve have to be distinguished, as indicated in Fig. 1.5.

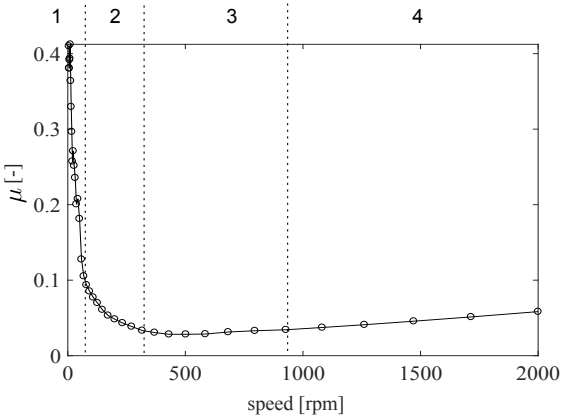

Fig. 1.5: *Friction under variation of speed shown in a Stribeck curve. Lubrication regimes: 1: Boundary friction, 2: Mixed lubrication, 3: Elastohydrodynamic lubrication, 4: Hydrodynamic lubrication.*

The different domains of the Stribeck curve are the following:

1. Boundary friction: At low speed the two bodies are in contact, high friction and wear occur.
2. Mixed lubrication: With increasing speed, the lubricant is able to build up a pressure and the contact force on the tips of the surface roughness is reduced.
3. Elastohydrodynamic lubrication: At a specific sliding speed, the friction reaches a minimum. The sliding components experience an elastic deformation due to high pressure.

4. Hydrodynamic lubrication: If the speed is high enough, a fluid film is built up and no contact occurs. Wear is minimized and friction increases with speed because of the viscous forces in the lubricant.

To measure the frictional force between to sliding partners under different conditions e.g. lubricants, several machines are commercially available. In small electric motors in contrast, the problem of friction cannot be reduced to a simple sliding contact, as the complex fluid-structure-interaction of the system in application involves more complex boundary conditions, such as very high shear rates, changes in lubrication regimes and dynamic effects as half-frequency whirling. This work therefore is based on the experimental setup developed and described in detail in Chapter 4, which was designed to represent the situation in applications.

1.2 Review on history and literature

In 1904, German physicist Arnold Sommerfeld, who was working on the foundation of quantum physics together with A. Einstein, M. Planck and N. Bohr, derived approximations for lubricant friction with the focus on application [105]. The important dimensionless parameter, established as 'Sommerfeld-number' So to characterize the bearing state, is named after him.

In those days, the application of the differential equations to real problems of physics was occupying many of the physicists, usually exploring more fundamental questions as the structure of atoms and quantum electrodynamics. In a discussion with experts of fluid dynamics Sommerfeld stated his opinion on the question of stability and whirling:

> *Es ist sehr merkwürdig und auf den ersten Blick unwahrscheinlich, daß der Couettesche Fall, wie Hopf und v. Mises gezeigt haben, bei unendlich kleinen Störungen stabil, alle übrigen Strömungsfälle nach Herrn Prandtl aber instabil sein sollen. Die Beobachtung läßt keinen solchen Unterschied erkennen, sondern es gilt in allen Fällen Instabilitäten oberhalb gewisser Grenzen, die allerdings sehr wohl von den näheren Umständen abhängen.* [96]

Also the students of Sommerfeld, Richard von Mises and Ludwig Hopf were working on this topic and Werner Heisenberg did his dissertation on the turbulent flow problem.

Due to the absence of numerical tools, simplification by approximation was an important technique in the middle of the 20th century.

In 1953, Dubois and Ocvirk [32] presented an approximate solution for short bearings, considering leakage flow and found experimental data to agree. Important aspects of maximum bearing temperature and effects of shaft deflection or misalignment were discussed as well.

Using a short approximation, Rhodes and W. Rouleau [99] theoretically studied, in 1965, the effect of sealed ends to prevent leakage. Friction values as a function of shaft eccentricity and attitude angle were given. Effects of porous bearing material were considered as well. This important effect, directly influencing bearing performance, became a new challenge in modeling and was accounted for in different ways: Joseph and Tao [50] applied Stokes' equations, Shir and Joseph [102] modified the Reynolds

equation using Darcy's law, leading to a flow velocity proportional to pressure and material parameters. The resulting pressure distribution was shown under variation of eccentricity and permeability.

The boundary conditions at a permeable wall, as they are found in the case of porous bearings, were given by Beavers and Joseph [14]. A wide overview on the topic was given by Morgan [76] in 1971.

In the same year, the effect of reduced friction of porous bearings was assigned to 'slip' by Goldstein and Braun [39].

With the focus on hydrodynamic lubrication, Murti analytically investigated bearing performance for long [79], finite [78] and short [80] bearings and published other work on the subject of slip and flow in porous media [81, 83, 82, 84]

More important contributions on this topic were given by Cusano [29] in 1973 and Prakash and Vsj in [93, 92].

Later more sophisticated modeling become possible and in 1978 Kumar [58] did also consider effects of turbulence. More analytical solutions were given for short [59] and for finite [61] bearings. He also published critical reviews, which state the problems in limits of the theory applied [60, 62].

With the strong increase in computation power, numerical solutions today allow to take into account any arbitrary effect of physics, such as viscous heating, flow in porous media [12] of any modeling and cavitation [100].

Even worn bearings with imperfect geometry can be analyzed [38, 10].

Of course a heavy simulation considering every detail cannot replace an exact analytical solution for the relevant parameters, therefore the old approximations mentioned above still find use in modeling and performance analysis.

The key performance parameters of journal bearing technology, load carrying capacity and friction under variation of speed, can be determined experimentally using a suitable technique. According to theory [45] these parameters depend on the relative position between shaft and bearing, which is more difficult to access experimentally. Especially on small bearings direct dynamic measurements can not be applied, as the fluid gap is in the range of μm.

German engineer Richard Stribeck first performed systematic experiments to investigate friction versus speed in 1902 [109]. To credit his work, such data is usually referred to as 'Stribeck curve'.

Several measurement techniques were proposed to measure friction: In 1985 Yong-Xin and Pei-Ming [131] measured friction at a shaft of $24mm$

of diameter using a balance. In [130] he performed measurements on a shaft of $4.5mm$ diameter and obtained high deviation between theory and measurement.

With the focus on MEMS applications, Brenner et al. [22] applied a $0.7\,mm$ leaf spring and strain gauges to reach measurement precision of $1\,\mu Nm$ with high error. Damping was needed to avoid vibrations. Another system based on strain gauges was proposed by Yao et al. [128]

For bigger shaft diameter of $50mm$ and $100mm$, some work was presented by Adatepe et al. [1] and Bouyer and Fillon [20] for the case of start-up friction.

A similar experimental technique as applied in this work was used by Kim et al. [56] who calculated coefficients of friction for discrete rotational speeds using assumptions for the contact geometry between shaft and bearing. Fabrication imperfections were not considered and the speed range limited to $5000\,rpm$ for constructive reasons.

The setup developed here allows for precise friction measurements at rotational speed up to $25000\,rpm$ and is described in detail in Sections 3 and 4. It allows for simultaneous detection of friction and relative displacement between shaft and bearing. For the calculation of friction values, deviations from the ideal geometry are considered, which is important for small bearings.

1.3 Overriding research questions and structure

The need of precise friction measurement techniques for small journal bearings to investigate lubrication performance of a new type of fluid, Ionic Liquids, as lubricant and the absence of experimental work [103] were the motivation for this thesis.

For small journal bearings, to date no suitable technique is available to perform precise friction measurements with boundary conditions close to the real application. As an additional lack, to date the important parameter in lubrication theory, eccentricity e, the relative displacement between shaft and bearing, was not possible to measure, as any established measurement technique from bigger bearings, cannot be applied on miniature bearings, without influencing the sensitive fluid structure interaction and therefore the bearing performance itself.

This thesis is structured according to the work flow of the research performed, which again appears in the order of the paper publications:

1. **Experimental setup.** The basis of this work, the apparatus developed is described in detail in chapter 4, allowing for precise friction measurements with simultaneous detection of the relative displacement between shaft and bearing. This provides the bearing trajectory under variation of parameters involved, and, analysed in the frequency domain, the dynamic behaviour of the system. In the friction measurement technique applied here, the knowledge of bearing eccentricity allows for calculation of more precise values of friction.

2. **Modelling friction considering thermal effects.** Friction measurements at high speed and high shear rates are accompanied by viscous heating, which directly influences fluid viscosity and therefore the friction measured in the hydrodynamic domain of lubrication. To model friction and the influence of parameters involved, effects of viscous heating cannot be neglected. This topic was addressed in detail in Chapter 5, again under consideration of dynamic effects of half-frequency whirling, identified by the simultaneous detection of friction and relative displacement between shaft and bearing.

3. **Ionic Liquids as lubricant.** Finally, using the hardware, technique and know-how acquired, the initial motivation to start this work was addressed: A selection of Ionic Liquids were applied as lubricants and measured friction compared to established theory, to investigate their lubrication performance. Considering effects of viscous heating in porous bearing material, measured friction was compared to theory and measurements using standard lubricants.

The work is put in a structure of a cumulative dissertation, each chapter is a paper publication and can be read and understood alone and independent from each other.

Chapter 2 provides the basics of the theory involved, which readers from different backgrouds might not be familiar with. Additional information on experimental aspects, which is not present in the following paper publication included in Chapter 4, is given in Chapter 3. The experimental technique developed is important for this work, as a major part of the time was spent to understand the physics involved and find approaches to make measurable the parameters of interest.

Basics and theory applied to bearing lubrication

2

As simple as possible, but not simpler.

ALBERT EINSTEIN, 1879-1955

Long time before high performance lubricants were available, the basic mathematics to describe pressure forces on a fluid, were given.

Back in 1755, Leonhard Euler published the Euler-equations [35], a general form of equation of continuity and conservation of momentum for compressible fluids, which were among the first differential equations written down, representing conservation of mass (2.1) and momentum (2.2).

$$\frac{\partial \rho}{\partial t} = -\nabla \cdot (\rho \mathbf{u}) \tag{2.1}$$

$$\underbrace{\rho \left[\frac{\partial \mathbf{u}}{\partial t} + (\mathbf{u} \cdot \nabla \mathbf{u}) \right]}_{\text{inertia forces}} = - \underbrace{\nabla p}_{\text{pressure forces}} + \underbrace{\mathbf{g}}_{\text{body forces}} \tag{2.2}$$

with velocity vector $\mathbf{u}$, pressure p and density ρ. These conservative equations don't consider any viscosity, friction and dissipation of energy.

Independent from each other, Navier and Stokes added in 1822 and 1845 the effect of viscosity η, a measure of a fluids resistance to a shear deformation $\dot{\gamma}$, it is exposed to, by a force per area τ:

$$\eta = \frac{\tau}{\dot{\gamma}} \tag{2.3}$$

Herewith they created the basis for calculations with Newtonian fluids. The famous Navier-Stokes equations consist of the conservation of momentum (2.4)

$$\rho \left[\frac{\partial \mathbf{u}}{\partial t} + (\mathbf{u} \cdot \nabla \mathbf{u}) \right] = -\nabla p + \eta \nabla^2 \mathbf{u} + \rho \mathbf{f} \tag{2.4}$$

with external forces $\mathbf{f}$ and the continuity equation (2.5)

$$\nabla \cdot \mathbf{u} = 0 \tag{2.5}$$

Assuming an incompressible fluid, steady state and no external forces, a simplification relates the fluid pressure p to fluid velocity $\mathbf{u}$, in case of laminar flow, where viscous forces are dominant.

$$\nabla p = \eta \nabla^2 \mathbf{u} \tag{2.6}$$

Train-engineer Tower, as first to experimentally clarify the essence of hydrodynamic lubrication in 1883 [115], reflecting Britain's advanced technology at that time. He found a small coefficient of friction, frictional

resistance merely depending on the load applied, but increasing with sliding speed. He also found frictional resistance to decrease at higher temperature.

With focus on bearing applications, British physicist Reynolds formulated the theory of lubrication in 1886 [97], which became the foundation of hydrodynamic lubrication. The equation assumes a Newtonian fluid with viscous forces dominating inertial forces, a laminar flow profile and a much smaller film thickness than the circumferential dimension B and length L, as given in Fig. 2.1. A commonly encountered form of the Reynolds equation for compressible fluids is given in [55]

$$\frac{\partial}{\partial x}\left(\frac{\rho h^3}{12\eta}\frac{\partial p}{\partial x}\right)+\frac{\partial}{\partial y}\left(\frac{\rho h^3}{12\eta}\frac{\partial p}{\partial y}\right)=\frac{1}{2}U\frac{\partial \rho h}{\partial x}+\rho\frac{\partial h}{\partial t}. \tag{2.7}$$

with the shaft surface velocity $U=\omega\, r_s$ and film thickness h. For incompressible fluids (2.7) simplifies to

$$\frac{\partial}{\partial x}\left(\frac{h^3}{12\eta}\frac{\partial p}{\partial x}\right)+\frac{\partial}{\partial y}\left(\frac{h^3}{12\eta}\frac{\partial p}{\partial y}\right)=\frac{1}{2}U\frac{\partial h}{\partial x}+\frac{\partial h}{\partial t}. \tag{2.8}$$

Solving this equation, one obtains the hydrodynamic pressure distribution, accounting for physical wedge, as well as normal motion of the surfaces $\frac{\partial h}{\partial t}$, which vanishes for the case of a steady film.

As this is a second-order partial differential equation, no closed-form, analytical solution is available.

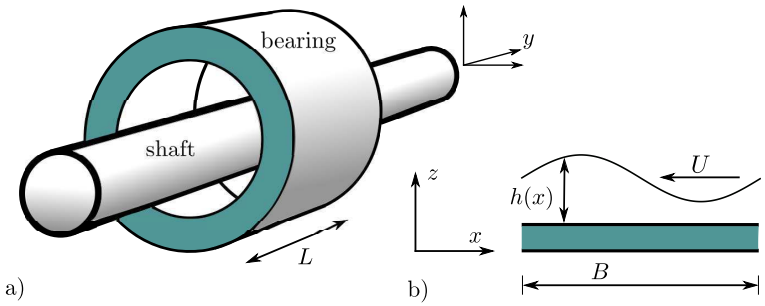

Fig. 2.1: *Journal bearing*

Based on the Reynolds equation in dimensionless form according to [55]:

$$\frac{\partial}{\partial \overline{x}}\left(\overline{h}^3\frac{\partial \overline{p}}{\partial \overline{x}}\right)+\left(\frac{B}{L}\right)^2\frac{\partial}{\partial \overline{y}}\left(\overline{h}^3\frac{\partial \overline{p}}{\partial \overline{y}}\right)=6\frac{\partial \overline{h}}{\partial \overline{x}}, \tag{2.9}$$

where $\overline{\square}$ denotes the dimensionless quantities: $\overline{x} = \frac{x}{B}$, $\overline{y} = \frac{y}{L}$, $\overline{h} = \frac{h}{h_{mean}}$, $\overline{t} = \frac{t}{t_{ref}}$, $\overline{P} = \frac{P}{P_{ref}}$. Using $P_{ref} = \eta\, B\, U/h^2_{mean}$ and $t_{ref} = B/U$, it is possible to get closed form solutions for limiting cases: depending on the ratio B/L of the fluid film, (2.9) can be simplified by neglecting either the first or the second term, as shown in the following sections.

2.1 Boundary conditions and approximations

1. Infinitely long approximation (ILA): $L >> B$, $(B/L)^2 << 1$, neglects pressure gradient in y-direction and simplifies to:

$$\frac{\partial}{\partial \overline{x}} \left(\overline{h}^3 \frac{\partial \overline{p}}{\partial \overline{x}} \right) = 6 \frac{\partial \overline{h}}{\partial \overline{x}} \tag{2.10}$$

2. Infinitely short approximation (ISA): $L << B$, $(B/L)^2 >> 1$, the pressure gradient in y-direction is dominant compared to the flow in sliding direction:

$$\left(\frac{B}{L} \right)^2 \frac{\partial}{\partial \overline{y}} \left(\overline{h}^3 \frac{\partial \overline{p}}{\partial \overline{y}} \right) = 6 \frac{\partial \overline{h}}{\partial \overline{x}} \tag{2.11}$$

where: x is the direction of movement, z is the normal direction and $\overline{h}(\overline{x}, \overline{t})$ is the film thickness.
Both approximations allow analytical solutions and therefore are very useful results [55]. For a finite bearing length, the equation can be solved numerically or by an approximate analytical method [45].

Reynolds' equation gives positive pressure in the converging part of the fluid gap and negative pressure in the diverging domain. This is possible at moderate pressure. At higher bearing pressure, the negative pressure might decrease below ambient pressure, which is not possible. Also a rupture of the fluid film due to cavitation is a problem, as it is difficult to know the precise position at which oil film rupture will occur.

For the circumferential pressure distribution, the following boundary conditions are applied to give approximate solutions according to the specific problem:

- *Sommerfeld's* boundary condition: In this case, negative and positive pressure are equally considered. Having the advantage of continuous

and symmetric pressure, negative pressure might reach values, which are never achieved physically.

- *Gümbel's* boundary condition neglects the negative part of the pressure completely by simply assuming zero pressure at the location of negative pressure. A discontinuity in pressure results. This approach of only considering positive pressure is also known as *half-Sommerfeld* boundary condition.

- *Reynolds's* boundary condition: To eliminate the discontinuity in pressure and oil flow involved in Gümbel's boundary condition, the oil pressure is assumed to terminate later at a position where both fluid pressure and gradient become zero. This is also known as the Swift-Stieber boundary condition.

A sketch of a bearing is given in Fig. 2.2 to illustrate the main parameters of interest, namely: bearing radius r_b, shaft radius r_s, radial loading F_r, attitude angle φ and eccentricity e . It is common to relate the eccentricity e to the fluid gap $c = r_b - r_s$, such that a dimensionless relative eccentricity $\epsilon = \frac{e}{c}$ is obtained. Applying these approximations to the bearings under test with $3\,mm$ inner diameter and length $L = 3mm$, pressure distributions and the relative displacement between shaft and bearing from theory are given in the following sections.

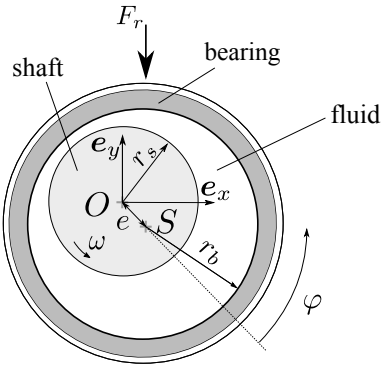

Fig. 2.2: *Shaft, bearing and fluid gap.*

Pressure distribution, infinitely long approximation

The infinite long approximation neglects pressure gradients in the axial direction. The flow problem therefore becomes two dimensional and pressure p can be obtained by integration of (2.10) according to Hamrock and Schmid [41] as given in (2.12):

$$p\left(\eta,\omega,\epsilon,\varphi\right)=\omega\eta\left(\frac{r_b}{c}\right)^2\cdot\frac{6\epsilon\sin\varphi\left(2+\epsilon\cos\varphi\right)}{\left(2+\epsilon^2\right)\left(1+\epsilon\cos\varphi\right)^2}+p_0 \tag{2.12}$$

where: p_0 is the pressure at maximum film thickness. The pressure is illustrated in Fig. 2.3 (a) for the full Sommerfeld boundary condition, and in Fig. 2.3 (b) for the half-Sommerfeld or Gümbel boundary condition. For illustration, the pressure in Fig. 2.3 is given for a typical bearing of $3\,mm$ inner diameter, constant viscosity of $\eta = 10\,mPas$, a radial clearance of $c = 10\,\mu m$, a shaft speed of $1000\,rpm$ and several relative eccentricities ϵ and the corresponding radial load F_r.

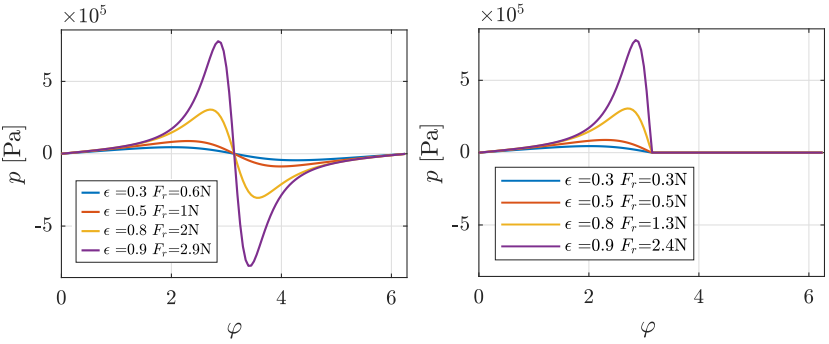

(a) Sommerfeld boundary condition.

(b) Gümbel boundary condition.

Fig. 2.3: *Infinitely long bearing approximation pressure solutions for several relative eccentricities ϵ and the corresponding radial load F_r.*

Pressure distribution, infinitely short approximation

For short bearings, the pressure gradient in axial direction is larger than the one in circumferential direction and, according to (2.11), the flow in sliding direction can be neglected. Integration leads to the simplified three dimensional pressure distribution given in (2.13):

$$p = \frac{3\eta\omega\epsilon}{c^2}\left(\frac{b^2}{4} - y^2\right)\frac{\sin\varphi}{(1+\epsilon\cos\varphi)^3} \tag{2.13}$$

For illustration, an example is given for a typical bearing at a relative eccentricity $\epsilon = 0.3$, constant viscosity of $\eta = 10\,mPas$ and a radial clearance of $c = 4\ \mu m$ in Fig. 2.4 (a) for the Sommerfeld boundary condition and in Fig. 2.4 (b) for the Gümbel boundary condition, neglecting the negative pressure.

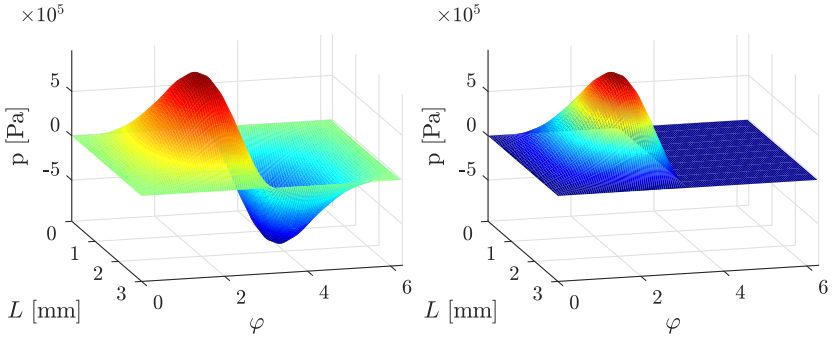

(a) Sommerfeld boundary condition.

(b) Gümbel or half-Sommerfeld boundary condition.

Fig. 2.4: *Infinitely short bearing approximation pressure solutions,* $\epsilon = 0.3$.

Depending on the pressure solution chosen, different forces act on shaft and bearing, and therefore, a different relative position between the two results. This will be shown after the introduction of the Sommerfeld number So in Section 2.3.

2.2 Sommerfeld number

In a bearing under low radial load, the shaft is well centred and the shear-flow, defined by the no-slip boundary conditions, fluid gap c and angular velocity ω, dominate over pressure and axial flow, which are neglected.

As first formulated by *Petroff* in 1883, the dominating circumferential friction by the fluid forces is given by:

$$F_{fric} = B\,L\,\eta\frac{\omega r_s}{c}, \tag{2.14}$$

describing a relationship between the geometry of bearing circumferential length B, bearing axial length L, r_s and c, fluid viscosity η and angular shaft velocity ω, and the radial load applied F_r to give a dimensionless friction μ as:

$$\mu = \frac{F_{fric}}{F_r} = \frac{B\,L}{F_r}\,\eta\frac{\omega r_s}{c}. \tag{2.15}$$

In hydrodynamic bearing theory, this value often is related to the relative gap $\Psi = \frac{c}{r_s}$[77], herewith we obtain:

$$\frac{\mu}{\Psi} = \frac{F_{fric}}{F_r}\frac{1}{\Psi} = \frac{B\,L}{F_r}\,\eta\omega\left(\frac{r_s}{c}\right)^2. \tag{2.16}$$

Substituting the active pressure p

$$p = \frac{F_r}{B\,L},$$

we obtain the Sommerfeld number So:

$$So = \left(\frac{r_s}{c}\right)^2\frac{\eta\omega}{p} \tag{2.17}$$

a dimensionless parameter containing all the relevant factors such as shaft radius r_s, radial clearance c, fluid viscosity η, angular velocity ω and the load carrying pressure p.

The *Sommerfeld* number So is used to characterize the bearing state. Doubling the rotational speed for example has the same effect on friction as an increase in viscosity η by a factor of two. Note the quadratic dependence on the fluid gap c, which is typically within some μm and difficult to determine. In some literature, the Sommerfeld number is used in an inverse form. The speed parameter ω sometimes is used as rpm or Hz. In the notation used here, ω is used in rad/s.

2.3 Eccentricity and relative displacement trajectory

To maintain a quasi static equilibrium between the external radial load F_r and the fluid forces, a relative position between shaft and bearing has to be found. This is typically described by a value of eccentricity e or relative eccentricity ϵ and an angle φ as illustrated in Fig. 2.2.

As given in [18], the expected eccentricity ratio ϵ is related for the infinite long approximation for both the full and half-Sommerfeld circumferential pressure distribution to the *Sommerfeld* number So:

$$So_{long,full} = \frac{\left(1-\epsilon^2\right)^{0.5}\left(2+\epsilon^2\right)}{12\pi^2\epsilon} \tag{2.18}$$

$$So_{long,half} = \frac{\left(2+\epsilon^2\right)\left(1-\epsilon^2\right)}{6\pi\epsilon\left(\pi^2(1-\epsilon^2)+4\epsilon^2\right)^{0.5}} \tag{2.19}$$

A dimensionless representation is plotted in Fig. 2.5 using the ILA and the ISA for bearings of equal diameter and length such that $d_b/L = 1$ as it is the case in the configuration under test. For the short bearing approximation

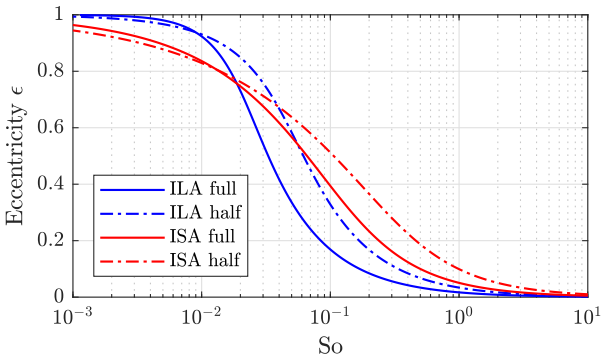

Fig. 2.5: *Eccentricity ratio ϵ in function of So for $d_b/L = 1$.*

ISA the relation for the full Sommerfeld boundary condition is given by:

$$So_{\text{short,full}} = \left(\frac{d_b}{L}\right)^2 \frac{\left(1-\epsilon^2\right)^{3/2}}{2\pi^2\epsilon} \tag{2.20}$$

and for the half-Sommerfeld-boundary condition:

$$So_{\text{short,half}} = \left(\frac{d_b}{L}\right)^2 \frac{\left(1-\epsilon^2\right)^2}{\pi\epsilon\left(\pi^2(1-\epsilon^2)+16\epsilon^2\right)^{0.5}} \tag{2.21}$$

Using some typical numerical values, relative eccentricity ratio ϵ for different bearing length and loadings are presented against speed in Fig. 2.6. The differences between the ISA and ILA with full and half Sommerfeld boundary conditions are only small for a specific bearing length, but a relevant deviation can be observed at different bearing lengths, where the approximations are not valid anymore.

In an alternative representation in Fig. 2.7, the contact angle information is included as well. The relative displacement between shaft and bearing is plotted in the available clearance c of the fluid gap for the half-Sommerfeld pressure boundary condition and for the ILA and ISA approximation for different speeds. Due to the complex mechanism in the domain of boundary and mixed lubrication, these models of hydrodynamic theory are of a limited validity at low speed. However, measured relative displacement trajectories and theory over the entire speed range fit astonishingly well.

Models of friction in the domain of hydrodynamic lubrication in contrast, provide too low friction at low speed as they don't consider solid friction and start from zero friction at zero speed.

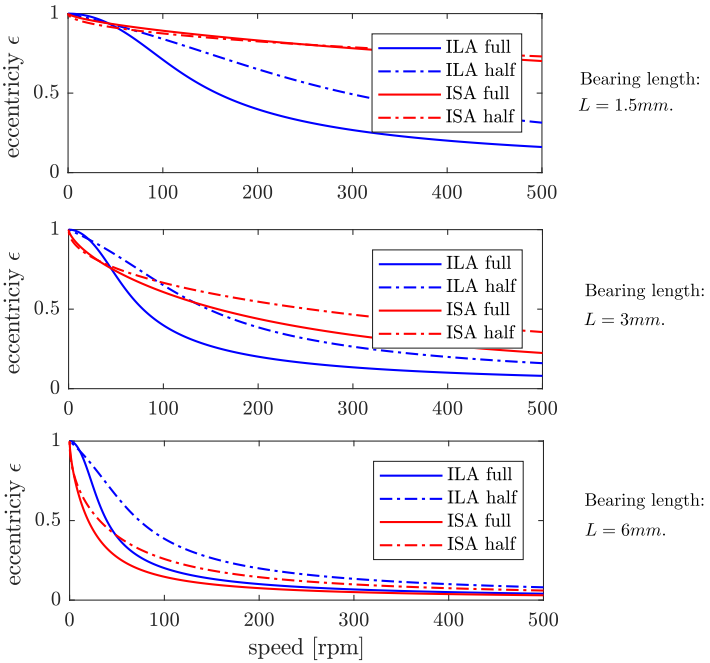

Fig. 2.6: *Expected relative eccentricity ϵ according to the ISA and ILA theory, both for full Sommerfeld and half Sommerfeld or Gümbel boundary conditions, mean gap with $c = 12.5\mu m$, $F_r = 1.2N$, viscosity $\eta = 55\, mPas$ and different speeds.*

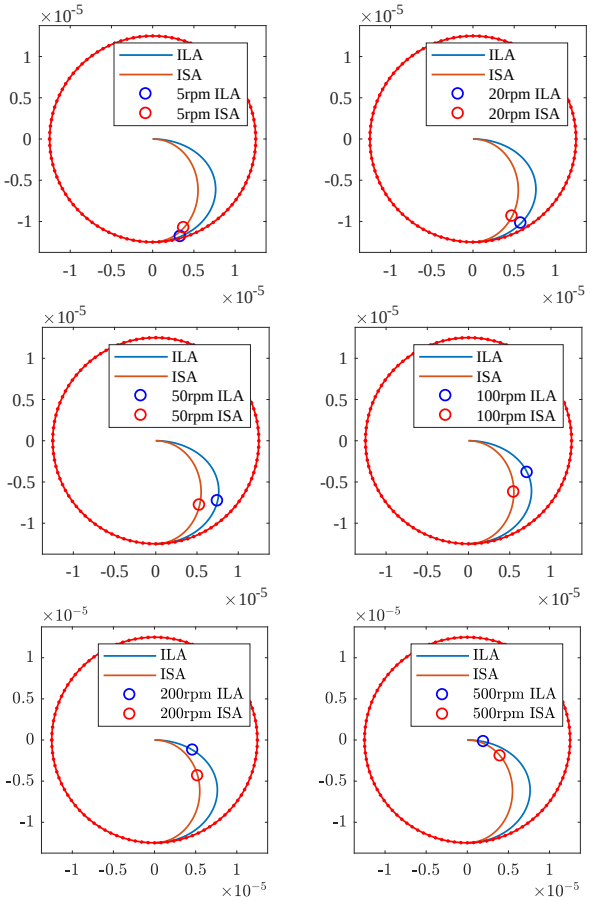

Fig. 2.7: *Shaft trajectory for half Sommerfeld solution, ILA and ISA, mean radial clearance $c = 12.5\mu m$, $F_r = 1.2N$, viscosity $\eta = 55\,mPas$ and different speeds.*

2.4 Friction models

Based on the *Sommerfeld*-number, containing all the important parameters of speed ω, viscosity η, radial clearance c and pressure p, several different models of friction were proposed to describe non dimensional friction values for different domains of applications.

Starting from the equation of *Petroff* for an ideally centred shaft

$$\frac{\mu}{\Psi} = \pi \, So, \tag{2.22}$$

with the relative gap $\Psi = \frac{c}{r_s}$, friction reduces in the case of a semicircular fluid contact, which might happen in the case of cavitation or a lack of lubricant, to

$$\frac{\mu}{\Psi} = \frac{\pi}{2} So. \tag{2.23}$$

An overview of some semi empirical approaches which have been developed to describe the friction for different domains of So is given in [121].

Falz suggested to write for highly loaded bearings at $So < 1$:

$$\frac{\mu}{\Psi} = 3.8 \cdot \sqrt{So}. \tag{2.24}$$

Vogelpohl modified this relation to

$$\frac{\mu}{\Psi} = 3 \cdot \sqrt{So}. \tag{2.25}$$

A formulation by *Leloup* suggests to distinguish between two domains:

$$\frac{\mu}{\Psi} = 0.72 + 2.6 \, So, \qquad So > 0.188 \tag{2.26}$$

$$\frac{\mu}{\Psi} = 2.88 \sqrt{So}, \qquad So < 0.188 \tag{2.27}$$

and *Vogelpohl* suggested the asymptotes

$$\frac{\mu}{\Psi} = \frac{\pi}{2} \, So, \qquad So > 10 \tag{2.28}$$

$$\frac{\mu}{\Psi} = 2\sqrt{So}, \qquad So < 0.1 \tag{2.29}$$

in case of a semicircular bearing. Of course all the theory only applies to the hydrodynamic domain of friction. At low speed solid contact and its friction has to be confronted, such that several new parameters might get involved.

The friction models introduced above were applied using parameters of typical porous journal bearings at radial clearance $c = 12.5\mu m$, fluid viscosity $\eta = 55\,mPas$ and $p = 66kPa$ and compared to a Stribeck friction measurement in Fig. 2.8. Note the wide spread domain of friction values covered by the different isothermal theories and effect of viscous heating, only visible in the measurement, leading to reduced values of viscosity and therefore friction, manifested in the measurement by a decrease of the slope at increasing speed.

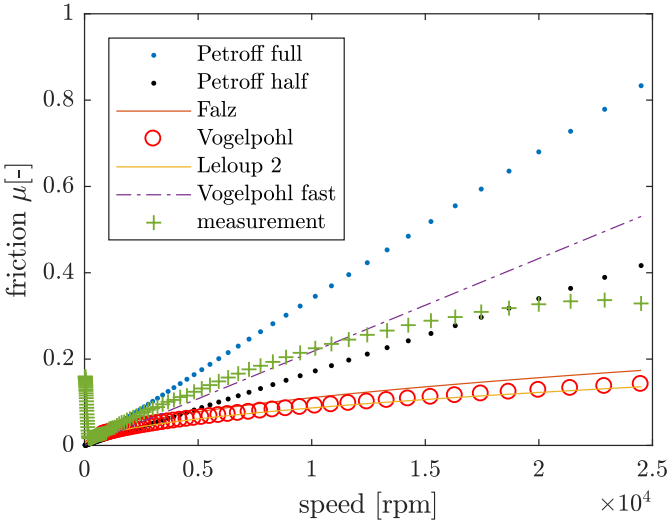

Fig. 2.8: *Different semi-empirical concepts of friction*

In this thesis the range of application at low speed and small Sommerfeld number So is of minor interest.

2.5 Thermal effects

To bring together precise friction measurements and any kind of theoretical or numerical approaches to quantify friction, the important parameter of fluid viscosity η is required. For all common lubrication fluids, it strongly depends on temperature.

The temperature at the fluid gap cannot be determined by any external temperature measurement, because the heat source is located at the fluid gap itself, which will be the hottest part of the bearing. In the hydrodynamic domain of lubrication, viscous heating in the fluid will contribute thermal energy, in other bearing states, solid friction will contribute heating and wear.

The importance of considering thermal effects was shown by an extensive survey by Khonsari [54]. A variation of lubricant viscosity as a function of temperature therefore must be considered in bearing design and analysis. Any model considering a change of lubricant viscosity under variation of lubricant temperature is generally referred to as thermohydrodynamic model.

Chapter 5 is dedicated to determine the temperature in the lubricant film using a combined theoretical, numerical and analytical approach. The thermal model developed thus allows to take into account effects of viscous heating.

2.6 Eccentricity ϵ and relative displacement

Experimental data, measuring the relative displacement between shaft and bearing are scarce and only available for bigger shaft diameters [32, 48, 113, 74, 65, 11], where various types of proximity sensors were used, which cannot be applied on miniature bearings without influencing the sensitive fluid– structure interaction.

In order to represent the situation of an application of interest, the system under test should be exposed to the same boundary conditions. This allows for exploration of the system behavior such as the extremely sensitive transition from mixed to hydrodynamic lubrication and dynamic phenomena, specially the half-frequency whirling. The setup developed is able to capture simultaneously both friction and relative displacement between shaft and bearing under conditions close to applications. It is described and characterized in detail in Sec. 3 and 4.

2.7 Half-frequency whirling

The well-known effect of half-frequency whirling, an instability of a dynamically rigid rotor in hydrodynamic fluid-film bearings, arises from shaft-fluid interaction:

Assuming a no slip boundary condition at the bearing and shaft surface, a shear flow results in case of a rotating shaft. Assuming a simple linear shear flow profile, an average flow speed of half of the shaft surface velocity is found in the fluid gap. The oil flow per unit bearing length at any position therefore only depends on the cross section area, which, illustrated in Fig. 2.9, is bigger at point B than at point A. In the case of an incompressible

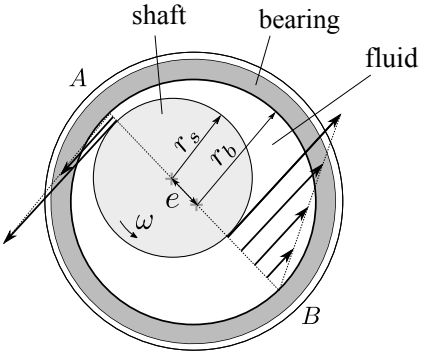

Fig. 2.9: *Illustration of shaft, eccentric bearing and fluid gap.*

fluid, shaft and bearing have to move relative to each other with frequency Ω_w, such that the excessive fluid resulting from the different flows in A and B, can be compensated [45]:

$$\frac{r_s\omega}{2}(c+e) - \frac{r_s\omega}{2}(c-e) = 2\,r_s e\,\Omega_w \tag{2.30}$$

where the radial clearance $c = r_b - r_s$ is given and whirling frequency is Ω_w. The shaft therefore will whirl in the same direction of shaft rotation at a frequency

$$\Omega_w = \frac{\omega}{2}, \tag{2.31}$$

as observed from (2.30). In cases of resonance of the system the instability commences near the first critical speed and occurs with a frequency around

half the rotational speed. For big machines this phenomena might be catastrophic, at small bearings an increase in vibration, noise and friction can be detected. Anyway it is most important to understand and master this effect.

In 1973 Capone [26] presented an analytical model of oil whirl for unloaded journal bearings and confirmed the results by some experimental tests. More data was presented for porous bearings [27]. Experimental evidence was given by Braun [21] and later in [36, 64, 117]. On the side of theory, a lot of work has been done and the reader is referred to [111, 40, 85, 86, 88, 68, 127, 30, 101, 69, 2]. Whirling can be detected

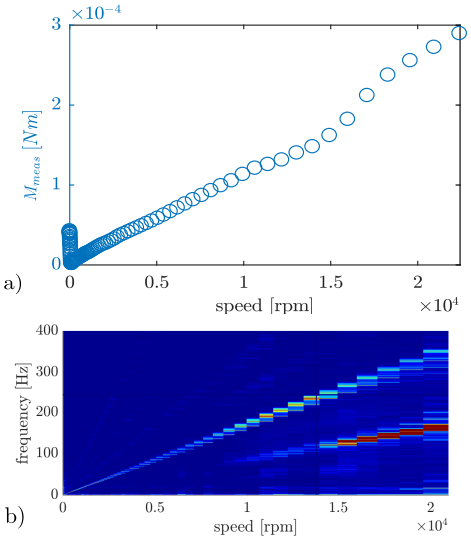

Fig. 2.10: *Simultaneous detection of friction in a) and relative displacement between shaft and bearing in b) reveals whirling displacement data in the frequency domain and an increase in friction at its onset.*

experimentally by capturing the relative displacement between shaft and bearing. A signal analysis in the frequency domain clearly reveals the onset of whirling as shown in Fig. 2.10 b). A simultaneous detection of friction (Fig. 2.10 a)) and relative displacement in b) allows to study also the effect of whirling on friction.

2.8 Taylor-Couette vortex

To analyse the stability of the couette flow in the gap c between rotating shaft and stationary cylinder, dimensionless *Reynolds*-numbers are looked at. The Reynolds number Re relates inertial forces to viscous forces considering the geometry involved. For the situation of the small fluid gap, it is defined as [43]:

$$Re = \frac{u_s c}{\nu}, \tag{2.32}$$

using the shaft surface speed $u_s = \omega r_s$, kinematic viscosity $\nu = \frac{\eta}{\rho}$ and the radial fluid gap c as characteristic length. Taking typical parameters $r_s = 1.5\,mm$, $c = 10\,\mu m$, a dynamic viscosity of $\eta = 0.01\,Pas$ and a density $\rho = 800\,kg/m^3$, we obtain a Reynolds number under variation of the rotational speed of the shaft as shown in Fig. 2.11. According to Taylor

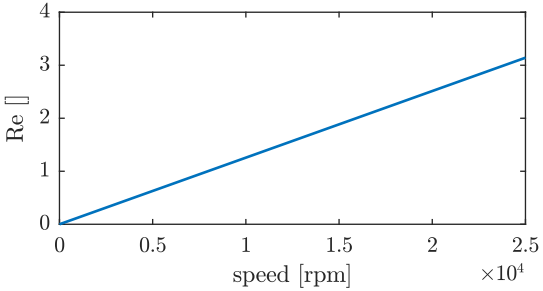

Fig. 2.11: *Reynolds number under variation of speed.*

[112], vortices are expected to develop in case of the Reynolds number passing a critical value Re_c, which is given as

$$Re_c = 41.2 \left(\frac{r_s}{c}\right)^{0.5} \tag{2.33}$$

Taking the parameters given above, a critical value for the Reynolds number is found as $Re_c = 504$. Viscous forces are dominant and even at big gaps, no such vortices have to be expected.

A numerical study on the subject was presented by Magère [70]. Andereck [5] considered inner and outer cylinder to rotate independently from each other in an experimental study. In our case, the outer cylinder, given by the bearing, does not rotate and the system remains at $R_o = 0$ on the stability map given in Fig. 2.12, which indicates a stable Couette flow.

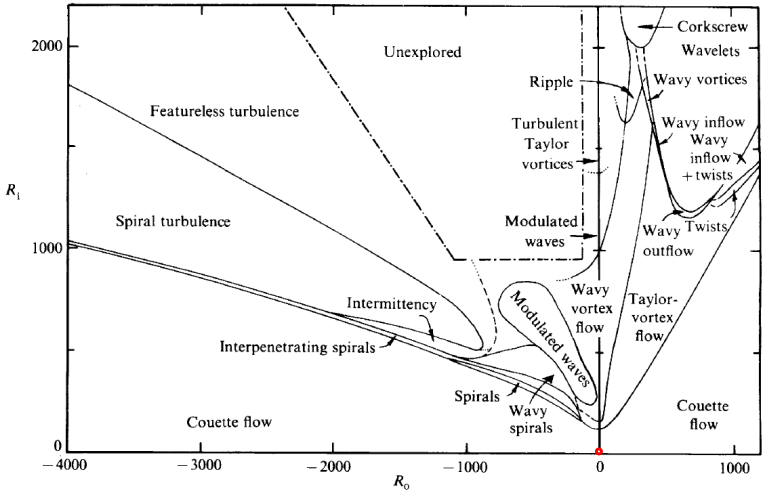

Fig. 2.12: *Flow regimes of rotating concentric cylinders. R_i and R_o are the inner and outer Reynolds numbers. The domain of the experiments are at $R_o = 0$ and $R_{i,max} = 3$, indicated by the red dot. Reprinted from [5] with permission of the Cambridge University Press.*

3 Experimental Setup

The measurement we get when we measure something is not a property of the thing measured.

NIELS BOHR, 1885 -1962

As the information concerning the experimental setup given in the paper publication in Section 4 is limited to the most relevant key factors and also the number of figures are limited, this section is dedicated to the experimental part to provide additional information regarding important details of the device.

Most of the experimental know-how, the technique applied and parts installed, grew during many hours in the lab and after analysis and comparison of nearly 3000 measurements. Parts were modified and changed according to the specific needs. Each modification allowed for more precise measurements, new insight and better understanding of the system behavior.

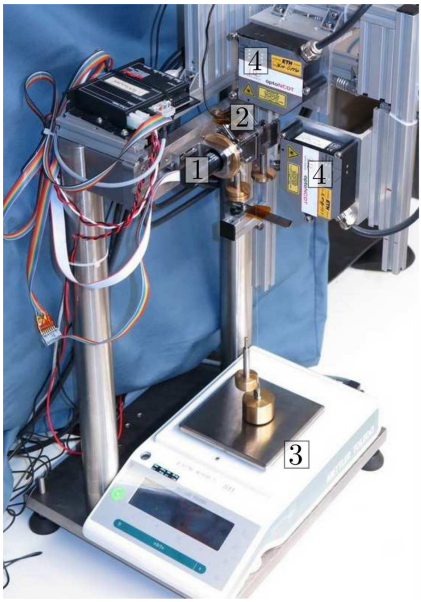

Fig. 3.1: *Overview of the experimental setup consisting of a driving motor (1) to move the shaft in the bearing unit under test (2), a balance (3) to measure friction and two laser systems (4) to capture the relative displacement between shaft and bearing.*

The experimental setup is shown in Fig. 3.1, more details in Fig. 4.1. Similar to application in electric motors, the bearings are pressed into a steel cylinder as shown in Fig. 3.2. After first unsuccessful concepts, the final

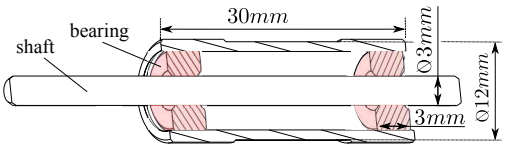

Fig. 3.2: *Cross section of the bearings, pressed into the steel cylinder.*

principle of measuring friction is illustrated in Fig. 3.3. Friction force is transmitted by a wire to the balance and recorded. To calculate the friction torque at the shaft using (3.1), the gravitation force of the weight F_w and geometry r_b, r_w need to be known.

$$M_{meas} = (r_w F_w - r_b F_b) \quad [Nm] \tag{3.1}$$

Considering fabrication imperfections and the relative displacement between shaft and bearing, s_x and s_y, captured by laser triangulation, further increases measurement precision and gives additional insight in the systems behavior and dynamics.

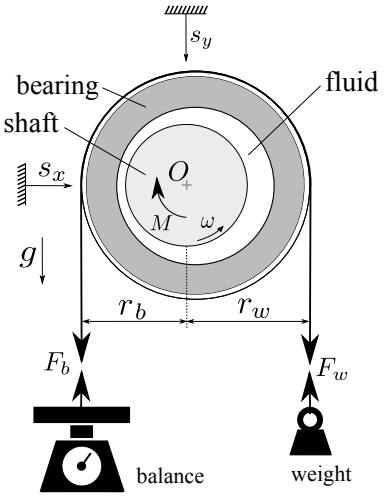

Fig. 3.3: *Sketch of the friction measurement technique*

3.1 Bearing calibration and run in

To obtain optimal bearing performance and low friction, the two bearings to be tested need to be well aligned and provide a smooth surface.

The bearings after the sintering process show geometrical imperfections. Best results are obtained with an alignment and calibration of the bearings in the position and situation of the final application. For good alignment of the bearings under test, a calibration device was built as shown in Fig. 3.4. This device is used to press the bearings into the steel cylinder as shown

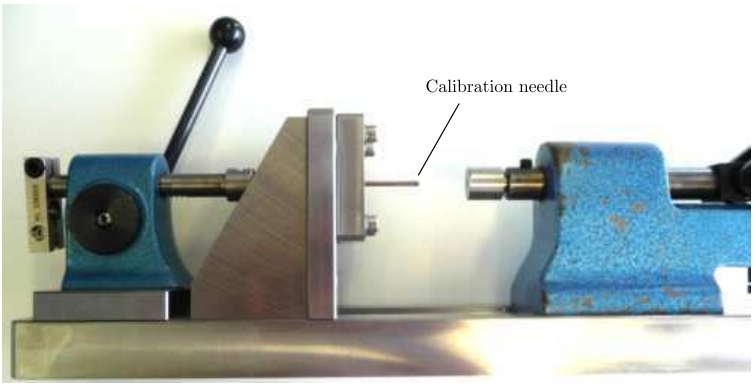

Fig. 3.4: *Bearing alignment and calibration tool, used to press the bearings in the sample cylinders.*

in Fig. 3.2, with a needle inside the bearings. In a clamped position, the needle is moved to smoothen the surface. The influence of the calibration is illustrated in the Stribeck-curves in Fig. 3.5: Moving the needle only four times through the bearing leads to the results of samples B50-1 and B50-3. A long time running-in reduces friction, but still is not good enough.

A lower friction and a transition to the hydrodynamic range at lower speed can be obtained (see sample B50-2 and B50-4 in Fig. 3.5), if the needle is moved many times and the bearing rotated in between. All measurements used and presented were obtained using a multiple calibration method and were run in such that no change in friction was visible between consecutive measurements. The run in behavior of well aligned and calibrated bearings typically is visible in the domain of mixed lubrication as the

sample	calibration	running in time
B50-1	simple	1 min.
B50-2	multiple	1 min.
B50-3	simple	1 hour
B50-4	multiple	1 hour

Tab. 3.1: *Running in and calibration: Overview of samples measured.*

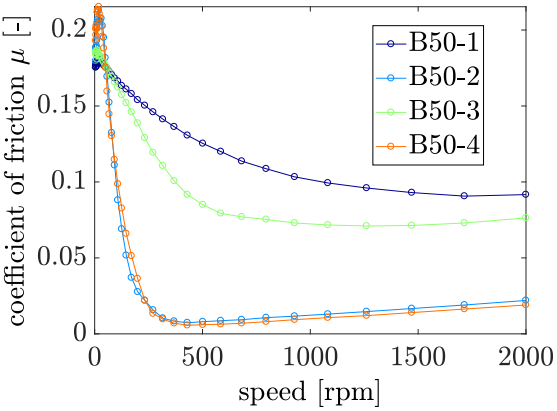

Fig. 3.5: *Stribeck-measurements for different calibration methods*

point of minimum friction is shifted towards lower speed during the run in process. At high speed, in the domain of hydrodynamic lubrication, run in effects are merely visible.

3.2 Driving motor

To perform precise Stribeck friction measurements under variation of speed, the driving motor needs to be driven at a controlled and known speed. Using an electric motor *EC22* by *maxon motor* with a nominal output power of $40\,W$ and a nominal output torque of $20\,mNm$, equipped with encoder and Hall sensors and an *EPOS2P* control in the *velocity control* mode, this task seemed to be mastered for the speed range from 0 to $25000\ rpm$, which is given by the maximum encoder frequency. To go to higher speed, a motor without encoder has to be applied, which brings limitations in precision at low speed. Using some stiff control parameters, the motor can be rotated precisely with constant speed, even at low speed. In case of big radial loading at low speed, the system operates in the domain of solid and mixed lubrication. Due to some remaining compliance at the motor control, effects of slip-stick at the bearing-shaft interface and elasticity in the wires installed to transmit the friction force to the balance, a rotation with a superimposed oscillation was observed.

The installation of a brass disc as shown in Fig. 3.6, providing additional inertia, significantly improved this point and led to more constant rotation at low speed.

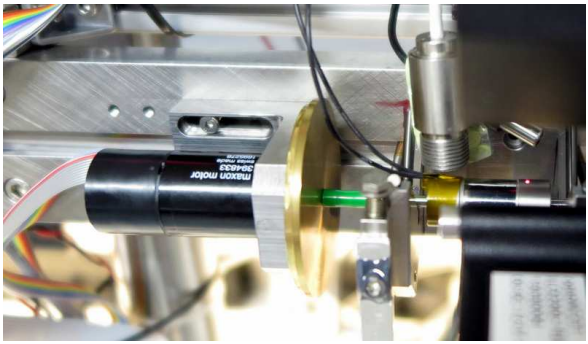

Fig. 3.6: *Driving motor maxon EC22 with encoder and brass disc to increase inertia. This photo was taken during temperature measurements on the cylinder unit. A green polymer tube is applied as elastic coupling between the driving shaft and the shaft of the unit under test.*

3.3 Coupling

The coupling between the driving shaft on the side of the motor and the shaft at the bearing unit, which can be exchanged to alter the radial clearance c, was first solved by an elastic coupling *BSK 1223 03/03* by *Sigerist*[1] as shown in Fig. 3.7. Small offsets between the two shafts, due to the installation of

Fig. 3.7: *Elastic coupling between the two shafts allows for eccentricity and misalignment but was identified to by the origin of heavy vibrations at high speed.*

shafts of different diameter, can be compensated.

A combination of imperfect alignment, coupling imperfections, unbalance and its soft and deformable structure led to problems of vibration at the rotating frequency at moderate and high speed. A successful elastic coupling was achieved using thermally activated shrinking tube, and, more suitable for frequent part exchange, an elastic polyurethane tube [2] from pneumatic technology as can be seen in Fig. 3.6 in green.

[1] http://www.sigerist.ch
[2] www.smcusa.com, art. 0425G-20

3.4 Bearings and support

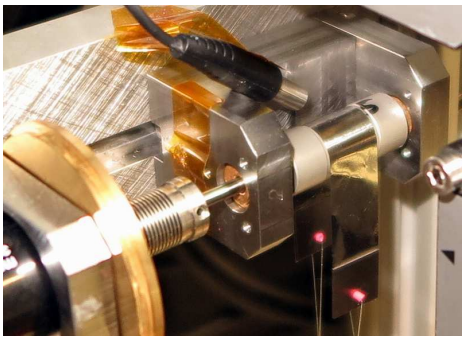

Fig. 3.8: *Support with sintered bearings of the same type as in the bearing unit under test*

To support the rotating shaft of the bearing unit, several possibilities were explored. For example the use of the same type of bearings as the bearings in the cylinder unit under test as shown in Fig. 3.8. But the need of a precise and stiff contact between shaft and support to capture the relative displacement between shaft and bearing by measuring the displacement of the bearing unit, did not allow for any elastic support. The final, successfully implemented concept of at steel prism as shown in Fig. 3.7 and 3.9 (b), provides a very precise and constant position of the shaft. The setup also allows for easy sample exchange without lubricant cross-contamination. To change the bearing unit and the shaft using bearings at the support (Fig. 3.8), the shaft had to be pulled through the bearings in axial direction. Using the concept of the steel prism, the

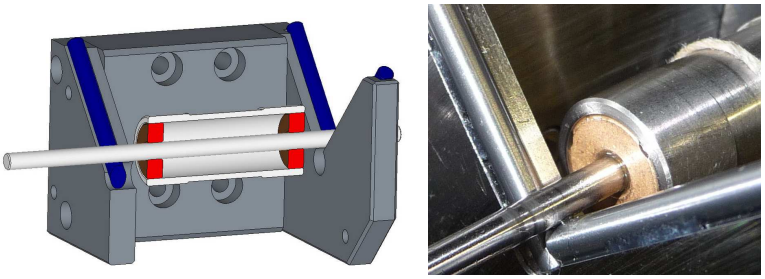

(a) CAD model of the bearing unit with shaft and the support in a semi cross section view.

(b) Close up view of the contact shaft-support.

Fig. 3.9: *Bearing unit and shaft on support*

shaft is simply put on the prism and cleaning is rather simple. Regarding the friction measurements and modelling, with or without the displacement measurement between shaft and bearing, a stable position of the shaft is of fundamental importance, since the model shown in Fig. 3.3 cannot be applied in case of an undefined floating shaft. The friction force between shaft and support is of minor importance, as the driving motor will overcome friction anyway and the measurement is not influenced directly. With regard to frictional heating, low and known friction at this point is preferred. Some lubricant from the bearings typically is found on the shaft as well.

3.5 Cable force transmission

Bearing eccentricity and geometrical deviations from symmetry in the range of μm are relevant and important to be considered as shown in Chapter 4.

The determination of the friction torque on the shaft using (3.1), requires precise knowledge of the active distances r_b and r_w illustrated in Fig. 3.3. Using any arbitrary rope, these parameters depend on the current state of the rope, it's ability to transmit shear forces, which again will depend on the direction of the force, the local position of the rope and many other unknowns.

To avoid any uncertain influences at this point, a precise steel band of $10\mu m$ thickness was applied. The transmission mechanism of the tensile forces from the rope to the cylinder now is assumed to happen symmetrically on both sides, such that after identification of the geometrical deviations (see Chapter 4) the relevant radii r_b and r_w don't depend on the load on the wire, time or other parameters which are not known.

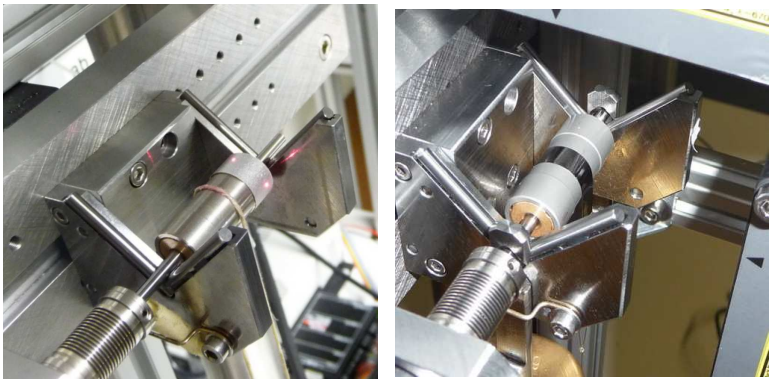

(a) Rope in contact with cylinder (b) Steel band of $10\mu m$ thickness

Fig. 3.10: *Friction force transmission from the cylinder to the balance.*

3.6 Influence of friction at the support

All types of bearings or supports come along with their specific properties with respect to stiffness, induced vibrations and friction, which is directly related to frictional heating. To minimize effects of frictional heating at high speed measurements, additional weights initially installed on the shaft to keep it in contact with the support (see Fig. 3.10 (b)) during measurements of low radial loading, were removed and the friction at the support analyzed and characterized as given in detail in Chapter 5. Considering thermal effects is important, as lubricant viscosity strongly depends on temperature. An exemplary illustration of the FEM solution for the temperature distribution in the device-under-test is given in Fig. 3.11 to show the effect of frictional heating at the support.

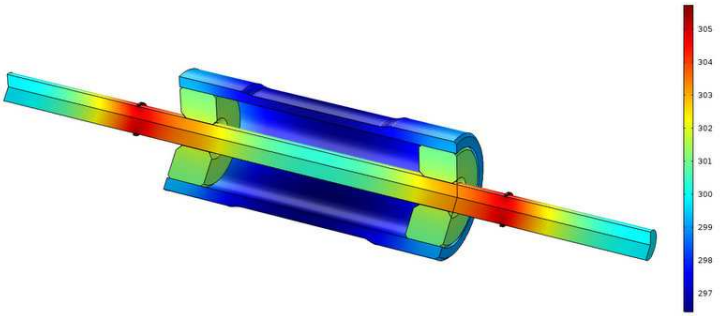

Fig. 3.11: *FEM solution of the temperature distribution. Note the symmetrically modeled heat source at the location of the support, where at the illustrated point in time the hottest temperature occurs.*

3.7 Laser triangulation for displacement measurement

Fig. 3.12: *Laser displacement measuring devices*

The laser displacement-measurement devices *ILD2300LL* by *Micro-Epsilon* were selected to provide optimal results on metallic surfaces. Their distorted measuring spot of $0.4-0.8\,mm$ length was aligned parallel to the axis of the shaft and adjusted on the shaft surface, such that best alignment and measurement precision on the cylinder is guaranteed (Fig. 3.12). Although the system was developed to be applied on metallic surfaces, the shiny machined and reflective outer cylinder surface did not provide precise results. An improvement and very good results were obtained using a sand-blasted surface providing diffuse reflectivity. The differences in surface topography is shown in the SEM images in Fig. 3.13.

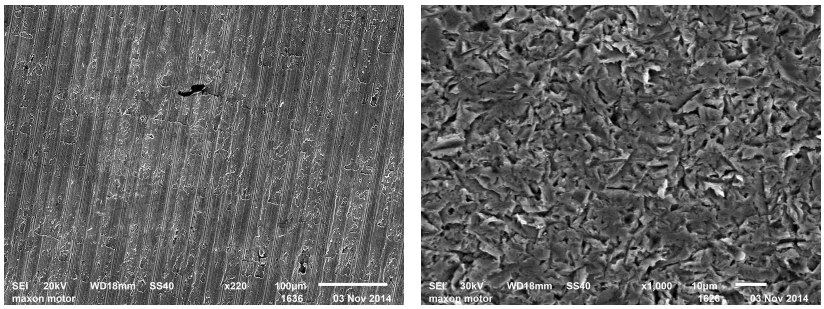

(a) Shiny cylinder surface after machining. (b) Sand blasted steel cylinder surface.

Fig. 3.13: *SEM images of the cylinder surfaces.*

Warm-up behaviour

The laser systems operate with some energy losses which lead to a moderate increase in temperature after startup. This is directly related to a drift in the displacement signal in the range of some μm. All measurements were taken after the equilibrium temperature was reached and no drift in the signal due to heating is registered in the displacement data.

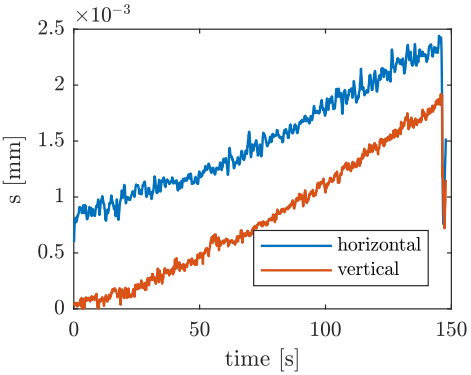

Fig. 3.14: *Laser displacement measurement signal drift during warm up*

Setup-Eigenfrequency

Displacement data analysis in the frequency domain in the form of a *Campell* diagram as given for example in Fig. 2.10, also allows to identify Eigenfrequencies of the mechanical setup, visible in Fig. 3.15, which are easily excited by any background vibration. Using this analysis, the system can easily be modified in stiffness, such that no Eigenfrequency is detected and

eventually interact with the systems dynamic or data acquisition.

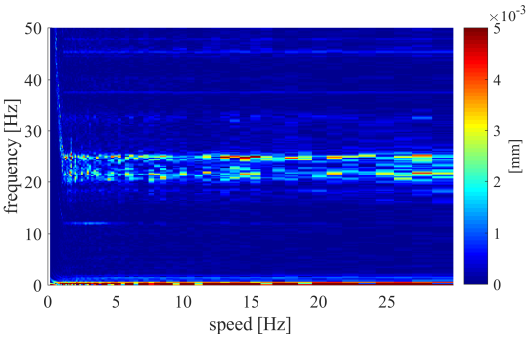

Fig. 3.15: *FFT analysis of displacement data with disconnected shaft.*

Friction and 2D measurements in small journal bearings

4

Published in:
M. Trachsel, R. Pittini, J. Dual, *Friction and 2D position measurements in small journal bearings*, Tribology International 102 (2016) 555-560, ISSN 0301679X. [1]

Measure what is measurable, and make measurable what is not so.

GALILEO GALILEI, 1564-1642

[1] Reprinted from Tribology International, 102, M. Trachsel, R. Pittini, J. Dual, *Friction and 2D position measurements in small journal bearings*, pp. 555-560, (2016), with permission from Elsevier.

Abstract

Shaft position and friction torque as a function of radial loading and rotational speed are important parameters in the theory of lubrication. However, to date values for small bearings taking into account manufacturing deviations are not available. The method described in this work allows precise friction torque and 2D position measurements on small journal bearings under variation of the important parameters: speed, radial loading, lubricant and gap width. If displacement is considered for the friction torque measurement, an improvement in measurement accuracy is achieved when compared to previously reported techniques. Geometrical deviations, which are of high importance in miniature bearings, are identified by two measurements in opposite direction of rotation and corrected.

4.1 Introduction

Small, self-lubricating, porous journal bearings are cheap, robust and widely applied in all kinds of machinery to support a rotating shaft with radial loading. Lubricant is dragged between the two bodies by viscous forces and reduces friction and wear. Depending on speed, gap-width, fluid viscosity, radial loading and other parameters, the shaft will be located at a specific position relative to the bearing.

Friction torque measurements in the range of μNm are extremely sensitive to all kinds of external forces and kinematic constraints which favor or prevent the formation of a fluid film necessary to separate the sliding bodies. Experiments, therefore, should reproduce the common case of unconstrained displacement with a radial load.

To capture the friction torque and measure both friction torque and displacement between the two interacting bodies, one can measure directly at the shaft or alternatively at the bearings. To allow eccentricity measurements with the new method presented in this paper, the shaft is supported in a stiff way. The friction created at the support excludes torque measurements at the shaft and the friction force is captured at the bearings and transmitted by a rope to a precise balance. A similar technique was applied in [130, 128, 56], assuming ideal geometries, which is not sufficient for miniature systems where fabrication imperfections cannot be neglected.

The relative displacement between shaft and bearing and bearing eccentricity are key parameters as was identified by Reynolds in 1886 [98] and integrated into theory for applications by Sommerfeld [105] at the beginning of the last century.

Displacement trajectories were obtained using numerical methods as published in various works: In [100] cavitation phenomena were simulated and in [66] models of porous media compared. Effects of surface roughness and misalignment were simulated in [120]. Turbulence was considered in [133] applying an approximate analytical method. The influence of permeability and an added reservoir was simulated in [12].

Experimental data measuring the relative displacement are scarce and only available for bigger shaft diameters [32, 48, 11, 65], where various types of proximity sensors were used, which cannot be applied on miniature bearings without influencing the fluid-structure interaction.

A domain of particular interest is the transition from mixed to hydrody-

namic lubrication analytically discussed in [47] for hydrodynamic bearings. The new method presented here is able to give additional insight and understanding.

To determine the friction torque at the shaft, the horizontal component of bearing eccentricity is considered in this work, presenting a novelty for this type of measurements with higher friction values at the points of high eccentricity. Geometrical deviations are identified by two measurements in opposite direction of rotation and considered in the evaluation of the friction torque.

With increasing speed, hydrodynamic forces center the shaft in the bearing: unstable domains might be reached and the well known whirling at about half the speed of rotation might occur [46, 2, 30, 68]. The setup allows dynamic phenomena to be investigated and whirling can be detected in the displacement data as shown in section 4.4.1.

4.2 Experimental setup

A steel shaft (DIN 1.2210) of $3mm$ nominal diameter is driven at controlled speed by an electric motor (*maxon EC-22* with encoder) and is supported on two V-shaped prisms built of hardened steel as shown in Fig. 4.1. To prevent it from lifting-off the support, the shaft is pulled down by two weights and kept in place in case of low radial loading. The sintered bronze bearings to

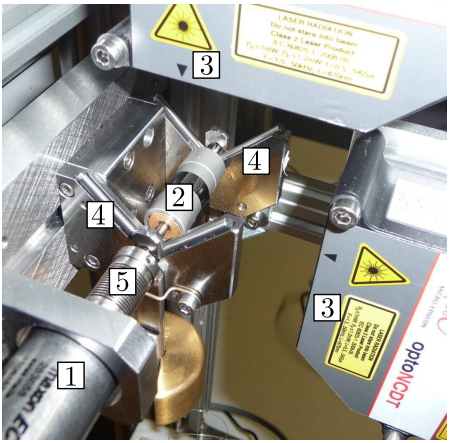

Fig. 4.1: *Measurement hardware: 1: electric motor, 2: steel cylinder with bearings, 3: laser devices, 4: prisms to support shaft, 5: flexible coupling.*

be measured are aligned on a steel needle of $3.003mm$ diameter and pressed in a steel cylinder. The needle is moved axially in the bearing to smooth the surface.

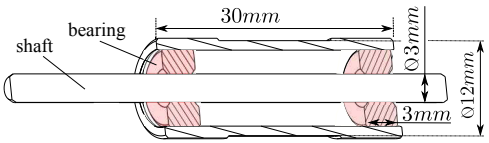

Fig. 4.2: *Cross-section of shaft and bearing unit.*

4.2.1 Friction torque measurement

The friction force is transmitted to a balance (METTLER TOLERO, *Pharmacy Line PHS*, $PH403S$, $1mg$ resolution) by a rope which is connected to a steel band having a $180°$ contact angle at the cylinder (Fig. 4.3). An internal calibration routine of the balance provides high accuracy and reproducibility. The radial load is altered by a variation of the weight F_w on the other side of the cylinder. The measured friction torque in this con-

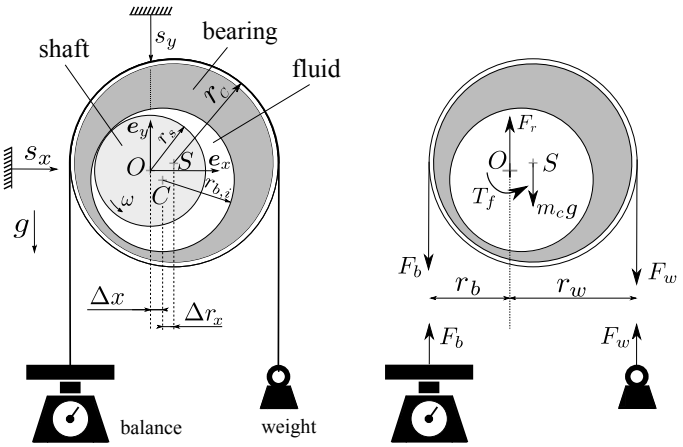

Fig. 4.3: *Principle of the Stribeck-measurement: Geometry and kinematics, reduction of the forces to the center of the shaft. Bearing imperfections and clearance $c = r_{b,i} - r_s$ are not to scale for sake of clarity. O: center of the shaft, C: center of journal bearing, S: center of outer cylinder. ω is shown in ccw direction.*

figuration is a function of the distances r_b and r_w of the forces F_b and F_w from the axis of rotation O. These are very important to know precisely. Therefore a stainless steel band of $10\mu m$ thickness is used in contact with the cylinder. A rope in contact with the cylinder as used by other authors [130, 56] was applied first but did not allow satisfactory precision and reproducibility because any arbitrary deformation of the rope results in imprecise measurements.

The nominal resolution of $50nNm$ is further increased by taking average values for at least 6 seconds at every speed. The signal of the balance is

digitally transmitted to the PC using $RS232$ and saved at the same sampling frequency of $10Hz$ as the laser measurements. Fig. 4.4 gives a schematic overview of the setup.

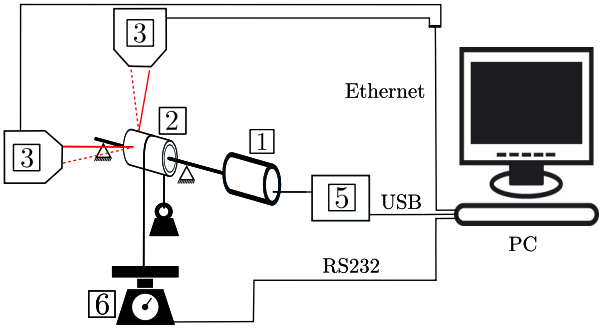

Fig. 4.4: *Schematic overview of the implemented system consisting of 1: electric motor $EC - 22$, 2: bearing unit, 3: laser devices $ILD2300LL$, 5: $EPOS2P$ motor control, 6: $Mettler\ Tolero, PH403S$.*

4.2.2 Displacement measurement

Two laser triangulation systems *ILD2300LL* by *Micro-Epsilon* are used to capture the displacement of the bearings in horizontal s_x and vertical s_y direction. Having a measuring range of $10mm$ the lasers are working at a wavelength of $670nm$. A distorted measuring spot between $120 \times 405\mu m$ and $125 \times 835\mu m$ is used and oriented with the longer dimension in the direction of rotation, positioned at the center of the shaft. Good results are obtained on a diffuse, sand-blasted steel surface. The influence of the cylinder curvature r_c on the displacement measurement is neglected: Assuming $s_x = 10\mu m$, an error in $s_y = r_c - \sqrt{r_c^2 - s_x^2} = 8nm$ is two orders of magnitude smaller than the data of interest. The displacement data were lowpass filtered by the lasersytem and digitally transmitted at $1.5kHz$ to the PC. An average value is taken over 150 samples and data are registered at $10Hz$. Data acquisition is controlled by *LabVIEW*. For analysis in the frequency domain non averaged data are used and a Hanning-window filter was applied. The noise of the signal is irrelevant, as can be observed in the

frequency domain shown Fig. 4.10.

Data shown here were obtained with a nominal $7\mu m$ radial gap, variable speed and some discrete radial loadings using porous journal bearings *Sint-B 50* with 20% porosity which got impregnated in vacuum with the non Newtonian lubricant *ISOFLEX PDB 38 CX 2000* by Klüber. Lubricant viscosity was measured using a cone-plate rotational measurement [2]and is shown in Fig. 4.5.

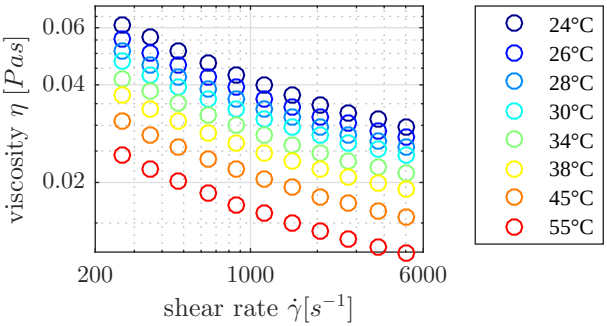

Fig. 4.5: *CX 2000 lubricant viscosity*

4.3 Method used to evaluate friction torque

To precisely capture the changes in displacement and friction torque at low speed, a logarithmic scaling of the speed steps is used. Data are recorded such that at least 6 complete turns of the shaft are performed at each speed to allow averaging out the effects of fluctuations over one revolution e.g. shaft imperfections. At higher speed, for every speed-step, data are registered for 6 seconds.

[2] *Paar Physica UDS200*

shaft diameter $2r_s$	$2.989mm$
bearing diameter $2r_{b,i}$	$3.003mm$
bearing clearance c	$7\mu m$
shaft speed ω	$5 - 20000rpm$
radial loading F_r	$0.25 - 10N$

Tab. 4.1: *Dimensions and parameter range*

4.3.1 Geometry and deviations

Using a contact, precision geometry measurement (*Schneider SKM250*) performed outside the setup, eccentricities between outer cylinder and inner bearing bore surface $|\boldsymbol{r}_{CS}|$ up to $20\mu m$ were detected. The horizontal component $\Delta r_x = \boldsymbol{r}_{CS} \cdot \boldsymbol{e}_x$ (see Fig. 4.3) is considered in the friction torque measurement as described in section 4.3.2. During the measurement the bearing is either in contact with the shaft at low speed or supported by the fluid and free to move within the bearing clearance $c = r_{b,i} - r_s$. The horizontal displacement of the bearing unit $\Delta x = \boldsymbol{r}_{OC} \cdot \boldsymbol{e}_x$ is calculated from the captured data s_x.

The friction torque at the shaft, T_f, is calculated from the data captured by the balance F_b, the known weight F_w, the variable distance r_b on the side of the balance and on the side of the weight r_w, considering the horizontal components of deviations Δr_x and the horizontal displacement Δx (see Fig. 4.3).

$$r_b = r_c - \Delta r_x - \Delta x \tag{4.1}$$

$$r_w = r_c + \Delta r_x + \Delta x \tag{4.2}$$

Knowing Δr_x and Δx, the torque induced by gravity T_g is considered as well in this quasi-static analysis. Gravity is assumed to act at the center S of the steel cylinder the bearings are pressed-in, which is heavier than the bearings. Depending on deviations Δr_x and horizontal displacement Δx the force of gravity $m_c g$ leads to an additional torque T_g which is considered in the calculation of the friction torque T_f to act at the center of the shaft O:

$$T_g = -m_c g \, \boldsymbol{r}_{OS} \times \boldsymbol{e}_y = m_c g \, (\Delta x + \Delta r_x) \tag{4.3}$$

The friction torque is measured for ccw and cw direction:

$$T_{f,ccw} = r_w\ F_w - r_b\ F_{b,ccw} + (\Delta x + \Delta r_x)\ m_c g \tag{4.4}$$

$$T_{f,cw} = -r_w\ F_w + r_b\ F_{b,cw} - (\Delta x + \Delta r_x)\ m_c g \tag{4.5}$$

4.3.2 Calibration by geometry identification

At high speed in the hydrodynamic domain, friction is not expected to show any dependence on the direction of rotation. According to theory [108] and measurements (Fig. 4.9), the shaft is well centered in the bearing and influences of horizontal displacement Δx are minimized.

The friction torque T_f according to (4.4) and (4.5) is written with corrected geometry (and $\Delta x = 0$):

$$r_b = r_c - \Delta r_x \tag{4.6}$$

$$r_w = r_c + \Delta r_x \tag{4.7}$$

and set equal for both directions of rotation at maximum speed. Equating (4.4) and (4.5) using (4.6) and (4.7), the geometrical deviation Δr_x is obtained:

$$\Delta r_x = r_c \cdot \frac{2F_w - F_{b,ccw} - F_{b,cw}}{2F_w + F_{b,ccw} + F_{b,cw} + 2m_c g}. \tag{4.8}$$

The effect and importance of the calibration procedure and consideration of Δr_x and the horizontal displacement Δx is illustrated in Fig. 4.6 with two measurements at a radial loading of $F_r = 0.33N$, performed over a speed profile up to $4000rpm$. A value of $\Delta r_x = 17.31\mu m$ was found. Not considering Δr_x leads to wrong results and even negative friction. The displacement values Δx and the vertical displacement are shown in Fig. 4.9(a).

In accordance with theory presented in [46] taking into account porosity and numerical investigations [100, 66, 120, 133, 12], in the case of low radial loading F_r the shaft is in contact with the bearing surface at low speed to lift off at some specific speed. This was identified by the simultaneous friction torque measurement to occur at (or in some cases slightly before) the speed of minimum friction.

The trajectories of relative displacement are centered in the available displacement range at top speed, as predicted by theory and experimentally verified. In the case of high radial loading F_r, of course this is not correct because fluid forces can not completely lift of the bearing.

The calibration method should be applied in stable domains, which can be identified by an analysis in the frequency-domain as shown in section 4.4.1. Whirling was identified to come along with an increase in friction which might result in imprecise values of Δr_x in case of asymmetric appearance in cw and ccw direction.

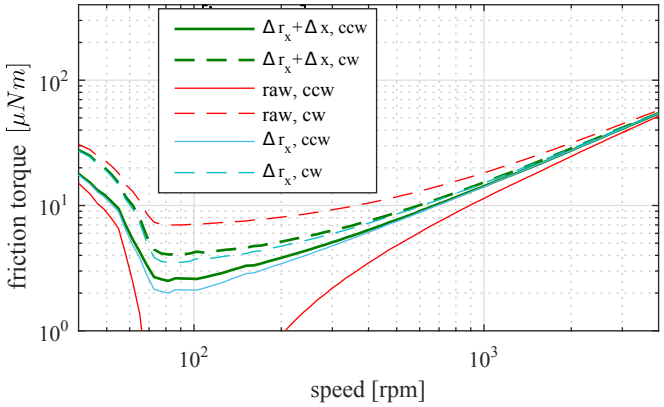

Fig. 4.6: *Effect of considering Δr_x and Δx for determining the friction torque. Note the strong influence of bearing imperfection $\Delta r_x = 17.31\mu m$ compared to the unprocessed raw data. The additional consideration of the horizontal displacement Δx during the measurement results in a slight increase in the friction torque at high eccentricity. Measurements in cw direction show higher friction at low speed, see Sec. 4.3.4 for details.*

Verification of eccentricity deviation

To verify the strong influences of the imperfections Δr_x, the bearing unit was rotated in 90° steps. At each position two measurements were taken. The resulting values Δr_x obtained from the calibration process according to (4.8) vary sinusoidally with the rotation angle of the bearing unit, which again proves their existence and verifies the calibration process.

4.3.3 Friction torque and gravity

The effect of gravity on the cylinder unit influences the total radial load and is considered in (4.9). Influence on the friction torque T_g according to (4.3) is shown in Fig. 4.7. Deviations Δr_x induce a torque T_g independent on

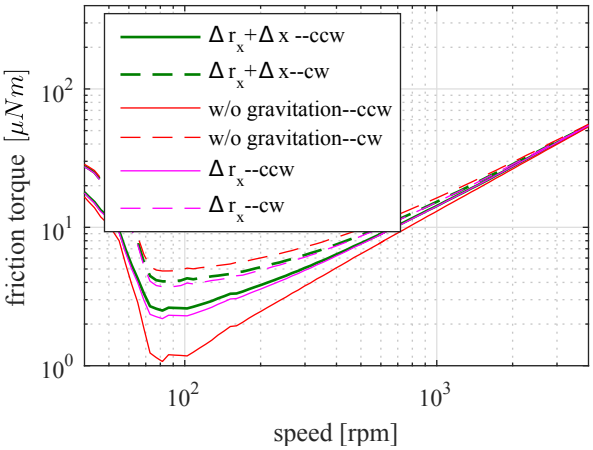

Fig. 4.7: *Effect of considering influence of gravity on cylinder unit for cw and ccw direction, $\Delta r_x = 17.31\mu m$, $F_r = 0.33N$. Δx is shown in Fig. 4.9(a). Not considering effects of gravity changes the friction torque measured depending on Δr_x and Δx.*

the direction of rotation and therefore, in this case, to a reduction in cw direction and an increase in ccw direction. Considering the torque induced by the variable displacement Δx leads to an increase of friction at high eccentricity for both cw and ccw direction.

4.3.4 Influence of the direction of rotation

The force F_w on the side of the weight is constant during the measurement. The force F_b on the side of the balance, in addition, has to counterbalance the force induced by the friction torque. Depending on the direction of rotation this is either added or subtracted. Note that the horizontal component of the radial load is zero, because of the geometry of the setup.

The overall radial loading F_r therefore depends on both the friction force and direction of rotation. The total radial load F_r can be expressed by:

$$F_r = F_w + F_b + m_c g. \tag{4.9}$$

At the transition from mixed to hydrodynamic lubrication, a higher friction was observed for cw direction. In addition to the effect of a higher radial load in cw direction due to friction, this could be explained by the fact that in ccw direction the cylinder can easily move up, lift the weight and a fluid film is built. In cw direction however, the rope is held fixed to the balance resulting in higher friction torque at the transition to the hydrodynamic domain and a shift of minimum friction towards higher speed can be noted in Fig. 4.7 and 4.8.

4.4 Measurements

Applying the method of calibration described in section 4.3.2 and considering the horizontal displacement Δx, various radial loadings F_r were applied. The measurements shown in Fig. 4.8 reveal the friction torque which, at high speed only slightly depends on the load applied as it is purely hydrodynamic. At low speed, the friction torque shows a significant dependence on the

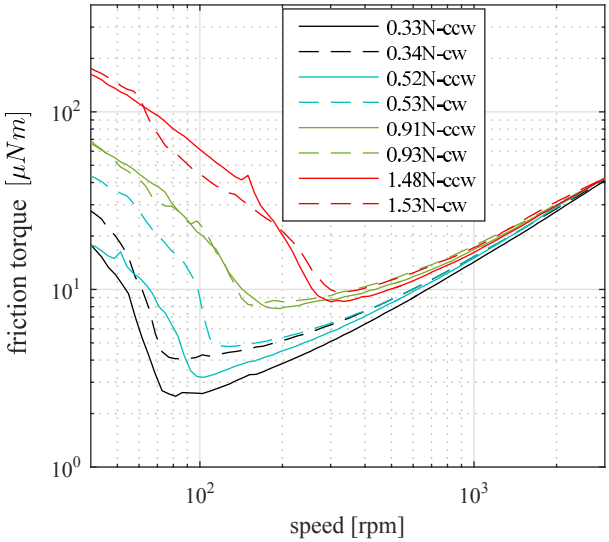

Fig. 4.8: *Friction torque measurements for different average radial loadings F_r and cw and ccw direction of rotation.*

radial load. Points of minimum friction are shifted towards higher speed with increasing load because higher viscous forces are needed to create the load carrying pressure needed for the transition to the hydrodynamic regime.

The corresponding displacement data are shown in Fig. 4.9. The curves are placed into the center at maximum speed and show the lift-off to occur at the points of minimum friction. At high radial load (Fig. 4.9(d)) the bearing remains centered at the bottom and merely lifts.

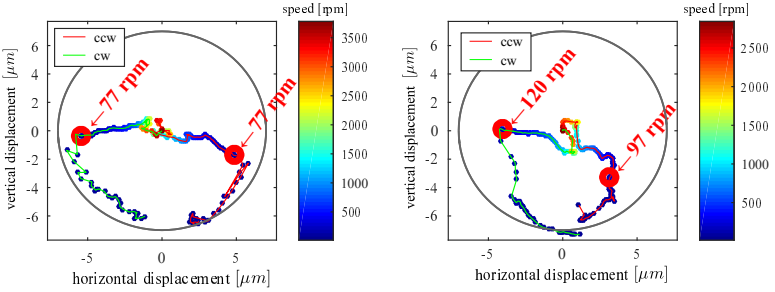

(a) Bearing center locus, $F_r = 0.33N$

(b) Bearing center locus, $F_r = 0.52N$

(c) Bearing center locus, $F_r = 0.91N$

(d) Bearing center locus, $F_r = 1.45N$

Fig. 4.9: *Displacement trajectories for cw and ccw direction of rotation and different radial loading F_r. Points of minimum friction (Fig. 4.8) are indicated in red.*

4.4.1 Dynamic effects

Due to the stiff support of the shaft, the dynamic fluid-structure interaction can be examined by an analysis in the frequency domain. At low radial loading the well known half frequency whirling [46, 2, 30, 68, 108] can be detected to start at some specific critical speed. Transforming the displacement signal for each speed-step into the frequency domain a representation in the Campell-diagram reveals important information about the system dynamics as vibration frequencies are identified: first and half-harmonics being noted in Fig. 4.10.

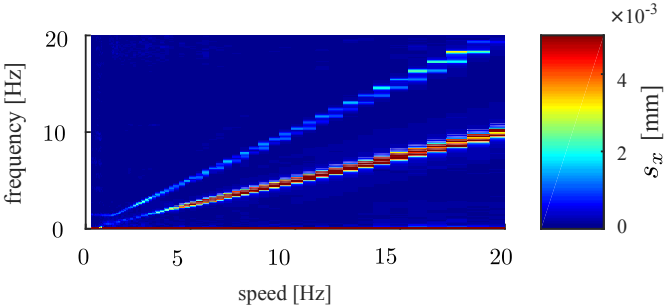

Fig. 4.10: *Campell-diagram of displacement in horizontal direction revealing first harmonic and half-frequency whirling. (ccw-measurement, $F_r = 0.25N$)*

4.5 Conclusions and discussion

A new setup was developed to study the performance of small bearings. Simultaneous detection of friction torque and displacement improves the precision of friction data and leads to a profound understanding of the fluid-structure interaction, which allows further optimization of parts involved according to specific applications.

The calibration procedure allows to measure standard bearings with arbitrary deviations from perfect geometry. The high sensitivity of the device allows for identification of small imperfections/phenomena which translate into large effects on the friction torque in the domain of mixed lubrication, such as run-in phenomena, geometrical deviations, surface structure and lubricant properties.

The laser measurements show the relative displacement between shaft and bearings under variation of speed. Points of minimum friction can be identified to be located close to the location of lift off in the case of low radial loading and data can be used to determine missing parameters for bearing analysis, such as permeability and coefficients of slip. The curves in Fig. 4.9 are not in perfect symmetry for the cw and ccw direction, which shows the strong sensitivity of the motion on the parameters in the region of minimum friction.

Due to the high flexibility of the system, all kinds of small bearings can be measured under different sets of parameters.

Thermal model 5

Published in:
M. Trachsel, R. Pittini, J. Dual. *A combined approach to study and model the effect of viscous heating in small porous, self lubricating journal bearings*, Tribology International 116C (2017) pp. 199-207, ISSN 0301679X.[1]

Thermodynamics is a funny subject. The first time you go through it, you don't understand it at all. The second time you go through it, you think you understand it, except for one or two small points. The third time you go through it, you know you don't understand it, but by that time you are so used to it, it doesn't bother you any more.

Arnold Sommerfeld, 1868-1951

[1]Reprinted from Tribology International, 116c, M. Trachsel, R. Pittini, J. Dual, *A combined approach to study and model the effect of viscous heating in small porous, self lubricating journal bearings*, pp. 199-207, (2017), with permission from Elsevier.

Abstract

Friction torque is one of the key performance parameters of journal bearings and it is strongly influenced by the temperature dependent lubricant viscosity. In small bearings, this temperature cannot be measured directly. Therefore, a combined experimental, numerical and analytical approach is used to determine the lubricant temperature for the application in instationary Stribeck measurements. The thermal model proposed returns temperature and it is verified by FE simulations. Based on friction measurements with a Newtonian reference oil and friction models, the change in temperature is detected in a second independent way as viscosity changes with temperature. Results are presented in function of speed, clearances and for both porous and nonporous bearings. Half-frequency whirling and its effect on friction was detected.

5.1 Introduction

Small, self-lubricating, porous journal bearings are widely used in all kind of different applications providing lifetime lubrication via the lubricant stored in the porous substrate. Lubricant dynamic viscosity η is an important parameter in bearing technology and key performance parameters such as load-carrying capacity, eccentricity ratio and friction depend on it as well as the established Sommerfeld-number: $So = \left(\frac{d_s/2}{c}\right)^2 \frac{\eta\omega}{p}$, a parameter to characterize the bearing state. Most importantly, dynamic viscosity η is strongly temperature dependent for most lubrication fluids. For accurate bearing performance analysis, the frictional heating and change in fluid temperature has to be considered which is generally referred to as a thermohydrodynamic (THD) model.

Several efforts in experimental quantification of lubricant temperature gave important insights into bearing performance. Knowing about the significance of thermal effects, Dubois and Ocvirk [32] applied thermocouples to their setup in 1953 using a shaft of $34.9mm$ in diameter. Similar to Tonnesen [113], working on a shaft diameter of $100mm$, they were able to capture additional data of pressure and shaft eccentricity to derive analytical expressions describing the bearing performance. Yong-Xin et al. [130] applied a thermistor $2mm$ from the bearing surface to measure the temperature during the experiments performed at steady-state. Using thermocouples, Qiu [95] found the temperature around the bearing not to depend on the circumferential angle at low radial loading. With the focus on start-up friction Bouyer and Fillon [20] identified friction to depend on the oil inlet temperature on externally pressurized bearings with $100mm$ in diameter. Temperature was measured using thermocouples. Mitsui [73] performed measurements at steady-state using a shaft diameter of $50mm$ and developed an analytical method to determine the temperature in the fluid film. In this case temperature was measured using thermocouples. The results revealed temperature gradients inside the bearing, which decrease as the eccentricity is reduced. In an externally pressurized bearing system Adatepe et al. [1] experimentally determined the fluid temperature applying thermocouples at the oil outlet.

To bring together measurements and theory, experimental data were compared to THD theory considering thermal expansion in [17]. Neacsu et al. [87] performed experiments to compare the simulated steady-state in

porous journal bearings. Temperature was measured using thermocouples at $1mm$ depth from the bearing surface to calculate the lubricant viscosity. More recently, a significant effort was spent in numerical work. A THD analysis considering effects of coupled stress was presented by Wang et al. [124]. Boubendir et al. [19] considered flow in porous media and obtained temperature distribution and isothermal lines for specific parameters. Lin and Wang [67] stated the significance of considering thermal effects in modeling and performed a THD analysis for non-Newtonian lubricants taking into account cavitation, however, no experimental results were presented.

To analytically access transient thermal problems, several lumped parameter thermal networks can be found in related work: A thermal network model was used by Perez and Kassakian [89] for high speed synchronous machines. Wu and Tan [125] modeled a spindle-bearing system and a thermal model for enclosed electric motors was presented by Kylander [63]. A thermal model for steady-state and transient solution was given by Mellor et al. [71] and Dikmen [31].

For small self-lubricating porous journal bearings, it is practically impossible to install any sensors close to the relevant fluid gap, because any modification would influence the fluid-structure interaction as well as the geometry of the bearings which typically are press-mounted, in this case as a pair into a steel cylinder (Fig. 6.2). Anyway, it is impossible to accu-

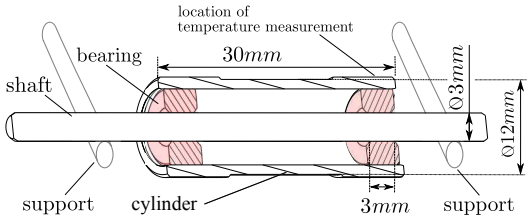

Fig. 5.1: *Cross section of the bearings pressed in a steel cylinder and rotating shaft.*

rately measure the temperature of the fluid in the gap of typically some μm thickness. Therefore, it is impossible to distinguish effects reducing friction which might be due to viscous heating [107], shear-thinning [28], surface slip [106, 91] and influence of the porous media at the fluid-structure interface [8, 120, 100] or cavitation [100, 87, 123].

The methodology and thermal model described in this work was de-

veloped and optimized to provide precise values of fluid temperature for time-varying friction measurements on small journal bearings. We use the setup described in [117] taking into account the ambient laboratory temperature and the friction measured. A similar friction measurement technique was used by Kim et al. [56]. The absence of an in- and outgoing oil-flow restricts the heat transport away from the fluid to heat conduction through shaft and bearings. These heat transport phenomena can be simulated accurately. Convective heat transfer to the ambient air was considered and identified with temperature measurements which were performed on the outer cylinder surface at the axial position of a bearing (Fig. 5.1) in the hydrodynamic domain of lubrication at steady state and different speeds to increase measurement accuracy.

A FE-model was used to determine the temperature at the fluid-gap using heating power $\dot{Q}_f$ calculated from the friction measurements and assigned as the heat source. These values were used to identify parameters of the model and to verify it.

The application of a temperature sensitive Newtonian viscosity standard works as an indirect determination of the fluid temperature via the friction torque measured precisely [117]. The THD-model therefore was verified by two independent approaches. Effects of the porous bearing material on the friction torque were considered and verified by measurements using non-porous bearings.

Simultaneous detection of 2D relative displacement between shaft and bearing using laser triangulation reveal the well known half-frequency whirl whose onset depends on the radial loading, fluid gap, bearing porosity and fluid viscosity and is also seen in an increase in friction.

5.2 Experimental setup

The apparatus used to measure bearing friction is illustrated in Figs. 5.1 and 5.2 and was described in detail in [117]. Two bronze bearings (porous type $B50$ with 20% porosity and non-porous) were pressed into a steel cylinder as shown in Fig. 5.1. A shaft of $3mm$ nominal diameter d_s is driven by an electric motor at controlled speed ω, the fluid gap c can be varied using shafts of different diameters. A radial load F_r is defined by a variable weight F_w and friction is transmitted by rope to a balance and recorded. The shaft is supported on a steel prism to provide a stiff contact and constant friction.

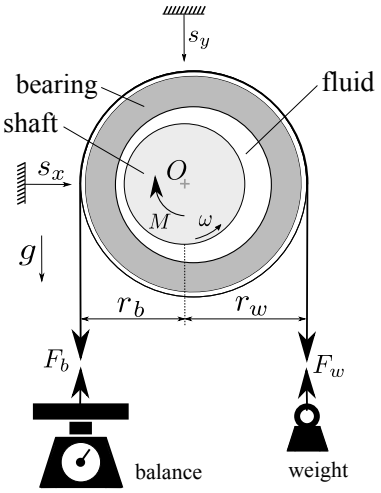

Fig. 5.2: *Friction measurement principle: rotating shaft, bearing unit, counterweight to define the radial loading and a balance to capture friction. Displacement s_x, s_y between shaft and bearing is captured using a laser triangulation sensor. See [117] for details.*

The friction torque $M_{meas}(\omega)$ with respect to the center of the shaft O is calculated using the tensile forces F_b on the side of the balance and F_w on the side of the weight. Fabrication imperfections were identified by two measurements in opposite direction of rotation and corrected, horizontal displacement s_x between shaft and bearing is captured by laser triangulation and considered for the calculation of the friction torque. A nominal resolution of $50nNm$ can be obtained. The frictional heating power $\dot{Q}_f$ is calculated as a function of time while varying ω for the illustrated case of ccw rotation:

$$\dot{Q}_f = M_{meas} \cdot \omega = (r_w F_w - r_b F_b) \cdot \omega \ \ [W] \tag{5.1}$$

A typical friction measurement performed over 100 discrete speed steps up to $24500\ rpm$ is plotted versus time in Fig. 5.3 a). The speed profile was chosen such that logarithmic speed steps are taken and at least three revolutions at each step are performed at low speed to average effects of shaft

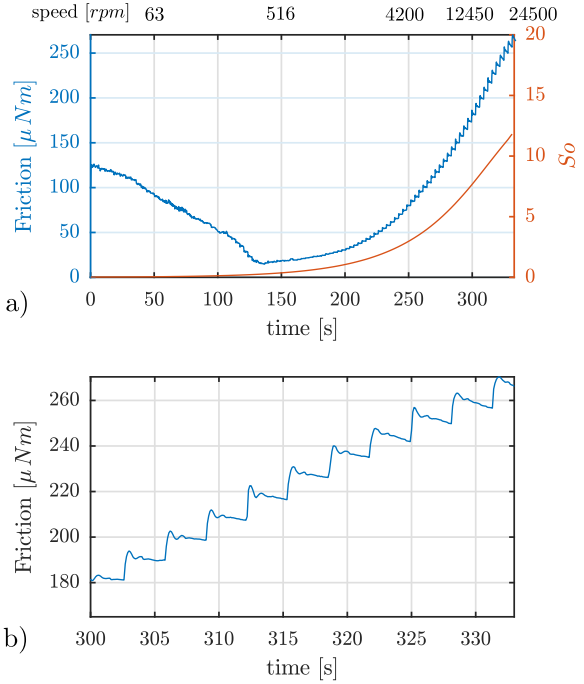

Fig. 5.3: *Friction measurement data for one bearing of a typical Stribeck measurement based on a speed ramp up to* $24500rpm$ *of discrete speed steps, showing a gradual decrease in friction after each step due to a reduction of fluid viscosity* η*. Radial clearance* $c = 17.5\mu m$*,* $F_r = 1.09N$*, fluid: Cannon N35 a) Friction measurement and Sommerfeld number* So*, b) Zoom in the speed range* $12450 - 24500rpm$*.*

inhomogeneities. The application of Newtonian viscosity standard oil [2] *N35* clearly shows the time depending decrease of friction in the hydrodynamic domain due to viscous losses heating up the lubricant and thus reducing its viscosity (Fig. 5.3b)). Viscosity values $\eta(T)$ of the fluid applied are given in Fig. 5.4.

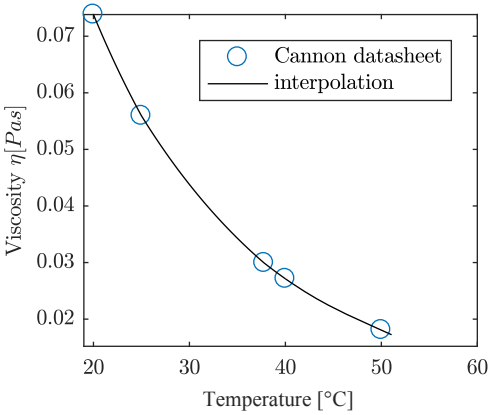

Fig. 5.4: *Viscosity values of CANNON $N35$ viscosity standard.*

Using the known motor torque constant $k_m = 3.74\ [mNm/A]$ and measured values of motor current at constant speed, the friction of the shaft on the support (Fig. 5.5) was identified to be of dry friction type and providing a friction torque at the shaft M_s depending on the radial load F_r:

$$M_s(F_r) = (70.8\ F_r + 162.8) \cdot 10^{-6}\,[Nm] \tag{5.2}$$

Considering the reaction principle at the contact, half of the friction power is assumed to go to the shaft and is considered as additional heat input in the two models built:

$$\dot{Q}_{sup} = 0.5\, M_s \cdot \omega \tag{5.3}$$

[2] www.cannoninstrument.com

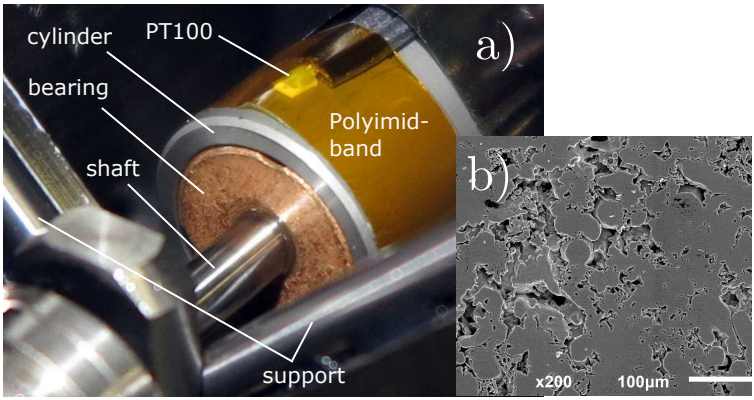

Fig. 5.5: *a) Temperature measurement on the cylinder surface using $PT100$ and IR-measurement on the Polyimid-band. The rotating shaft is supported on a steel prism [117]. b) SEM image of the porous bearing inner surface.*

5.3 Modeling temperature distribution and heat transfer

As the temperature distribution in the bearing is important and difficult to measure, a combined approach of temperature and friction measurement in combination with FEM and modeling of friction was chosen.

5.3.1 Boundary conditions

The heat flux from the uncovered outer part of the rotating shaft to the surrounding air, for both the FEM and analytical model, was obtained using the heat transfer coefficient α_s given in [6] and shown in Fig. 5.6:

$$\alpha_s = Nu \, \frac{\lambda_a}{d_s} \quad [W/m^2K] \tag{5.4}$$

The *Nusselt* number

$$Nu = 0.1 \; Re^{2/3} \tag{5.5}$$

is obtained from the *Reynolds* number, given as

$$Re = \frac{\omega \; {d_s}^2}{2\nu}, \tag{5.6}$$

using thermal properties of air at $20°C$: $\nu = 1.51 \cdot 10^{-5} \; m^2/s$, $\lambda_a = 0.0257 \; W/mK$ and shaft diameter $d_s = 0.003 \; m$. The heat transfer co-

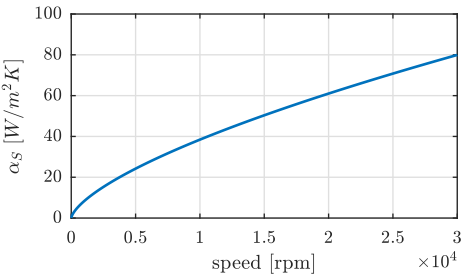

Fig. 5.6: *Coefficient of heat transfer α_S on the rotating shaft to surrounding air [6].*

efficient α_c on the cylinder surface, the side surfaces of the bearings and on the inner part of the shaft, which is covered by the cylinder, was assumed to be constant and identified using measurements at steady state. Using simultaneous temperature measurements at the outer cylinder and the bearing side surface by applying two $PT100$ elements, a contact resistance of $R_{bc} = 2.6\,K/W$ was identified in the press-fit between bearings and cylinder, which is in agreement with data published in [25].

5.3.2 FE-model

A numerical model was built using *COMSOL*. Heat flows and boundary conditions are shown in Fig. 5.7. Considering the axial symmetry of the components, the FE-model was built symmetrically with a symmetric heat source. This simplification is justified by the fact that at high speed, where

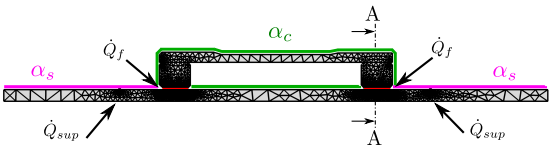

Fig. 5.7: *Visualization of the mesh, boundary conditions of convective heat transfer, α_s and α_c.*

the viscous losses are important, the shaft is well centered in the bearing as derived from established theory [46] and experimentally shown by Trachsel et al. [117] for this specific setup. Qiu [95] experimentally found the temperature not to depend on the circumferential angle at low eccentricity. Parts were modeled with thermal properties given in Tab. 5.1. The friction power $\dot{Q}_f$ is obtained from the measurement according to (5.1) and assigned as heat source to the modeled fluid film (Fig. 5.7) of actual thickness c.

	bronze bearings		cylinder	shaft	fluid
material	porous	nonporous	ETG100	steel 1.2210	oil
conductivity $\lambda\ [W/mK]$	32	58	33	33.5	0.14
density $[kg/m^3]$	6500	8700	7800	7850	850
heat capacity $[J/kgK]$	435	496	460	475	1670
heat capacity $C\ [J/K]$	1.81	2.81	4.66	1.85	$6.7\,10^{-4}$

Tab. 5.1: *Material properties used in the FE-model.*

Frictional heating from the support $\dot{Q}_{sup}$ obtained from (5.3) is assigned to the shaft at the specific position.

An average fluid film temperature is considered to compare with the model developed. A visualization of the simulated temperature is shown in Fig. 5.8a) for the bearing unit at the end of a typical Stribeck measurement and in Fig. 5.8b) for the temperature profile under variation of speed in the cross section $A - A$ indicated in Fig. 5.7. To identify the convective heat

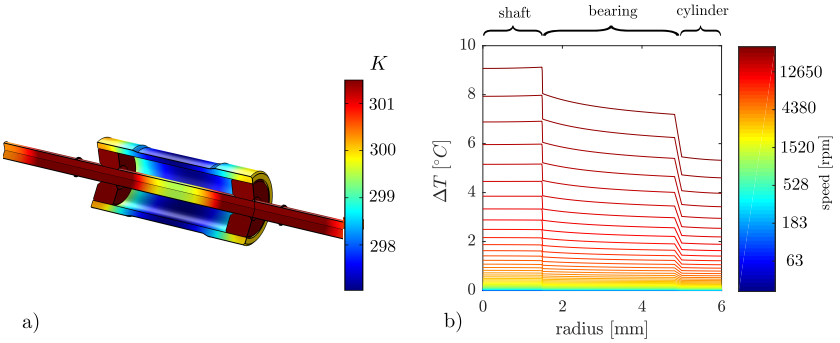

Fig. 5.8: *a) Numerical solution of the temperature distribution in the bearing system at* $24000\,rpm$ *after* $330s$. $c = 12.5\mu m$ *b) Temperature profile at section* $A - A$ *(see Fig. 5.7) under variation of speed. Note the steps at the interfaces. The speed was varied from* $30 - 24500\,rpm$ *as given in Fig. 5.3 a). The time between each line is* $5s$.

transfer α_c, temperature and friction measurements were performed after calibration at steady-state and different constant speeds. Temperature measurements on the outer cylinder surface (Figs. 5.1 and 5.5) using a $PT100$ resistance temperature detector were compared to the average surface temperature of the numeric solution. A value of $\alpha_c = 35W/m^2K$ was found for the simulation to best fit the measured temperature as shown in Fig. 5.9. $PT100$ measurements were verified using a contactless *IR*-measurement by a *Micro-Epsilon CT-SF22-C3* . To allow the *IR*-measurement, a Polyimid film was used to increase the relative spectral emissivity in the wavelength of interest.

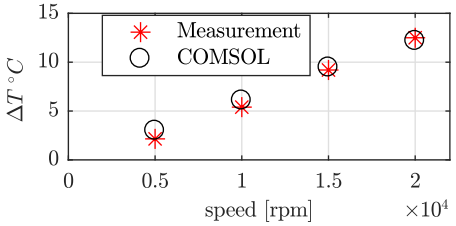

Fig. 5.9: *Measurement and simulation of the equilibrium surface temperature differences after $30min.$ at different constant speeds. Radial clearance $c = 17.5\mu m.$*

5.3.3 Lumped parameter model (LPM)

In order to simplify the evaluation of the Stribeck measurements, a LPM was developed to describe the thermal behavior of the system, in particular the fluid temperature T_f. The model allows to take into account viscous heating and an automated measurement analysis without big numerical effort.

Already a model consisting of only one single thermal mass representing the overall heat capacity given in Tab. 5.1 and relevant phenomena of heat exchange, allows to predict fluid temperature for slow changes in speed ω and heating power $\dot{Q}_f$ for cases of homogeneous heating.

However, a typical Stribeck measurement performed over a wide range of speed in a short lapse of time, in contrast, is associated with inhomogeneous temperature strongly dependent on time. Therefore, the LPM shown in Fig. 5.10 does not only represent the thermal mass and surface, but also considers heat transfer resistance between bearing and cylinder and the one of the fluid film. The thermal mass of the shaft was divided into two pieces, to better represent the temperature distribution along the shaft. According to the geometry of the bearing unit, 42% were assigned to the inner part of the shaft C_{s1}, the remaining 58% belong to the outer parts of the shaft C_{s2}.

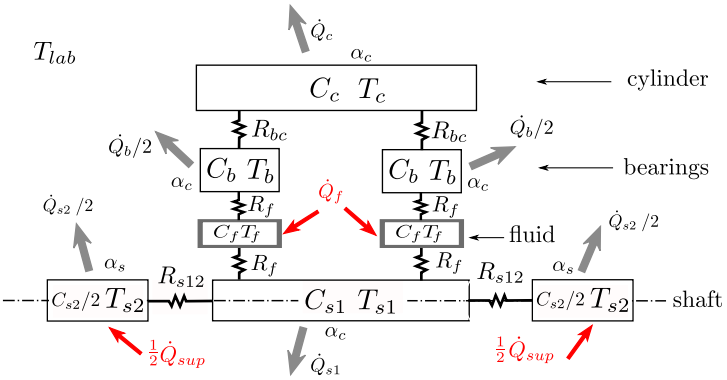

Fig. 5.10: *Lumped parameter thermal model (LPM) representing thermal masses C, heat exchange to the environment $\dot{Q}$ and internal heat transfer resistances R.*

Energy balance shaft elements

Based on this model, the equations of heat exchange [16] are written for the two shaft elements C_{s1} and C_{s2} as given in Eqs. (5.7) and (5.8):

$$C_{s1}\ \frac{\partial}{\partial t} T_{s1} = P_{f1} - P_{12} - \dot{Q}_{s1} \tag{5.7}$$

$$C_{s2}\ \frac{\partial}{\partial t} T_{s2} = \dot{Q}_{sup} + P_{12} - \dot{Q}_{s2} \tag{5.8}$$

with incoming heat fluxes from the support $\dot{Q}_{sup}$ (5.2). The heat flux from the fluid to part one of the shaft C_{s1} is denoted as P_{f1}, the one from part one of the shaft to part two, P_{12}, etc. (b: bearing, c: cylinder, f: fluid). The internal heat fluxes P were obtain ed proportional to the temperature differences of the elements involved:

$$P_{f1} = \frac{T_f - T_{s1}}{R_f} \tag{5.9}$$

$$P_{12} = \frac{T_{s1} - T_{s2}}{R_{s12}}, \tag{5.10}$$

were R_f is the conductive heat transfer resistance of the lubricant film. Assuming laminar shear flow in the fluid film, R_f was modeled in function

of the bearing clearance c, length l_b and diameter d_s to be:

$$R_f = \frac{0.5\,c}{l_b d_s \pi \lambda_f} \tag{5.11}$$

such that the overall heat transfer resistance between shaft and bearing is accurately represented. The heat conductivity $\lambda_f = 0.14W/mK$ for a typical mineral oil [23] was used.

The heat transfer resistance R_{s12} between the two shaft elements C_{s1} and C_{s2} was modeled as constant and controls the heat exchange $\dot{Q}_{12}$ between the shaft elements C_{s1} and C_{s2} and therefore the temperature in the fluid film. Using different types of friction measurements $M_{meas}\,(t)$ under variation of the fluid gap, $R_{s12} = 5\,K/W$ was found to minimize the integral of the difference between COMSOL solution of the fluid temperature and LP-model fluid temperature T_f.

Outgoing convective heat fluxes on the inner part of the shaft $\dot{Q}_{s1}$ was modeled identically to the COMSOL-model with constant heat transfer coefficient $\alpha_c = 35W/m^2K$ as given in Eq. (5.12):

$$\dot{Q}_{s1} = \alpha_c A_{s1}\,(T_{s1} - T_{lab}) \tag{5.12}$$

Convective heat transfer from the outer shaft element $\dot{Q}_{s2}$ was modeled dependent on the shaft speed (Eq. 5.4) using a coefficient of heat transfer α_s as given in Fig. 5.6:

$$\dot{Q}_{s2} = \alpha_s A_{s2}\,(T_{s2} - T_{lab}) \tag{5.13}$$

Energy balance fluid

The incoming heat flux from the viscous heating $\dot{Q}_f$, according to (5.1), goes to the energy balance of the fluid film C_f, given in Eq. (5.14):

$$C_f\,\frac{\partial}{\partial t} T_f = \dot{Q}_f - P_{f1} - P_{fb} \tag{5.14}$$

with conductive heat flux P_{f1} to the shaft element C_{s1} and to the bearings

$$P_{fb} = \frac{T_f - T_b}{R_f}. \tag{5.15}$$

Energy balance bearings and cylinder

The heat exchange for the remaining heat capacities of the bearings C_b and cylinder C_c are given in Eqs. (5.16) and (5.17).

$$C_b \frac{\partial}{\partial t} T_b = P_{fb} - P_{bc} - \dot{Q}_b \tag{5.16}$$

$$C_c \frac{\partial}{\partial t} T_c = P_{bc} - \dot{Q}_c \tag{5.17}$$

Outgoing convective heat fluxes on the outer cylinder surface, $\dot{Q}_c$, and on the bearing $\dot{Q}_b$, was modeled identically to the COMSOL-model with constant heat transfer coefficient $\alpha_c = 35 W/m^2 K$ as given in Eqs. (5.18) and (5.19):

$$\dot{Q}_c = \alpha_c A_c \left(T_c - T_{lab}\right) \tag{5.18}$$

$$\dot{Q}_b = \alpha_c A_b \left(T_b - T_{lab}\right) \tag{5.19}$$

considering the involved free surfaces of bearing A_b and cylinder A_c. Conductive heat flux from the bearing to the cylinder, P_{bc}, is obtained by the temperature difference of the elements involved

$$P_{bc} = \frac{T_b - T_c}{R_{bc}} \tag{5.20}$$

and constant resistance R_{bc} from measurements.

The internal heat fluxes P_{ij} and heat exchange to the surrounding $\dot{Q}$ to the are shown in Fig. 5.11b) for a typical Stribeck measurement. Note the negative heat fluxes P_{12} and P_{fs}, as at low speed, the friction of the support is dominant. Equations (5.7), (5.8), (5.16) and (5.17) were solved using the *MATLAB* solver *ode23s*. The temperatures differences ΔT with respect to T_{lab} are shown in Fig. 5.11a). Note the strong dependence on the change in speed, which is a function of time and the big temperature difference between the parts which shows the importance of considering temperature inhomogeneities. The correlation between speed and time is identical to the one given in Fig. 5.3a).

The fluid-temperature T_f found using this model was verified by comparing to the solution for the fluid temperature obtained by *COMSOL* for friction measurements using different shaft diameters, porous and non porous bearing material and different measurement duration (Figs. 5.13, 5.14).

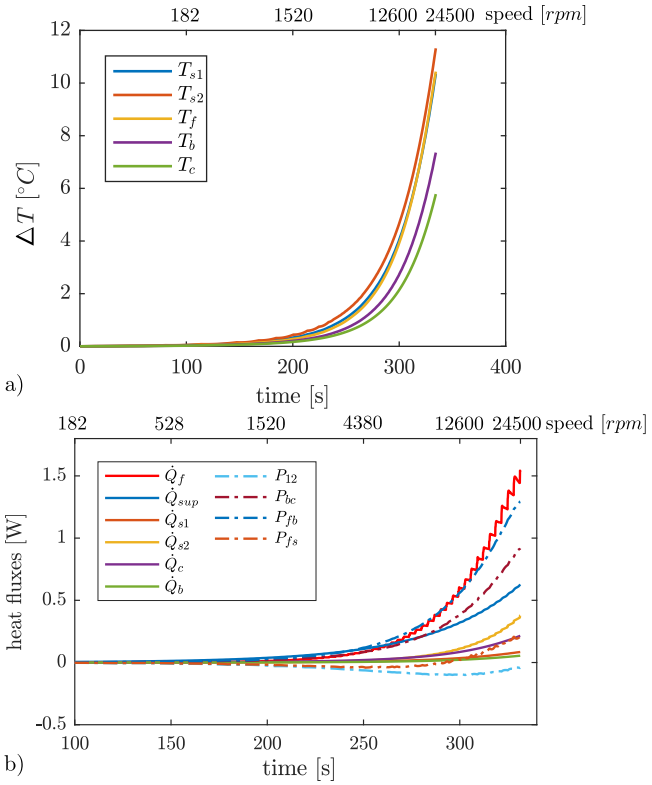

Fig. 5.11: *Solution of the LP-model.* $c = 12.5\mu m$*, porous bearings: a) Temperatures, note the large temperature differences between the elements at the end of the measurement (t=330s) b) Internal heat fluxes* P_i *and in and outgoing heat fluxes* Q_i*. The correlation between speed and time is identical to the one given in Fig. 5.3a).*

The LPM presented, now allows to determine the lubricant temperature evolution during a Stribeck measurement, without the need of FE-simulations. Friction models for the domain of hydrodynamic lubrication always depend on viscosity $\eta(T)$, which strongly depends on temperature T.

5.4 Friction Measurements

The high precision friction measurement [117] in combination with a temperature sensitive Newtonian fluid are used to investigate effects of viscous heating: The model described in Sec. 5.3.3 returns the fluid temperature at each point in time of the friction measurement. This allows to determine the viscosity, which only depends on temperature in the case of the Newtonian fluid applied (Fig. 5.4).

Using established theory of lubrication [46], the friction torque in the hydrodynamic (HD) domain of lubrication (see So-number in Fig. 5.3) can be well approximated using the law by Petrov and describing forces of a Couette shear flow on the shaft surface:

$$M_{HD} = \frac{u_s}{c}\frac{d_s}{2}\eta \cdot l_b d_s \pi \tag{5.21}$$

using the surface speed on the shaft $u_s = \omega\frac{d_s}{2}$. In the case of a THD model, viscosity η is a function of fluid temperature T_f:

$$M_{THD} = \frac{u_s}{c}\frac{d_s}{2}\eta\left(T_f\right) \cdot l_b d_s \pi. \tag{5.22}$$

5.4.1 Porous bearings

The friction torque measured M_{meas}, using porous bearings, was found to be smaller than M_{THD} for all fluid gaps c tested, as the shear rate at the shaft surface reduces in the domain of the pores. This phenomena is known and a friction model according by Goldstein and Braun [39] considering the porous bearing material and a reduction of friction by the factor Θ was applied in the hydrodynamic domain for an ideally centered shaft:

$$M_{THD,p} = \frac{u_s}{c}\frac{d_s}{2}\eta\left(T\right) \cdot l_b d_s \pi \cdot \Theta \tag{5.23}$$

using a reduction of friction by the factor Θ:

$$\Theta = \frac{1}{1 + \frac{\sqrt{\kappa}}{c\beta}}. \tag{5.24}$$

This describes well the measurements shown in Fig. 5.13 in the hydrodynamic domain using slip coefficient $\beta = 0.2$ and permeability $\kappa = 4 \cdot 10^{-13}\, m^2$ for Stribeck measurements with different fluid gap c and is in accordance with the values given in [39]. A Θ-value of 0.79, 0.84 and 0.89 was used for the different gaps $12.5\mu m$, $17\mu m$ and $c = 25\mu m$ as shown in Fig. 5.12. In the comparison between measurement and theory in Fig.

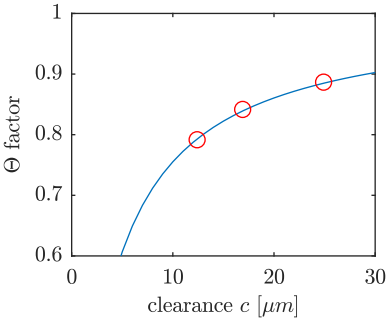

Fig. 5.12: *Factor Θ in function of radial clearance c.* $\kappa = 4 \cdot 10^{-13}\, m^2$, $\beta = 0.2$.

5.13 b), one can clearly see the influence of viscous heating and effect of

porous media, which both depend on the fluid gap c: Due to the increased shear rate, a smaller fluid gap c of course is directly related to an increased friction torque. However, viscous heating is also increased, thereby reducing friction. Also the reduction in friction Θ due to the porous material is bigger at smaller fluid gaps, as given in Fig. 5.12.

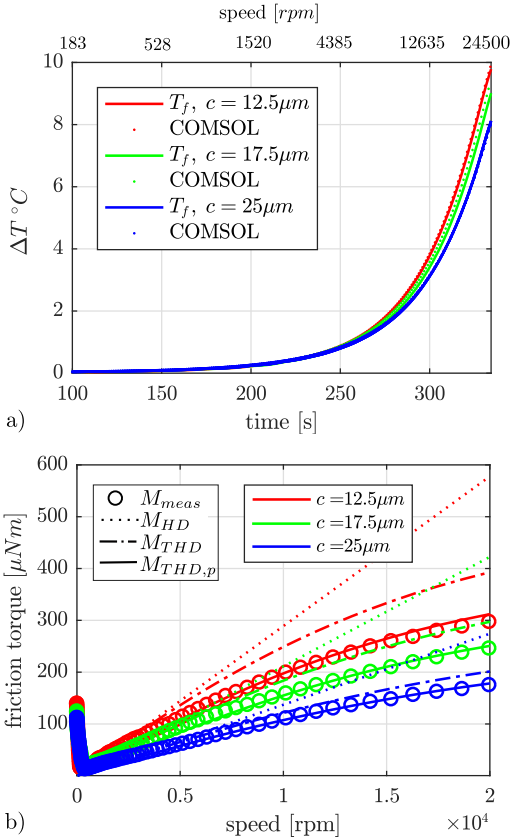

Fig. 5.13: *Porous bearing material: a) Temperature solution T_f of LP-model and COMSOL. b) Friction measurements M_{meas} at different radial clearances c and models neglecting viscosity changes due to frictional heating M_{HD}, considering thermal effects M_{THD} and additionally considering pores $M_{THD,p}$.*

5.4.2 Non porous bearings

Using non porous bronze material for the bearings, thermal properties of the models needed to be adjusted as heat capacity and thermal conductivity are different (Tab. 5.1). No further reduction Θ of friction is needed for the model M_{THD} to fit the measurements M_{meas} in absence of whirling because no pores are present (Fig. 5.14 c)).

For measurements in this setup close to applications, the use of non porous bearings in the domain of hydrodynamic lubrication is not simple, as the system is unstable at high speed and tend to exhibit the well known phenomena of half-frequency whirling [30, 2, 46, 107, 68], which comes together with an increase in friction.

The simultaneous detection of friction torque and relative displacement between shaft and bearing s allows to identify whirling phenomena and understand the reason for any change in friction which is due to whirling. Note the increase in friction in Fig. 5.15a) at $15000\,rpm$ where whirling at half of the frequency of rotation starts. Non porous bearings of course are not able to store any lubricant and therefore they are of no further importance for any application in this configuration. They were only used to investigate the effect of the porous material.

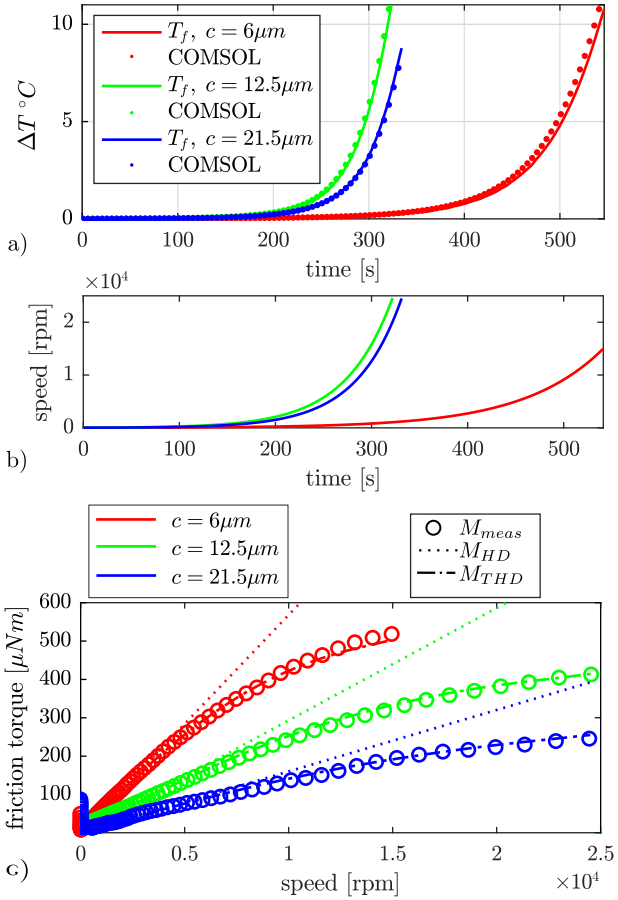

Fig. 5.14: *Non porous bearing material: a) Temperature solution T_f of LP-model and COMSOL. b) Speed profiles. c) Friction measurements M_{meas} at different radial clearances c and model M_{HD}: neglecting frictional heating, M_{THD}: considering thermal effects.*

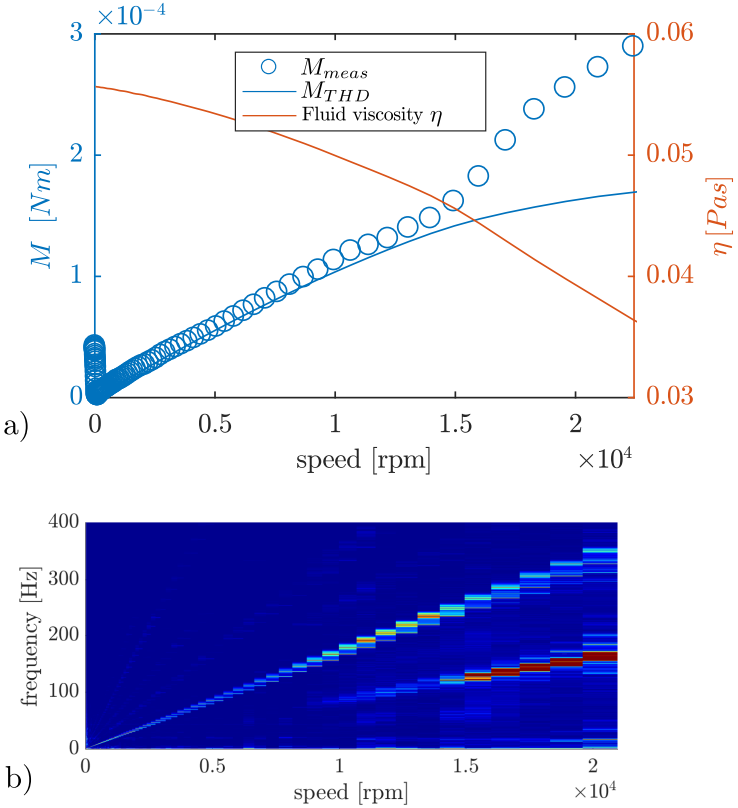

Fig. 5.15: *Simultaneous detection of friction torque M_{meas} (a) and relative displacement s_x between shaft and bearing (b) reveal effects of half-frequency whirling on friction. a) Friction measurement M_{meas}, theory M_{THD} and viscosity value η. b) Campell-diagramm of horizontal relative displacement s_x.*

5.5 Conclusions

The methodology and model described allows to precisely determine fluid temperature for the application in Stribeck measurements using miniature journal bearings without the need of difficult installation of temperature measurement devices. The fluid temperature can be calculated from the heating power produced by the measured friction torque and the solution of the thermal problem using Finite elements or a calibrated lumped parameter (LP) model.

Precisely calibrated, temperature sensitive Newtonian viscosity standard fluids were used and show the accuracy of the model. A comparison of porous and non-porous bearing material shows a reduced friction in the porous case as a function of the fluid gap. No friction reduction related to slip was needed for the non porous bearing as the model agreed with the experiments. A simultaneous measurement of the relative displacement between shaft and bearing allows to detect the dynamic phenomena of half-frequency whirling in line with an increase in friction at the same rotational speed.

Knowing the local temperature, the important value of lubricant viscosity $\eta(T)$ can be determined and thermohydrodynamic models in bearing analysis can be used to investigate bearing performance.

Using a precise friction measurement, effects of frictional heating, shear thinning, surface slip or flow in porous media can be investigated and distinguished. A contact-less detection of whirling is needed at low radial loading to avoid any false interpretation of friction measurement data, as half-frequency whirling leads to an increase in friction and to a false data interpretation if it is not detected.

Acknowledgments

The author likes to thank James Bartolo and Anubhav Jain for the fruitful discussions and support in programming.

Ionic Liquid Lubrication

6

submitted to:
M. Trachsel, R. Pittini, J. Dual. *Evaluation and quantification of friction using Ionic Liquids in small, self lubricating journal bearings*, Tribology International

L'essentiel est invisible pour les yeux.

LE PETIT PRINCE,
ANTOINE DE SAINT-EXUPÉRY,
1900-1944

Abstract

Four low viscosity Ionic Liquids were evaluated as lubricants in self lubricating porous journal bearings. Precise friction measurements performed under boundary conditions close to applications are presented under variation of the fluid gap and radial loading both in the domain of hydrodynamic and mixed lubrication up to high speed and high shear rates. A comparison to a standard lubricant and verification using a Newtonian reference is given and lowest friction was found for the low viscosity Ionic Liquids at the speed of minimum friction. Applying a thermohydrodynamic friction model, Newtonian fluid behavior was found for the Ionic Liquids in the hydrodynamic domain of lubrication up to high shear rates.

6.1 Introduction

In small electric motors, the efficiency of the electromagnetic part is limited, mainly by manufacturing processes and uncertainties of the parts involved. Therefore, the mechanical losses provide some potential for improvement in efficiency and are mainly to be found in the bearings, which are typically located as pairs, as far apart as possible in axial direction to provide a maximum of stiffness and precision. They provide a precise relative position between rotor and stator, and are able to carry a load. Due to fabrication uncertainties, costs and their extreme sensitivity with respect to impacts and overload, ball bearings are rarely found in this application and the low cost alternative of sintered journal bearings is chosen more often. Porous bronze bearings provide low friction and a lifetime lubrication via the lubricant stored in the pores. As there is typically no maintenance nor exchange of lubrication fluid in small bearings, the operating time is given by the integrity and presence of the lubricant. Due to the tremendous importance in industry, lubrication technology has strongly developed since crude oil first was used as a lubricant on a cotton spinning mill in Pittsburgh in 1845 [7].

Lately, a new type of fluid became available: Ionic liquids were developed as chemical reactants and solvents. Ionic liquids (ILs) are salts, which are in the liquid state at room temperature. They consist of large, asymmetric ions, which makes it difficult to build a regular crystalline structure. Considering properties of thermal and chemical stability and low volatility, ILs come along with important aspects of lubricants under severe conditions [90, 72, 94, 104, 15, 129]. Since the first application of ILs as lubricants [129], the research on this topic increased rapidly. Bermúdez et al. [15] presented a review on ILs as lubricants including their ability to interact with nano additives. An overview of application of ILs in the domain of research in tribology is given by Minami [72] and Somers et al. [104]. Applying standard tests of tribology, already a lot of good results were obtained using ILs in lubrication technology [13, 75, 4, 57, 114, 42, 49].

The unique properties of ILs also led to domains of research aiming to understand the molecular interaction with other material. Xiao et al. [126] found the film thickness for three ILs in elastohydrodynamic lubrication to depend on speed. Using an electrical potential at an IL lubricated contact, Atkin [9] was able to modify the molecule structure and lubricity, which

was detected using atomic force microscopy. Espinosa-marzal et al. [34] measured friction in the nano scale using colloidal probe atomic force microscopy. Due to their unique structure, ILs are able to interact not only with surfaces but also with different kinds of additives that influence their properties. With the focus on tribology, several studies were performed on this topic [52, 132, 119, 37, 122]

With regard to application under vacuum conditions, e.g. in space, several studies were performed evaluating IL lubrication: Holzbauer et al. [44] started a screening with some fluids, showed viscosity measurements, wetting properties and outgassing. Ball-on-disk type tribotests and wear tests were performed by Suzuki et al. [110] under high vacuum conditions. A good thermal stability, low volatility and low friction was reported. Kałdoński and Wojdyna [51] investigated liquid lubricants for space engineering and analyzed fluid properties and friction for two ILs. Tribochemical reactions of ILs under vacuum condition were analyzed by Kawada et al. [53].

Burrell et al. [24] reported shear thinning for several ILs. The magnitude of shear thinning decreased with increasing water content. The diluted ILs are reported to behave Newtonian. Amann et al. [3] performed rheological studies on ILs aiming to understand the low friction values. Orientation of molecules was explored and correlated with viscosity. A non Newtonian effect of shear thinning was observed depending on the molecule orientation.

Application in self lubricating porous journal bearings

Summarizing the review of different branches of research given above, ILs have already proven to have a great potential in lubrication technology and are able to push the limits of application towards new domains.

However, the fluid-structure interaction in small, porous journal bearings is more complex than in a typical measurement device of tribology or rheology. Depending on the bearing state, characterized by the dimensionless Sommerfeld number So, one might have to deal with surface chemistry and tribology at low speed and high radial loading, or fluid dynamics and rheology at high speed and low load. This is even a simplifying assumption. The complex interaction at the porous bearing material exhibits a combination of both tribology and rheology at all bearing states and so far can only be addressed experimentally to identify the lubrication properties of the specific fluids for the specific case. This is presented here for the first time.

Aiming to explore solutions for low friction and for vacuum applica-

tion, in this paper we present the application of ILs as lubricant in small porous journal bearings of $3.002\,mm$ inner diameter using precise friction measurements together with a modelling of friction, which sheds new light on a difficult problem. Applying the setup described in [117, 116], friction torque is measured under variation of the important parameters of rotational speed ω, radial loading F_r and bearing clearance c. A simultaneous detection of friction and relative displacement between shaft and bearing allows detecting effects of half frequency whirling and its influence on friction. Therefore a correct interpretation of friction measurement data is guaranteed. To compare the lubrication performance of different fluids and identify anomalies which reduce friction, like effects of shear thinning or surface slip, measurements were compared to theory of thermohydrodynamic lubrication. Effects of viscous heating and bearing porosity were modelled as shown in [118]. The new measurements obtained for ILs are compared to those using a non-Newtonian standard lubricant $CX2000$ by Klüber as reference and Newtonian viscosity standard mineral oils.

6.2 Experimental setup

The apparatus used to measure bearing friction is illustrated in Figures 6.2-6.1 and was described in detail in [117]. Two bronze bearings (porous type $B50$ with 20% porosity) were pressed into a steel cylinder which is a typical method of installation in small electrical motors.

The friction torque $M_{meas}(\omega)$ with respect to the centre of the shaft O is calculated using the tensile forces F_b on the side of the balance and F_w on the side of the weight. Fabrication uncertainties were identified by two measurements in opposite direction of rotation and corrected. Horizontal

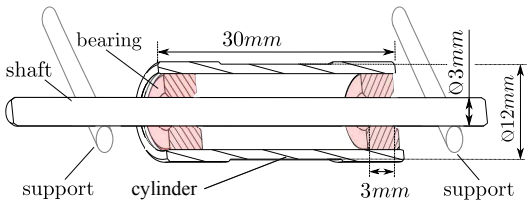

Fig. 6.1: *Cross section of cylinder unit with bearings, shaft and support.*

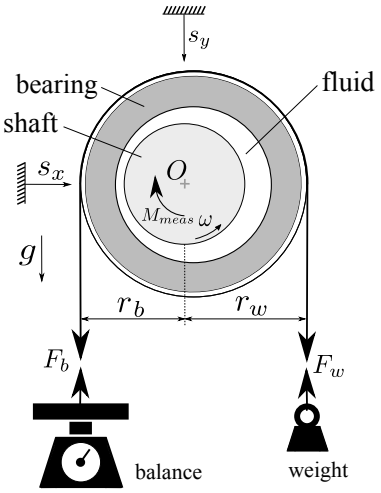

Fig. 6.2: *Friction measurement principle: rotating shaft, bearing unit, counterweight to define the radial loading and a balance to capture friction M_{meas} between the rotating shaft and the bearings. Displacement s_x, s_y between shaft and bearing is captured using two lasers. See [117] for details.*

displacement s_x between shaft and bearing is captured by laser triangulation and considered for the calculation of the friction torque. A nominal resolution of $50nNm$ can be obtained. Friction torque M_{meas} is calculated for the illustrated case of ccw rotation:

$$M_{meas} = (r_w F_w - r_b F_b) \cdot \omega \ \ [Nm] \tag{6.1}$$

Measurements were performed over 100 discrete speed steps within $330s$ and up to $20000\ rpm$ and analysed versus speed or the dimensionless Sommerfeld number So and compared to theory. Average values of the measured friction were taken at each speed, no additional filter was applied.

Using precise steel shafts (DIN 1.2210) of two different diameters d_s $(2.970mm,\ 2.980mm)$, measurements were performed with two different radial clearances c of $11\mu m$ and $16\mu m$. Rotational speed in function of time and the resulting average shear-rates $\dot{\gamma}$, the fluid is exposed to, are given in Figure 6.4. The radial load was set to $1.09\,N$ for the analysis in

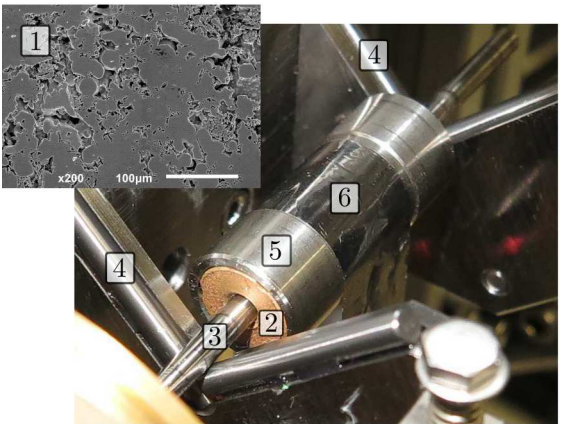

Fig. 6.3: *Hardware: (1) SEM image of the porous bearing material, (2) bearing, (3) shaft of $3\,mm$ diameter, (4) support prism, (5) cylinder, (6) steel band to transmit friction force.*

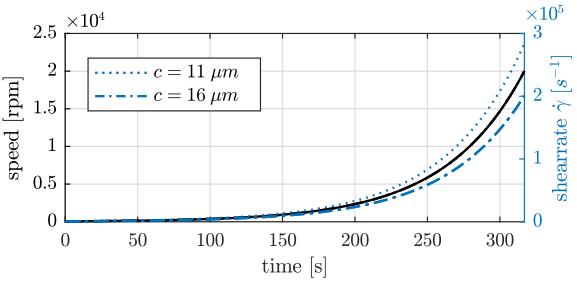

Fig. 6.4: *Speed profile (black, scale at the left) applied during a typical Stribeck-measurement. Resulting average shear rates (blue, scale at the right) for radial clearances $c = 11\,\mu m$ and $16\,\mu m$.*

the hydrodynamic domain of lubrication which corresponds to an average pressure of $64\,kPa$.

6.2.1 IL lubrication

For an application in porous journal bearings, as they are used for example in small electric motors, lubricant viscosity is an important parameter and therefore a selection criteria for the ILs. High viscosity fluids cannot be used at high speed in the domain of hydrodynamic lubrication, as the friction losses would be too high. The ILs tested were purchased from *Ionic Liquids Technologies GmbH* with $> 99\%$ purity and are listed in Table 6.1. The viscosity of all fluids applied was measured for different temperatures

Abbrev.	η [mPas] @ 25°C	**Name**
IL-23	30.4	1-Ethyl-3-methylimidazoliumbis(trifluoromethylsulfonyl)imide
IL-30	29.2	Triethylsulfonium bis(trifluoromethylsulfonyl)imide
IL-32	94.4	Butyltrimethylammonium bis(trifluoromethylsulfonyl)imide
IL-116	63.6	Diethylmethyl-(2-methoxyethyl)ammonium bis(trifluoromethylsulfonyl)imide
CX2000	38.2 at 1150 s^{-1}	Klüber ISOFLEX PDB 38 CX 2000
N10	15.15 at 25°C	Newtonian viscosity standard mineral oil by *CANNON*
N35	55.9 at 25°C	Newtonian viscosity standard mineral oil by *CANNON*

Tab. 6.1: *Fluids tested*

and shear rates using an *Anton Paar UDS200* and a cone-plate geometry. Measurement data are shown in Figure 6.5 for the fluids applied. Viscosity $\eta\,(T_f)$ for the ILs was found not to depend on shear rate in the range from $100\,s^{-1}$ to $5000\,s^{-1}$; they behave as Newtonian fluids. However, in the application in small journal bearings, much higher shear rates $\dot{\gamma}$ are reached, as illustrated in Figure 6.4 for the ideally centred situation.

The measured viscosity of the non Newtonian standard lubricant *CX2000* by *Klüber* is given vs. the shear rate $\dot{\gamma}$ in Figure 6.5 a) for several temperatures together with IL viscosity values at $25^\circ\,C$. Figure 6.5 b) displays the dependence of ILs viscosity on temperature together with the viscosity η of *CX2000* at a shear rate of $1150\,s^{-1}$. Note the similar low dependence on temperature of the low viscosity Ionic Liquids IL23 and IL30 as obtained for the highly developed lubricant *CX2000*.

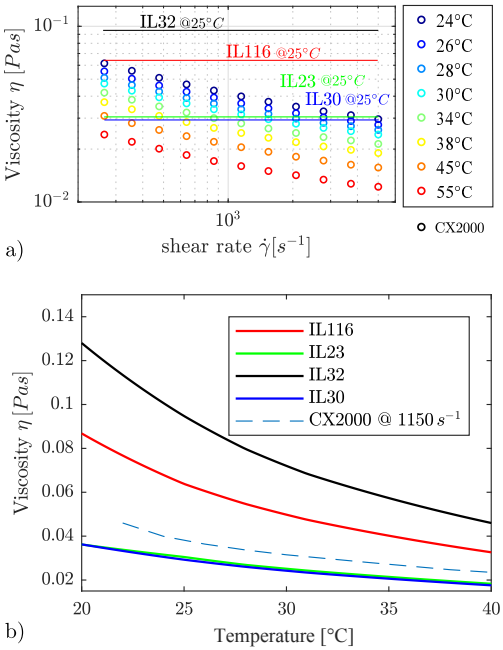

Fig. 6.5: *Viscosity values $\eta(T_f)$ measured using an Anton Paar UDS200 rheometer: a) Viscosity η vs. shear rate $\dot{\gamma}$ shows shear thinning for CX2000 and Newtonian behavior of the ILs. b) Viscosity values under variation of temperature.*

6.3 Friction measurements and theory

To quantify friction and identify unknown effects which potentially reduce it by effects of shear-thinning or surface slip, the values of measured friction torque M_{meas} was compared to established theory of lubrication [46]: The friction torque in the hydrodynamic (HD) domain of lubrication can be well approximated using the law by Petrov [46] using the forces of a Couette shear flow on the shaft surface

$$M_{HD} = \frac{u_s}{c}\frac{d_s}{2}\eta \cdot l_b d_s \pi. \tag{6.2}$$

The surface speed on the shaft is $u_s = \omega \frac{d_s}{2}$. Eccentricity can be neglected because the shaft is well centred in the bearing hole in this domain as verified by simultaneous detection of friction and relative displacement (Figure 6.12 b).

6.3.1 Thermohydrodynamic (THD) lubrication

In the case of a THD description, fluid viscosity η is a function of temperature T_f, therefore friction torque M_{HD} (6.2) is written as:

$$M_{THD} = \frac{u_s}{c} \frac{d_s}{2} \eta\left(T_f\right) \cdot l_b d_s \pi. \tag{6.3}$$

To determine the temperature T_f in the fluid gap, a lumped parameter model was built and verified using FE models and Newtonian viscosity standard fluids for friction measurements. The thermal model is illustrated in Figure 6.6 and explained in detail in [118]. Knowing the evolution of the fluid temperature T_f during a measurement, the actual value of viscosity $\eta(T_f)$ can be used to calculate M_{THD}.

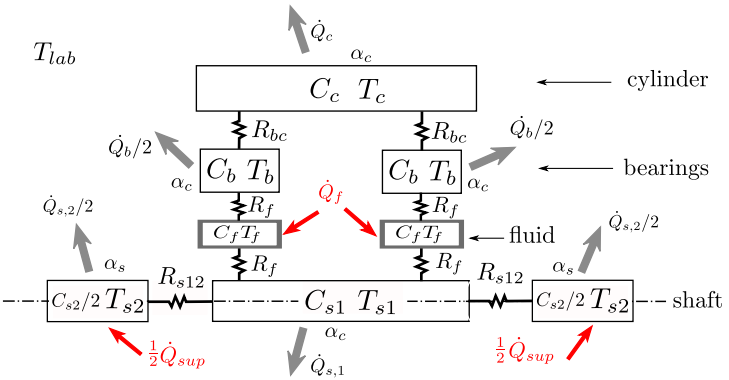

Fig. 6.6: *Lumped parameter thermal model used to determine the fluid temperature T_f. For details see [118]. $\dot{Q}_f$: frictional heating, $\dot{Q}_{sup}$: friction at the support, $\dot{Q}_i$: outgoing heat fluxes, C_i: thermal masses, R_i: heat transfer resistance, T_f: fluid temperature.*

For porous bearings, friction torque at the shaft is smaller then M_{THD}, depending on the fluid gap c used, because the shear rate at the shaft surface is reduced in the domain of the pores. This is known and a friction model according to Goldstein and Braun [39] considering the porous bearing material and a reduction of friction by the factor Θ was applied in the hydrodynamic domain for an ideally centred shaft:

$$M_{THD,p} = \frac{u_s}{c}\frac{d_s}{2}\eta\left(T_f\right) \cdot l_b d_s \pi \cdot \Theta \tag{6.4}$$

with the factor Θ:

$$\Theta = \frac{1}{1 + \frac{\sqrt{\kappa}}{c\beta}}, \tag{6.5}$$

using a slip coefficient $\beta = 0.2$ and bearing permeability $\kappa = 4 \cdot 10^{-13}\, m^2$. An experimental verification using non-porous journal bearings was presented in [118]. Values of measured friction torque M_{meas} vs. speed in RPM and a comparison to the different models described by M_{HD} (6.2), M_{THD} (6.3) and $M_{THD,p}$ (6.4) are given for the four ILs and the standard lubricant *CX2000* in Figure 6.7. Note the huge deviation between M_{HD} and M_{THD} for $CX2000$ in Figure 6.7 e). Considering measured values of viscosity $\eta(\dot{\gamma}, T)$ given in Figure 6.5, M_{THD} also includes shear thinning, which contributes the major part of the deviation $M_{HD} - M_{THD}$, as the temperature elevation for $CX2000$ is the smallest of all fluids as shown in Figure 6.9.

To allow a dimensionless presentation of friction data vs. So, we use a coefficient of friction μ considering the tangential force on the shaft surface $F_t = M_{meas}/\left(0.5\, d_s\right)$:

$$\mu := \frac{F_t}{F_r} = \frac{M_{meas}}{0.5\, d_s\, F_r}. \tag{6.6}$$

The radial loading F_r is calculated by the force of the load applied F_w, the force measured by the balance F_b and the weight of the cylinder unit $F_c = m_c\, g$:

$$F_r = F_w + F_b + F_c. \tag{6.7}$$

To compare measurements to theory, we use a coefficient of friction $\mu_{THD,p}$

$$\mu_{THD,p} := \frac{M_{THD,p}}{0.5\, d_s \cdot F_r}. \tag{6.8}$$

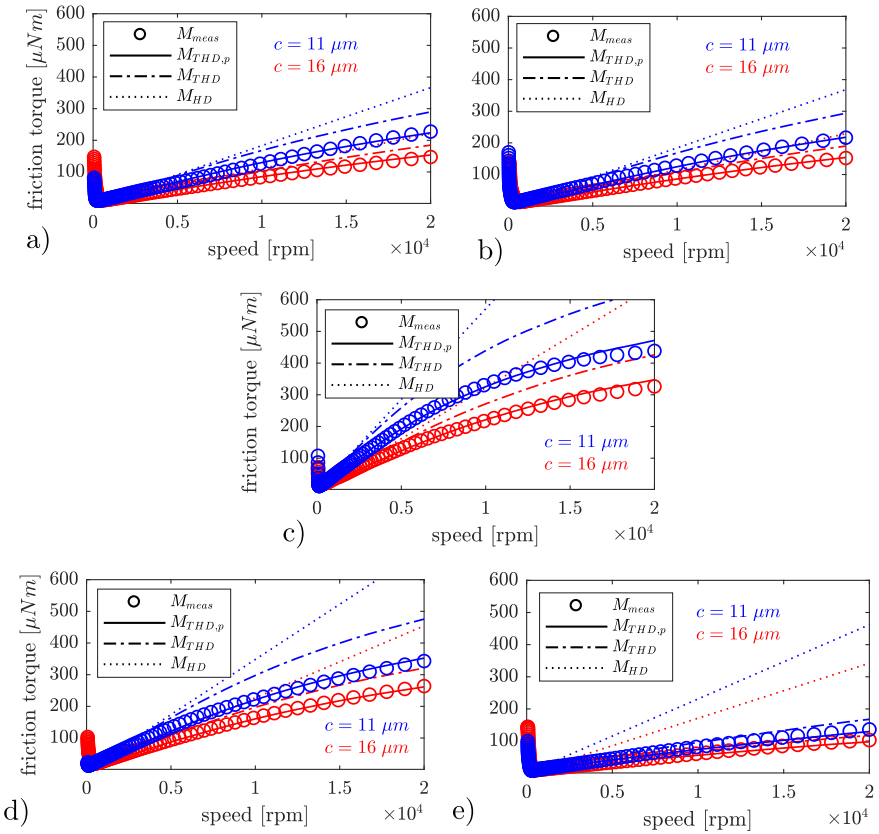

Fig. 6.7: *Friction torque measurements M_{meas} compared to the friction models M_{HD}, M_{THD} and $M_{THD,p}$ using radial clearances $c = 11\mu m$ and $16\mu m$ for the different fluids a): IL23, b): IL30, c): IL32, d): IL116, e): CX2000.*

The dimensionless presentation of the coefficient of friction μ vs. So is given for each fluid for radial clearances $c = 11\mu m$ and $16\mu m$ in Figure 6.8. Note the good agreement of measurement and theory of thermohydrodynamic lubrication in the domain of high speed and high So number. Due to the different values of viscosity $\eta(T)$, both the coefficient of friction μ and the range of the Sommerfeld number So differ significantly, depend-

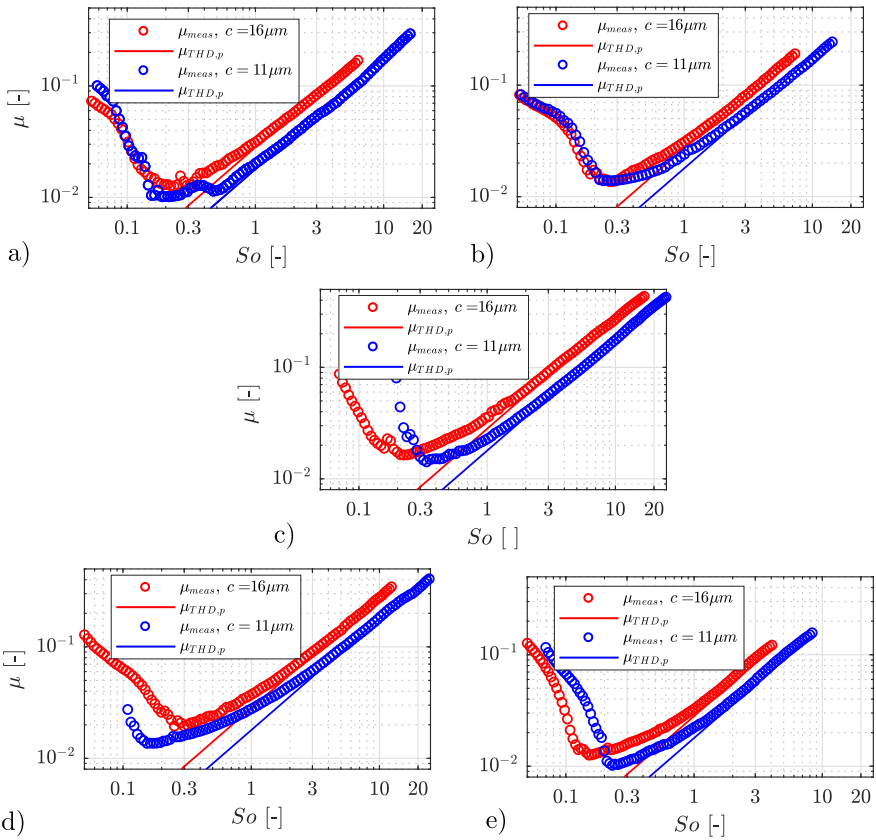

Fig. 6.8: *Stribeck curves μ_{meas} vs. So, together with the modelled coefficient of friction $\mu_{THD,p}$ using the two radial clearances $c = 11\mu m$ and $16\mu m$ and the fluids a): IL23, b): IL30, c): IL32, d): IL116, e): CX2000.*

ing on the fluid applied. All ILs tested behave Newtonian in the domain of hydrodynamic lubrication which is mainly dominated by rheology with the important parameter fluid viscosity $\eta(T_f)$. Viscosity η was found not to depend on the shear rate $\dot{\gamma}$. Due to this, the ILs tested under laboratory conditions show higher friction when compared to the shear thinning

standard lubricant *CX2000* at high speed in the domain of hydrodynamic lubrication. This is not the case in the domain of mixed lubrication, at the point of minimum friction. An analysis of this point will be presented in Sec. 6.3.2. The temperature elevation ΔT during the measurement is important to consider as fluid viscosity $\eta(T_f)$ and therefore also the Sommerfeld number So depend on temperature T_f. The change in temperature T_f is given vs. So in Figure 6.9 a) and vs. speed in Figure 6.9 b), respectively for all measurements and both gap width c and an equal speed profile up to 20000 rpm. The advantage of a high performance, non-Newtonian shear thinning

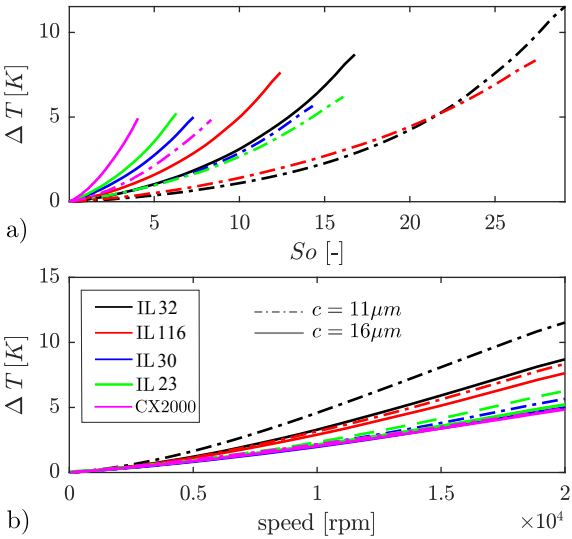

Fig. 6.9: *Temperature elevation at the fluid ΔT_f due to viscous heating obtained from the thermal model [118] shown in Figure 6.6. Data are given vs. Sommerfeld number So in a) and vs. speed in b).*

lubricant (CX2000) not only leads to the smallest temperature elevation at the fluid ΔT_f, but also to the smallest change in So, which allows application over a wide range of parameters. The highest change in temperature and widest variation in So is found for the high viscosity fluids at the smallest radial clearance c. These fluids are favorably applied at lower speed to avoid excessive viscous heating.

6.3.2 Mixed lubrication, high shear rates

To further investigate the lubrication properties of the ILs under test, the radial load was increased to $4.5\,N$. At high pressure of $p = 250\,kPa$, the viscous forces are not able to lift the bearings to an ideally centred position and the fluid is exposed to extremely high and undefined shear rates. In the following we focus on the point of minimum friction in the Stribeck curve. One typical friction torque measurement according to (6.1) up to $1500\,rpm$ for each fluid is given in Figure 6.10. Due to the high eccentricity, an increased friction was found when compared to $\mu_{THD,p}$ for all fluids. Measurements were performed using steel (*DIN 1.2210*) and

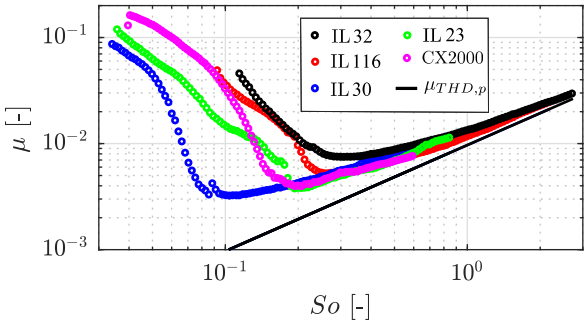

Fig. 6.10: *Stribeck measurements using a steel shaft at a radial load of $4.5\,N$ and radial clearance $c = 6.8\mu m$. Due to the high bearing eccentricity, measured friction is higher as predicted by $\mu_{THD,p}$ for an ideally centred shaft.*

polished ceramic ($Zr0_2$) shafts of identical diameter of $2.9884\,mm$ which was measured using an optical method (*Z-Mike 1220*) and a resulting radial clearance of $c = 6.8\,\mu m$. Ceramic shaft material is used in some applications in small electric motors and known to bring favourable frictional properties. The ceramic-IL-interaction therefore is a good candidate for low friction. Points of minimum friction μ_{min} were extracted from the measurements and are shown in Figure 6.11 for the four ILs applied and for both steel and ceramic shaft material.

Taking into account the fluid viscosity given in Figure 6.5, a dimensionless presentation of the coefficient of friction μ vs. So in Figure 6.11 a)

reveals lubrication performance. The transition to hydrodynamic lubrication according to theory [46] is influenced by the key parameters viscosity η, speed ω, pressure p and clearance c. Here we only changed the lubricant which is taken into account in the So number.

The application of highly viscous IL32 and IL116 in this experiment does not significantly shift the point of minimum friction and the transition to hydrodynamic lubrication towards lower speed, but simply results in higher friction. In Figure 6.11 a) and b) one can clearly see lowest friction for IL30 for both steel and ceramic shaft material and for IL23 in the case of ceramics without significant shift towards higher speed. This anomaly probably is due to the special molecular structure of the ILs and their surface interactions, such that fluid viscosity is not the only important parameter at this point. Values of minimum friction show a clear dependence on fluid

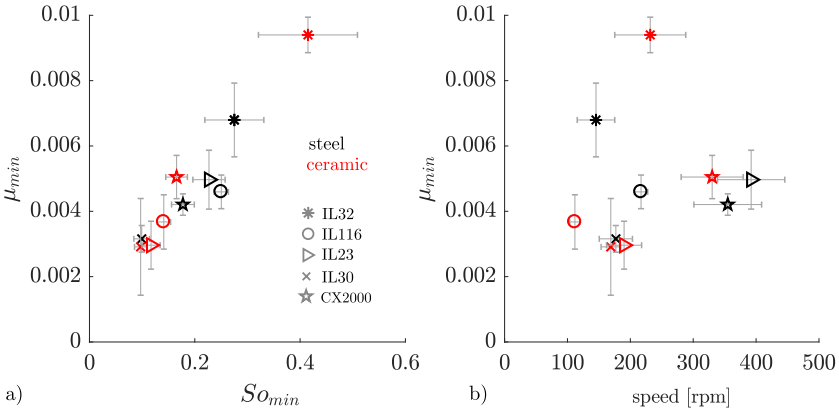

Fig. 6.11: *Values of minimum friction μ_{min} vs. the corresponding So-number in a) and at the corresponding speed n_{min} in b). $F_r = 4.5$ N, applied shaft materials are steel and ceramic. $c = 6.8\,\mu m$. Note the low friction of IL30, IL23 and IL116 when compared to the standard lubricant CX2000 taken as reference.*

viscosity, lowest friction was found for the lowest viscosity. Note the values of the non Newtonian standard lubricant *CX2000* in Figure 6.11, which neither shows lowest friction, nor a transition to hydrodynamic lubrication at low speed.

In case of Newtonian mineral oil viscosity standards N10 and N35 by *CANNON* the transition to hydrodynamic lubrication, identified by the point of minimum friction, clearly is found to occur at lower speed for the higher viscosity fluid N35 for all clearances c applied when compared to the low viscosity N10 as shown in Figure 6.12. As the friction measurements at

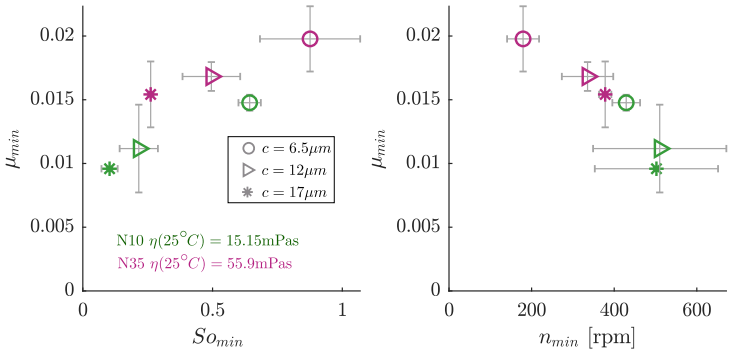

Fig. 6.12: *Values of minimum friction μ_{min} at the corresponding So-number in a) and at the corresponding speed n_{min} in b) for Newtonian viscosity standard fluid N10 and N35. $F_r = 1.14$ N. Note the speed of minimum friction n_{min} in b) and the transition to the domain of hydrodynamic lubrication shifted towards higher speeds for the low viscosity fluid N10.*

the point of minimum friction in the Stribeck curve is extremely sensitive to any influence, measured friction data were filtered using *MATLAB filtfilt* and average values of several measurements using identical parameters were taken for this analysis after a sufficient running in. Bearings were identified to be well run-in by consecutive Stribeck measurements at $F_r = 4.5\,N$ and low speed, that did not show any changes in the point of minimum friction, neither in friction nor at the corresponding speed. Run-in effects are significant and illustrated in Figure 6.13 using six consecutive measurements, IL23 as lubricant and 1.5N radial loading.

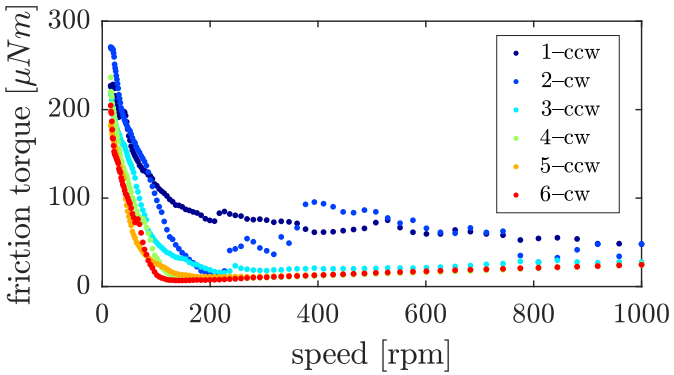

Fig. 6.13: *Effects of running-in illustrated using consecutive measurements in clockwise and counter clockwise direction of rotation. Lubricant IL23, radial clearance* $c = 6.5\mu m$, $F_r = 1.5N$.

6.3.3 Half frequency whirling, fluid gap and bearing locus

The well known phenomena of half frequency whirling [30, 2, 46, 107, 68], is favored to occur at low radial loading, big fluid gaps and Newtonian fluids. A simultaneous detection of relative displacement between shaft and bearing by contact less laser triangulation allows to detect effects of half frequency whirling, which never occurred in the data shown here. For illustration see the displacement data of the friction measurement of IL30 and $c = 11\mu m$ in Figure 6.14 a) where only the first and higher harmonics are weakly visible. In case of half frequency whirling, an increase in friction was detected as

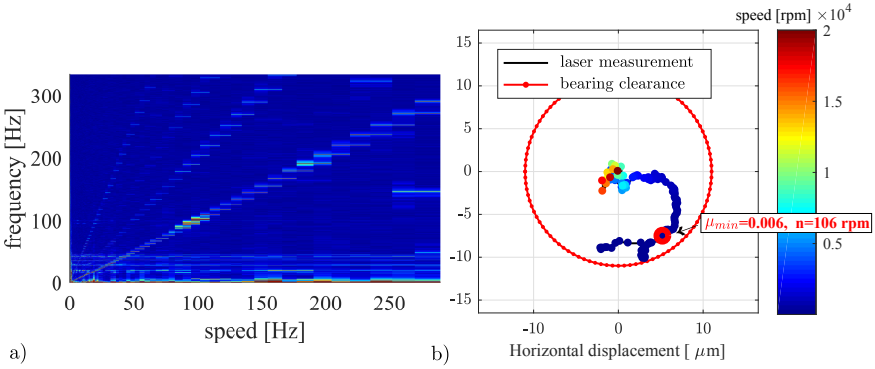

Fig. 6.14: *Relative displacement data captured by laser triangulation [117] for IL30, $c = 11\mu m$: a) Campell diagram used to prove the absence of half frequency whirling. b) Bearing locus, averaged for each speed. Note the point of minimum friction, μ_{min} and corresponding speed n_{min} indicated in red, which is found at a very thin fluid film.*

shown in Figure 6.15 for a configuration with non-porous bearings. For a correct interpretation of friction measurement data, therefore it is important to know the dynamic state of the system. Displacement signals were verified for each measurement to justify the absence of whirling phenomena. An analysis of the displacement data s_x and s_y as average values for each speed reveals the relative displacement trajectory under variation of rotation speed as given in Figure 6.14 b). Note the well centred shaft in

the domain of hydrodynamic lubrication at higher speed, which justifies to neglect eccentricity in the models of friction in the domain of hydrodynamic lubrication. The simultaneous detection of friction and relative displacement allows to locate the point of minimum friction μ_{min} in the relative displacement, as indicated in Figure 6.14 b), just before the contact between shaft and bearing opens.

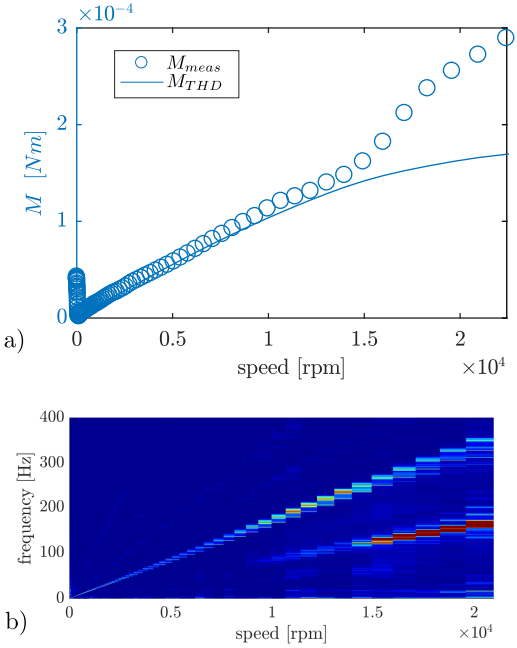

Fig. 6.15: *Simultaneous detection of friction a) on a non-porous bearing and relative displacement b) reveals effects of whirling on friction. Note the increase in friction at the onset of whirling.* $F_r = 0.54$ *N, clearance* $c = 26\mu m$*, Newtonian fluid CANNON N35.*

6.4 Conclusions

All Ionic Liquids applied as lubricant in porous, self lubricating bearings show a Newtonian behavior in the domain of hydrodynamic lubrication. The friction measured can be described by established theory, considering a reduction of friction by the reduction of viscosity due to effects of viscous heating and the porous bearing material. No shear thinning or additional effects of surface slip were observed within the parameters applied here.

Looking at the point of minimum friction in the domain of mixed lubrication in the Stribeck curve, lowest friction was found for the low viscosity fluids IL30 and IL23. Regarding the shaft material, ceramics shows lower friction when compared to steel for IL23, while the high viscosity IL32 shows lower friction with steel.

The corresponding speed of the points of minimum friction, the transition to the hydrodynamic domain of lubrication, does not significantly depend on the fluid viscosity, as it is expected from theory and verified for Newtonian fluids.

The good lubrication properties of the low viscosity fluids and the anomalies at the transition from mixed to hydrodynamic lubrication cannot be explained by established theory. An explanation might by found e.g. on basis of surface chemistry, the molecular structure and their surface interaction or improved slip models might explain this points discovered using the measurement technique presented.

The standard fluid *CX2000* taken as reference, at this point shows higher friction as well as a transition to hydrodynamic lubrication at quite high speeds.

With focus on applications in vacuum condition, other criteria as thermal- and long term stability, wear and volatility have to be considered.

Summary and Outlook

7

If I have seen further than others, it is by standing upon the shoulders of giants.

Isaac Newton, 1642-1727

The setup developed and described in Chapter 3 and 4, the foundation of this thesis, allows for precise friction measurements on small self lubricating journal bearings, as well as ball bearings, under variation of the relevant parameters of speed, radial clearance and loading. The shaft speed can be driven, precisely controlled, from 0 to $25000\,rpm$, radial clearance can be chosen by the parts installed and the loading altered over a wide range by applying different weights of known mass. After evaluation of different bearing solutions for the rotating shaft, the support of the shaft on a steel prism finally provided the most smooth support and was a key enabling element for precise measurements of relative displacement.

Considering the experiences gained and summarized in Chapter 3, the parameter range of the technique presented can easily be extended, e.g. to higher speeds using another driving system.

The high resolution of nominal $50\,nNm$ allows for all kinds of investigations, which influence the friction torque. The use of a precise balance to measure the friction provides several advantages when compared to the work of Kim et al. [56], as internal calibration routines can be used and compensation for typically encountered perturbations as temperature, pressure or humidity is already provided. To make use of this high precision, the process of identifying and compensating deviations from ideal geometry, as explained in Section 4, is of major importance for this measuring technique. Not considering fabrication and mounting eccentricities may lead to false results in all domains of the Stribeck curve and therefore to a misinterpretation of lubrication performance when comparing different lubricant and bearing systems.

The relative displacement between shaft and bearing, captured by contactless laser triangulation, provides additional insight into the systems behavior, including the fluid-structure interaction. The effect of half-frequency whirling can dramatically change the state of the system and higher friction will be detected. The onset of this instability is quite complex, it was found to happen more likely in case of low radial loadings, non porous bearing material, big fluid gaps and Newtonian behaviour of the lubricant.

Accounting for the relative displacement between shaft and bearing for the determination of friction, an increase in measurement precision is obtained compared to a system without this information as shown in Chapter 4. The increase in precision is dominant in the domain of mixed lubrication, at the point of minimum friction, where a maximum of horizontal relative displacement is detected. At high speed, in the domain of hydrodynamic

lubrication, the shaft is well centred in the bearing and relative displacement data is of minor importance for the determination of friction.

Applying the technique of simultaneous detection of friction and relative displacement between shaft and bearing around the speed of minimal friction, the important lift-off, the opening of the contact between shaft and bearing, can be observed and analysed for different parameters. This new insight into the bearing behaviour bridges the gap between work in Tribology, focussing on the surfaces sliding in contact, and research in Rheology and Fluid Dynamics, describing the physics in the hydrodynamic domain of lubrication.

Friction measurement analysis and modelling at high speed has to take into account effects of viscous heating, leading to a reduction of fluid viscosity due to the increase in temperature and therefore to a reduction of friction in the domain of hydrodynamic lubrication. A model to deal with this was developed and verified as presented in Chapter 5. To compare friction measurements at high speed, it is very important to apply approaches of thermohydrodynamic lubrication, considering effect of viscous heating. Otherwise the possibility of a meaningful comparison would be limited to some specific sets of parameters (speed profile $\omega(t)$, fluid gap c, fluid viscosity η) which are unknown and eventually not available. The importance of thermohydrodynamic models is illustrated in the Figs. 6.13 and 6.14, were the huge deviations between measurement and theory are visible for the isothermal model. The effect of porous bearing material on friction was investigated using non porous material and considered in the model. The reduction of friction due to the pores sometimes is referred to as a type of surface slip, although its origin is to be found on macroscopic scale. The friction models derived provide high precision friction values in the domain of hydrodynamic lubrication, at high speed and moderate radial loading.

Using the setup and techniques developed, Ionic Liquids were applied as lubricants in porous, self-lubricating journal bearings as described in Chapter 6. Considering the viscous heating and the reduction of viscosity linked to that, and effects of porous bearing material, measurement analysis revealed Newtonian fluid behaviour over the entire range of shear rates applied. Therefore, compared under laboratory conditions and atmospheric pressure, Ionic Liquids cannot compete with highly developed, modern non-Newtonian lubricant systems, as shear thinning is a key ability for low friction at high speed. Effects of surface slip or supra-fluidity on moleculare scale, as reported in literature, were not observed using the parameters applied.

In the domain of mixed lubrication, the low viscosity fluids showed lower friction and a transition to the domain of hydrodynamic lubrication at lower Sommerfeld numbers So when compared to the highly developed, non Newtonian standard lubricant taken as reference.

Outlook

From a theoretical point of view, friction analysis and modelling in the domains of solid and mixed lubrication has not been addressed so far in this thesis. An extension of the models to these domains will provide a more complete description of friction, mainly encountered during start-up and at heavy load. The good results of low friction in these domains for the IL lubrication as presented in Chapter 6 motivates for a more detailed analysis. In these domains, tribochemistry takes an important role and has to be looked at, as bearing and lubricant integrity are strongly influenced and significant wear might occur.

Beyond the basic application in friction measurements under laboratory conditions, some more potential in Ionic Liquid lubrication can be uncovered when going towards more difficult environment as low pressure, vacuum conditions and high temperature, where standard lubrication systems cannot be applied any more.

Potentially even more hidden lubrication capacity can be found in the application of IL lubrication in combination with suitable additives of the family of nano material, which have the possibility to interact with both the surface and the fluid molecules and therefore modification of the molecular interaction according to the specific needs. An open point, which has not been addressed so far, is the long term stability of the IL lubricant candidates at different surrounding conditions.

Using the data of simultaneous detection of friction and relative displacement between shaft and bearings, the old models of hydrodynamic lubrication and the simplifications of half- and full Sommerfeld pressure boundary conditions can be critically compared to the behaviour of the real system. An often mentioned justification for neglecting the negative pressure in the half-Sommerfeld solution is the fact that classic lubrication fluids cannot support sub-ambient pressure and will evaporate. With the application of ILs, especially in the domain of high pressure gradients, friction and relative displacement trajectories under variation of speed eventually look different.

As small electric motors are often used at low radial loading, at least on

the back side of the shaft, were no torque is applied, whirling phenomena are worth being looked at in detail. Using precise relative displacement measurements, the additional dynamic forces due to whirling can be calculated under consideration of the mass of the bearing unit. To reduce friction, it might be useful for some specific cases, to reduce the gap c to avoid whirling phenomena and accept some additional viscous losses due to the increased shear rate and herewith obtain reduced overall energy losses.

References

[1] Adatepe, H., Bıyıklıoglu, A., and Sofuoglu, H. (2011). An experimental investigation on frictional behavior of statically loaded micro-grooved journal bearing. *Tribology International*, 44(12):1942–1948.

[2] Amamou, A. and Chouchane, M. (2014). Nonlinear stability analysis of long hydrodynamic journal bearings using numerical continuation. *Mechanism and Machine Theory*, 72:17–24.

[3] Amann, T., Dold, C., and Kailer, A. (2012). Rheological characterization of ionic liquids and ionic liquid crystals with promising tribological performance. *Soft Matter*, 8(38):9840.

[4] Amann, T., Dold, C., and Kailer, A. (2013). Complex fluids in tribology to reduce friction: Mesogenic fluids, ionic liquids and ionic liquid crystals. *Tribology International*, 65:3–12.

[5] Andereck, D. (1986). Flow regimes in a circular Couette system with independently rotating cyclindes. *Journal of Fluid Mechanics*, 164:155–183.

[6] Anderson and Saunders (1953). Convection from an isolated heated horizontal cylinder rotating about its axis.

[7] Anderson, K. J. (1991). A History of Lubricants. *MRS Bulletin*, 16(10):69.

[8] A.Neacsu and B.Scheichl (2011). Hydrodynamic Lubrication in Porous Journal Bearings : Comparison Between Experimental and Simulation Data. Technical report, Austrian Center of Competence in Tribology, Austria.

[9] Atkin, R. (2013). Influence of Ion Structure and Surface Potential on Ionic Liquid Lubrication. In *World Tribology Congress*, pages 1–4, Torino, Italy.

[10] Awasthi, R. K., Sharma, S. C., and Jain, S. C. (2007). Performance of worn non-recessed hole-entry hybrid journal bearings. *Tribology International*, 40(5):717–734.

[11] Balasoiu, A. M. (2012). *A self-circulation porous bearing with a wrapped-around reservoir*. PhD thesis, Akron.

[12] Balasoiu, A. M., Braun, M. J., and Moldovan, S. I. (2013). A parametric study of a porous self-circulating hydrodynamic bearing. *Tribology International*, 61:176–193.

[13] Battez, a. H., González, R., Viesca, J., Blanco, D., Asedegbega, E., and Osorio, a. (2009). Tribological behaviour of two imidazolium ionic liquids as lubricant additives for steel/steel contacts. *Wear*, 266(11-12):1224–1228.

[14] Beavers, G. S. and Joseph, D. D. (1967). Boundary conditions at a naturally permeable wall.

[15] Bermúdez, M.-D., Jiménez, A.-E., Sanes, J., and Carrión, F.-J. (2009). Ionic liquids as advanced lubricant fluids. *Molecules (Basel, Switzerland)*, 14(8):2888–908.

[16] Böckh, P. V. and Wetzel, T. (2009). *Wärmeübertragung. 6. Auflage*.

[17] Boncompain, R. (1986). Analysis of Thermal Effects in Hydrodynamic Bearings. *Journal of Tribology-Transactions of the Asme*, 108(2):219 – 224.

[18] Booser, M. M. K., R., E., and R., E. (2008). journal bearings. In *applied tribology*, volume 4, chapter 8 journal. Applied Tribology: Bearing Design and Lubrication, Second Edition.

[19] Boubendir, S., Larbi, S., and Bennacer, R. (2011). Numerical study of the thermo-hydrodynamic lubrication phenomena in porous journal bearings. *Tribology International*, 44(1):1–8.

[20] Bouyer, J. and Fillon, M. (2011). Experimental measurement of the friction torque on hydrodynamic plain journal bearings during start-up. *Tribology International*, 44(7-8):772–781.

[21] Braun, A. (1982). Porous bearings. *Tribology International*, 15(5):235–242.

[22] Brenner, W., Haddad, G., Detter, H., Popovic, G., Vujanic, a., and Delic, N. (1997). The measurement of minimotors and micromotors torque-characteristic using miniaturized cable brake. *Microsystem Technologies*, 3(2):68–71.

[23] Bruce, R. W. (1988). *CRC Handbook of Lubrication: Theory and Practice of Tribology, Theory and Design*, volume 2. CRC Press.

[24] Burrell, G. L., Dunlop, N. F., and Separovic, F. (2010). Non-Newtonian viscous shear thinning in ionic liquids. *Soft Matter*, 6(9):2080.

[25] Camilleri, R., McCulloch, M. D., and Howey, D. (2014). Experimental investigation of the thermal contact resistance in shrink fit assemblies with relevance to electrical machines. *7th IET International Conference on Power Electronics, Machines and Drives (PEMD 2014)*, pages 0444–0444.

[26] Capone, E. (1973). OIL WHIRL IN JOURNAL BEARINGS UNDER NO LOAD CONDITIONS. *Wear*, 26:207–217.

[27] Capone, E. and D'Agostino, V. (1974). Oil whirl in porous metal bearings. *Meccanica*, 9(2):121–129.

[28] C.E. Snyder, J., Gschwender, L., and Sharma, S. (2001). Liquid Lubricants and Lubrication. In Bharat, B., editor, *MODERN tribology handbook*, chapter Liquid Lub. CRC Press.

[29] Cusano, C. (1973). the effect of variable permeability on the performance characteristics of porous bearings. *wear*, 23:55–62.

[30] de Castro, H. F., Cavalca, K. L., and Nordmann, R. (2008). Whirl and whip instabilities in rotor-bearing system considering a nonlinear force model. *Journal of Sound and Vibration*, 317:273–293.

[31] Dikmen, E. (2010). *Multiphysical effects on high-speed rotordynamics*. PhD thesis, Twente.

[32] Dubois, G. B. and Ocvirk, W. (1953). Analytical derivation and experimental evaluation of short-bearing approximation for full journal bearings. Technical report, Cornell University.

[33] Egypt (1882). Transport of a colossus, from a tomb at El Bersheh.

[34] Espinosa-marzal, R. M., Liu, K., Arcifa, A., Rossi, A., and Spencer, N. D. (2013). Uncovering the crucial properties for IL-mediated lubrication. In *World Tribology Congress*, volume 4, pages 4–5, Torino, Italy.

[35] Euler, L. (1755). Principes generaux du mouvement des fluides.

[36] Fan, C. C., Syu, J. W., Pan, M. C., and Tsao, W. C. (2011). Study of start-up vibration response for oil whirl, oil whip and dry whip. *Mechanical Systems and Signal Processing*, 25(8):3102–3115.

[37] Fan, X. and Wang, L. (2015). Ionic liquids gels with in situ modified multiwall carbon nanotubes towards high-performance lubricants. *Tribiology International*, 88:179–188.

[38] Fillon, M. and Bouyer, J. (2004). Thermohydrodynamic analysis of a worn plain journal bearing. *Tribology International*, 37(2):129–136.

[39] Goldstein, M. E. and Braun, W. H. (1971). Effect of velocity slip at a porous boundary on the performance of an incompressible porous bearing. Technical Report February, NASA.

[40] Guha, S. K. (1986). Study of Conical Whirl Instability of Externally Pressurized Porous Oil Journal Bearings With Tangential Velocity Slip. *Journal of Tribology*, 108(2):256.

[41] Hamrock, B. J. and Schmid, S. R. (2004). *Fundamentals of Fluid Film Lubrication Second Edition*.

[42] Hernández Battez, A., Bartolomé, M., Blanco, D., Viesca, J. L., Fernández-González, A., and González, R. (2016). Phosphonium cation-based ionic liquids as neat lubricants: Physicochemical and tribological performance. *Tribology International*, 95:118–131.

[43] Herwig, H. and Schmandt, B. (2015). *Strömungsmechanik*.

[44] Holzbauer, R., Merstallinger, A., and Brenner, J. (2006). IONIC LIQUIDS AS NEW LUBRICANTS FOR SPACE. Technical Report 1, seibersdorf research.

[45] Hori, Y. (2006a). *Hydrodynamic Lubrication*. Springer.

[46] Hori, Y. (2006b). Hydrodynamic Lubrication. In *Hydrodynamic Lubrication*, chapter Porous Bearings, pages 109–112. Springer.

[47] Illner, T., Bartel, D., and Deters, L. (2015). Determination of the transition speed in journal bearings under consideration of bearing deformation. *Tribology International*, 82:58–67.

[48] Jakeman, R. W. and Parkins, D. W. (1987). Theoretical and experimental orbits of a dynamically loaded hydrodynamic journal bearing. *Tribology Series*, 11(iii):355–362.

[49] Jiménez, A. E., Bermúdez, M. D., and Iglesias, P. (2009). Lubrication of Inconel 600 with ionic liquids at high temperature. *Tribology International*, 42(11-12):1744–1751.

[50] Joseph, D. D. and Tao, L. N. (1966). Lubrication of a Porous Bearing—Stokes' Solution. *Journal of Applied Mechanics*, 33(4):753.

[51] Kałdoński, T. and Wojdyna, P. (2011). Liquid lubricants for space engineering and methods for their testing. *Journal of KONES*, 18(1).

[52] Kamimura, H., Kubo, T., Minami, I., and Mori, S. (2007). Effect and mechanism of additives for ionic liquids as new lubricants. *Tribology International*, 40(4):620–625.

[53] Kawada, S., Watanabe, S., Kondo, Y., Tsuboi, R., and Sasaki, S. (2013). Tribochemical Reaction of Ionic Liquids under Vacuum Condition. In *World Tribology Congress*, pages 2–4, Torino, Italy.

[54] Khonsari, M. M. (2008). A Review of Thermal Effects in Hydrodynamic Bearings . Part I: Slider and Thrust Bearings. *Tribology Transactions*, 30(October 2014):37–41.

[55] Khonsari, M. M. and Booser, E. R. (2008). *Applied Tribology, Bearing Design and Lubrication*. Tribology Series. John Wiley & Sons, Ltd, Chichester, UK, 2 edition.

[56] Kim, H. J., Park, I. K., Seo, Y. H., Kim, B. H., and Hong, N. P. (2014). Wire tension method for coefficient of friction measurement of micro bearing. *International Journal of Precision Engineering and Manufacturing*, 15(2):267–273.

[57] Kondo, Y., Koyama, T., Tsuboi, R., Nakano, M., Miyake, K., and Sasaki, S. (2013). Tribological Performance of Halogen-Free Ionic Liquids as Lubricants of Hard Coatings and Ceramics. *Tribology Letters*, 51(2):243–249.

[58] Kumar, V. (1978). A LUBRICATION EQUATION INCLUDNG SLIP VELOCITY FOR HYDRODYNAMIC POROUS BEARINGS IN THE LOWER TURBULENT REGIME - A PERTURBATION APPROACH. *Wear*, 51:25–37.

[59] Kumar, V. (1980a). Estimation of the performacne of a norrow porous journal bearing with hydrodynamic turbulent lubrication considering slip velocity and arbitrary wall thickness. *Wear*, 64:355–365.

[60] Kumar, V. (1980b). Porous metal bearings — A critical review. *Wear*, 63(2):271–287.

[61] Kumar, V. (1981a). Hydrodynamic load capacity of a full porous journal bearing of finite length in the turbulent regime considering slip flow and curvature. *Wear*, 67(2):167–176.

[62] Kumar, V. (1981b). Plain hydrodynamic bearings in the turbulent regime - A critical review. *Wear*, 72(1):13–28.

[63] Kylander, G. (1995). *Thermal modelling of small cage induction motors*. Number 265.

[64] Laha, S. and Kakoty, S. (2011). Non-linear dynamic analysis of a flexible rotor supported on porous oil journal bearings. *Communications in Nonlinear Science and Numerical Simulation*, 16(3):1617–1631.

[65] L.Costa and Miranda (2003). Temperature, Flow, and Eccentricity Measurements in a Journal Bearing with a Single Axial Groove at 90 degree to the Load Line. *Lubrication Science*, 15(February):167–180.

[66] Lin, J., Hwang, C., and Yang, R. (1996). Hydrodynamic lubrication of long, flexible, porous journal bearings using the Brinkman model. *Wear*, 198:156–164.

[67] Lin, J. and Wang, L. (1990). Thermohydrodynamic Analysis of Finite-Width, Partial-Arc Journal Bearings with Non-Newtonian Lubricants : Part II. *Tribology International*, 23(3):211–216.

[68] Lin, J. R. and Hwang, C. C. (2002). Hopf bifurcation to a short porous journal-bearing system using the Brinkman model: Weakly nonlinear stability. *Tribology International*, 35:75–84.

[69] Ma, H., Li, H., Zhao, X., Niu, H., and Wen, B. (2013). Effects of eccentric phase difference between two discs on oil-film instability in a rotor-bearing system. *Mechanical Systems and Signal Processing*, 41(1-2):526–545.

[70] Magère, E. (1999). *Numerical study of transitions in taylor-couette flow*. PhD thesis, EPFL.

[71] Mellor, P., Roberts, D., and Turner, D. (1991). Lumped parameter thermal model for electrical machines of TEFC design. *IEE Proceedings B Electric Power Applications*, 138(5):205.

[72] Minami, I. (2009). Ionic liquids in tribology. *Molecules (Basel, Switzerland)*, 14(6):2286–305.

[73] Mitsui, J. (1987). A study of thermohydrodynamic lubrication in a circular journal bearing. *Tribology International*, 20(6):331–341.

[74] Mokhtar, M., Rafaat, M., and Shawki, G. (1984). Experimental Investigations into the Performance of Porous Journal Bearings.

[75] Mordukhovich, G., Qu, J., Howe, J. Y., Bair, S., Yu, B., Luo, H., Smolenski, D. J., Blau, P. J., Bunting, B. G., and Dai, S. (2013). A low-viscosity ionic liquid demonstrating superior lubricating performance from mixed to boundary lubrication. *Wear*, 301(1-2):740–746.

[76] Morgan, V. T. (1969). Porous metal bearings. In *Perspectives in Powder Metallurgy Fundamentals, Methods, and Applications*, chapter 15.

[77] Muhs, D., Wittel, H., Voßiek, J., and Jannasch, D. (2013). Tribologie. In *Roloff/Matek Maschinenelemente*, volume 0, pages 522–576.

[78] Murti, P. R. K. (1971a). Hydrodynamic lubrication of finite porous bearings. *wear*.

[79] Murti, P. R. K. (1971b). Hydrodynamic lubrication of long porous bearings. *Wear*, 18(6):449–460.

[80] Murti, P. R. K. (1972a). Hydrodynamic lubrication of short porous bearings. *Wear*, 19(1):17–25.

[81] Murti, P. R. K. (1972b). Some Aspects of Slip-flow in Porous Bearings. *Wear*, 19:123–129.

[82] Murti, P. R. K. (1973a). Effect of slip-flow on pressure distribution in narrow porous bearings. *Wear*, 25(3):365–372.

[83] Murti, P. R. K. (1973b). Lubrication of finite porous journal bearings. *Wear*, 26(1):95–104.

[84] Murti, P. R. K. (1974). Squeeze films in full porous metal bearings. *Wear*, 30(2):257–265.

[85] Muszynska, A. (1986). Whirl and whip—Rotor/bearing stability problems. *Journal of Sound and Vibration*, 110:443–462.

[86] Muszynska, A. (1988). Stability of whirl and whip in rotor/bearing systems. *Journal of Sound and Vibration*, 127:49–64.

[87] Neacsu, I. A., Scheichl, B., Vorlaufer, G., and Eder, S. J. (2014). Experimental validation of the simulated steady-state behavior of porous journal bearings. Technical report, AC2T research GmbH, Wien.

[88] Pai, R. and Majumdar, B. (1992). Theoretical analysis on conical whirl instability of unloaded submerged oil journal bearings. *Wear*, 152:309–316.

[89] Perez, I. J. and Kassakian, J. G. (1979). a Stationary Thermal Model for Smooth Air-Gap Rotating Electric Machines. *Electric Machines & Power Systems*, 3(3-4):285–303.

[90] Pham, M. Q., Yoon, H. S., Khare, V., and Ahn, S. H. (2014). Evaluation of ionic liquids as lubricants in micro milling - Process capability and sustainability. *Journal of Cleaner Production*, 76:167–173.

[91] Prakash, J. (1999). Effect of Velocity Slip in an Infinitely long prugh porous journal bearing. *Tribology Transactions*, 1.

[92] Prakash, J. and Vij, S. K. (1976). Effects of velocity slip in axially undefined porous bearings. *wear*, 38(9):245–263.

[93] Prakash, J. and Vsj, S. K. (1974). Analysis of Narrow Porous Journal Bearing Using Beavers-Joseph Criterion of Velocity Slip. *asme*, (June 1974):348–354.

[94] Predel, T., Pohrer, B., and Schlücker, E. (2010). Ionic Liquids as Alternative Lubricants for Special Applications. *Chemical Engineering & Technology*, 33(1):132–136.

[95] Qiu, Z. L. (1995). *A theoretical and experimental study on dynamic characteristics of journal bearings*. PhD thesis, University of Wollongong.

[96] Rechenberg, H. (2010). *Werner Heisenberg - die Sprache der Atome*.

[97] Reynolds, O. (1886a). On the Theory of Lubrication and Its Application to Mr. Beauchamp Tower's Experiments, Including an Experimental Determination of the Viscosity of Olive Oil. *Philosophical Transactions of the Royal Society of London*, 177:157–234.

[98] Reynolds, O. (1886b). On the Theory of Lubrication and Its Application to Mr. Beauchamp Tower's Experiments, Including an Experimental Determination of the Viscosity of Olive Oil. *Philosophical Transactions of the Royal Society of London*, 177:157–234.

[99] Rhodes, C. A. and W. Rouleau (1965). Hydrodynamic lubrication of narrow porous metal bearing with sealed ends. 8:474–480.

[100] Scheichl, B., Neacşu, I. A., and Kluwick, A. (2015). A novel view on lubricant flow undergoing cavitation in sintered journal bearings. *Tribology International*, 88:189–208.

[101] Schweizer, B. (2009). Oil whirl, oil whip and whirl/whip synchronization occurring in rotor systems with full-floating ring bearings. *Nonlinear Dynamics*, 57(4):509–532.

[102] Shir, C. and Joseph, D. (1966). Lubrication of a Porous Bearing—Reynolds' Solution. *Journal of . . . .*

[103] Simmons, G. F. (2013). *Journal Bearing Design, Lubrication and Operation*. Dissertation, Luleå.

[104] Somers, A., Howlett, P., MacFarlane, D., and Forsyth, M. (2013). A Review of Ionic Liquid Lubricants. *Lubricants*, 1(1):3–21.

[105] Sommerfeld, A. (1904). Zur hydrodynamischen Theorie der Schmiermittelreibung. *Zeitschrift für Mathematik und Physik*, 50:97–155.

[106] Spikes, H. and Granick, S. (2003). Equation for Slip of Simple Liquids at Smooth Solid Surfaces Equation for Slip of Simple Liquids at Smooth Solid. *Langmuir*, 19(May):5065–5071.

[107] Stachowiak, G. W. (2006). Hydrodynamic lubrication. In *Engineering Tribology*, chapter Hydrodynam. 3 edition.

[108] Stachowiak, G. W. and Batchelor, A. W. (2014). Engineering Tribology. In *Engineering Tribology*, chapter Hydrodynam, pages 105–210. Elsevier.

[109] Stribeck, R. (1902). Die Wesentlichen Eigenschaften der Gleit- und Rollenlager. *Zeitschrift des Vereines Deutscher Ingenieure*, 46:1341–1348.

[110] Suzuki, A., Shinka, Y., and Masuko, M. (2007). Tribological Characteristics of Imidazolium-based Room Temperature Ionic Liquids Under High Vacuum. *Tribology Letters*, 27(3):307–313.

[111] Szeri, A. Z. (1983). Dynamic Properties of Lubricant Films. *Fluid Film Lubrication: Theory and Design*, pages 132–168.

[112] Szeri, A. Z. (2014). *Flow Stability and Transition*. Number 1.

[113] Tonnesen, J. (1964). EXPERIMENTAL TECHNIQUES FOR ROTORDYNAMICS ANALYSIS. In N. F. Rieger, editor, *Rotordynamics 2*, chapter EXPERIMENT, pages 271–281. Springer.

[114] Totolin, V., Minami, I., Gabler, C., and Dörr, N. (2013). Halogen-free borate ionic liquids as novel lubricants for tribological applications. *Tribology International*, 67:191–198.

[115] Tower, B. (1883). First report on friction experiments. *Proc. Inst. Mech. Eng.1*, pages 632–666.

[116] Trachsel, M., Dual, J., and Pittini, R. (2016a). Friction measurements on small journal bearings. In *XXIV ICTAM*, number August, pages 1–2, Montreal.

[117] Trachsel, M., Pittini, R., and Dual, J. (2016b). Friction and 2D position measurements in small journal bearings. *Tribology International*, 102:555–560.

[118] Trachsel, M., Pittini, R., and Dual, J. (2017). A combined approach to study and model the effect of viscous heating in small porous, self lubricating journal bearings. *Tribology International*, 166(C):199–207.

[119] Tunckol, M., Durand, J., and Serp, P. (2012). Carbon nanomaterial-ionic liquid hybrids. *Carbon*, 50(12):4303–4334.

[120] Van Buuren, S. W., Hetzler, H., Hinterkausen, M., and Seemann, W. (2012). Novel approach to solve the dynamical porous journal bearing problem. *Tribology International*, 46(1):30–40.

[121] Waldemar, S. and Rudolf, R. (1996). *Maschinen- und Konstruktion-selemente 3*.

[122] Wang, B., Wang, X., Lou, W., and Hao, J. (2010). Rheological and tribological properties of ionic liquid-based nanofluids containing functionalized multi-walled carbon nanotubes. *Journal of Physical Chemistry C*, 114(19):8749–8754.

[123] Wang, J. and Khonsari, M. (2008). Effects of oil inlet pressure and inlet position of axially grooved infinitely long journal bearings. Part I: Analytical solutions and static performance. *Tribology International*, 41(2):119–131.

[124] Wang, X. L., Zhu, K. Q., and Wen, S. Z. (2001). Thermohydrodynamic analysis of journal bearings lubricated with couple stress fluids. *Tribology International*, 34(5):335–343.

[125] Wu, L. and Tan, Q. (2016). Thermal Characteristic Analysis and Experimental Study of a Spindle-Bearing System. *Entropy*, 18(8):271.

[126] Xiao, H., Guo, D., Liu, S., Pan, G., and Lu, X. (2010). Film Thickness of Ionic Liquids Under High Contact Pressures as a Function of Alkyl Chain Length. *Tribology Letters*, 41(2):471–477.

[127] Y. Hori and Okoshi, K. (2006). Stability of a Rotating Shaft — Oil Whip. In *hydrodynamic lubrication*.

[128] Yao, Z., Zhang, Q., Tao, Y., and Zhang, X. (2000). A new approach to measure the friction coefficient of micro journal bearings. *Tribology International*, 33(7):485–489.

[129] Ye, C., Liu, W., Chen, Y., and Yu, L. (2001). Room-temperature ionic liquids: a novel versatile lubricant. *Chemical Communications*, pages 2244–2245.

[130] Yong-Xin, Q., Ji, M., Yi-Geng, T., Gui-Ru, Z., Gao-Yi, S., and Guo-Liang, W. (1985). Investigation of sintered bronze bearings under high-speed conditions.

[131] Yong-Xin, Q. and Pei-Ming, W. (1985). Theoretical analysis and experimental investigation of a porous metal bearing.

[132] Yu, B., Liu, Z., Zhou, F., Liu, W., and Liang, Y. (2008). A novel lubricant additive based on carbon nanotubes for ionic liquids. *Materials Letters*, 62(17-18):2967–2969.

[133] Zhang, Y., Hei, D., Liu, C., Guo, B., Lu, Y., and Müller, N. (2014). An approximate solution of oil film forces of turbulent finite length journal bearing. *Tribology International*, 74:110–120.

List of publications

M. Trachsel, R. Pittini, J. Dual. *Evaluation and quantification of friction using Ionic Liquids in small, self lubricating journal bearings*, submitted to Tribology International in September 2017

M. Trachsel, R. Pittini, J. Dual. *A combined approach to study and model the effect of viscous heating in small porous, self lubricating journal bearings*, Tribology International 116C (2017) pp. 199-207, ISSN 0301679X.

M. Trachsel, R. Pittini, J. Dual. *Friction and 2D position measurements in small journal bearings*, Tribology International 102 (2016) 555-560, ISSN 0301679X.

M. Trachsel, R. Pittini, J. Dual. *Friction measurements on small journal bearings*, Proceedings of the 24th International Congress of Theoretical and Applied Mechanics, Montréal, Canada.